The Indian summer monsoon and Its variability in the Mid-Holocene and Last Millennium – A modelling view

A thesis submitted to the University of Hyderabad
For the degree of
Doctor of Philosophy

In

Earth, Ocean and Atmospheric Sciences

By

Tejavath Charan Teja Reg. No: 15ESPE09

Under the supervision of

Prof. Karumuri Ashok



Centre for Earth, Ocean and Atmospheric Sciences
School of Physics
University of Hyderabad
Hyderabad - 500046
Telangana, India
2021

Declaration

I hereby declare that this PhD thesis entitled "The Indian summer monsoon and Its variability in

the Mid-Holocene and Last Millennium – A modelling view" is the result of an investigation

carried out by me in the Centre for Earth, Ocean and Atmospheric Sciences, School of Physics,

University of Hyderabad, Hyderabad under the guidance/supervision of Prof. Karumuri Ashok. This

work is a bonafide research work and free from plagiarism. I also declare that the thesis has not

been submitted previously in part or in full to this or any other University or Institution for the

award of any degree or diploma.

A report on the plagiarism statistics from the University of Hyderabad librarian is enclosed.

Place: University of Hyderabad, Hyderabad.

Date:

Tejavath Charan Teja

Reg.No. 15ESPE09

CEOAS, School of Physics

University of Hyderabad

Gachibowli

Hyderabad, PIN 500046.



Certificate

This is to certify that the PhD thesis entitled "The Indian summer monsoon and Its variability in the Mid-Holocene and Last Millennium – A modelling view" by Mr. Tejavath Charan Teja bearing the Reg. No. 15ESPE09 in partial fulfillment of the requirements for the award of Doctor of Philosophy in the Centre for Earth, Ocean and Atmospheric Sciences (CEOAS), School of Physics, University of Hyderabad is a bonafide work carried out by him under my supervision/guidance. This thesis has not been submitted previously in part or in full to this or any other University or Institution for the award of any degree or diploma. Any text, illustration, tables, figures, etc., used in the thesis from other sources have been duly cited. He has completed the following requirements as per PhD regulations of the University:

- (a) Completion of the course work as per the University rules.
- (b) Regular submission of six months progress report.
- (c) Presentation of his work to the PhD doctoral committee members.
- (d) Publication of at least one research paper in a refereed research journal.

Prof. Karumuri Ashok (Supervisor)

(Head, CEOAS)

(Dean, School of Physics)

Frams 1301 31/5/12

UNIVERSITY OF HYDERABAD NOTIFICATION OF RESULTS

Course Work: Ph.D., Centre for Earth and Space Sciences,

Month & Year: April'2017 Semester -II

Sl.	Regn.No.	Name of the Student	CC			COURSES & ND GRADES	NO OF
No		* , .	ES 801 Credits 4	ES 805 Credits 3	ES 806 Credits 4	ES 807 Credits 3	ES 811- 830 Credits 2
1	13ESPE01	KONETI SUNITHA	Pass	Pass	Pass	Pass	Pass
2	13ESPE03	DEBASHRI GARAI	Pass	Pass	Pass	Exempted	Pass
3	15ESPE01	FABA FRANCIS	Pass	Pass	Pass	Pass	Pass
4	15ESPE02	HEMADRI BHUSHAN AMAT	Pass	Pass	Pass	Fail	Pass
5	15ESPE03	K. MALLESH	Pass	Pass	Pass	Exempted	Pass
6	15ESPE04	CHENNU RAMU	Pass	Pass	Pass	Pass	Pass
7-	15ESPE05	GOVARDHAN DANDU	Pass	Pass	Pass	Pass	Pass
Q	15ECDE07	POVALALIGITA.	Dogg	Docc	Docc	Docc	Pacc
9	15ESPE09	TEJAVATH CHARAN TEJA	Pass	Pass	Pass	Pass	Pass
10	15ESPE10	KUMAR	Pass	NA ·	Pass	NA	Pass
11	16ESPE01	RESHMA M.R.	Pass	NA	Pass ·	Exempted	Pass
12	16ESPE02	SEEDABATTULA V BALAJI MANASA RAO	Pass	NA	Pass	NA	Pass
13	16ESPE04	SUNIT MOHANTY.	Pass	NA	Pass	NA .	Pass
14	16ESPE05	TARUN THOMAS T.	Pass	NA	Pass	NA	Pass

Course No. Title of the Course

ES 801 Earth system sciences -4 ES 805 Research Mehtodology -3

ES 806 Mathematics for Earth Sciences -4

ES 807 Interdisciplinary course -3

ES 811-830 Special Paper on Spectified Research Topic -2

NA - NOTAPPEARED

Dated: 29.05.2017

To

Head, Centre for Earth and Space Sciences Dean School of Physics

1600 2000 Control of Examination 30-

Dedicated to my family



In loving memory of my precious 6 years

Contents

Ack	nowledgement	s .	•	•	•	•	•	•	•	•	•	•	•	•	•	•	•	i
List	of publications	s .	•		•	•									•			iii
Pap	ers presented i	n the	con	ıfere	nce/	sem i	inar	•	•						•	•		iv
List	of abbreviatio	ns	•			•	•	•	•	•								v
List	of figures .		•	•	•	•	•	•	•	•	•	•		•	•	•		viii
List	of tables .		•	•	•	•	•	•	•	•	•	•		•	•	•		xiv
Abs	tract		•	•	•	•	•	•	•	•				•	•	•		xvi
1 In	troduction																	1
	1.1 The current	day	India	an sı	ımm	er m	onso	on	•							•		1
	1.2 The El Niño) - Sc	outhe	ern C)scil	latio	n.		•									6
	1.3 ENSO impa	icts o	n th	e Inc	lian s	sumr	ner i	non	soon	and	l asso	ociat	ed m	echa	anisn	ns		9
	1.4 Indian sumı	ner r	nons	soon	duri	ng th	ne M	id-H	lolod	ene	and	Last	Mil	lenni	ium			12
	1.4.1 Proxy	-data	a bas	sed s	tudie	es.	•				•							12
	1.4.1.1	The	Mic	l-Ho	locei	ne										•		12
	1.4.1.2	The	Las	t Mi	llenn	ium		•		•								14
	1.4.2 Mode	elling	bas	ed st	udie	s.		•		•								16
	1.5 Objectives a	and S	Scop	e of	the s	tudy												17
	1.6 Summary		•															18
2 D	atasets and r	neth	odo	olog	\mathbf{y}													20
	2.1 Datasets .		•					•										20
	2.1.1 CMII	95 Hi	stori	ical s	simu	latio	ns			4		4						20

	2.1.2 PMIP3 Last Millennium simulations .	•	•	•	•	•	•	•	•	22
	2.1.3 PMIP3 Mid-Holocene simulations .							•	•	23
	2.1.4 Observational and Reanalysis datasets							•	•	24
	2.2 Methodology							•	•	24
	2.3 Validation of the CMIP5 Historical simulations							•	•	26
	2.4 Summary				•					32
3 I	Indian summer monsoon variability during	g the	e La	st N	/Iille	enni	ium	l		33
	3.1 Last Millennium analysis					•		•	•	33
	3.1.1 Annual cycle	•						•	•	33
	3.1.2 Mean state	•						•	•	35
	3.1.3 Simulated interannual variability of ISM	•			•	•		•	•	35
	3.1.4 El Niño-Southern oscillation and ISM					•		•	•	40
	3.2 MWP and LIA analysis				•					41
	3.2.1 Annual cycle									41
	3.2.2 Mean state					•				43
	3.2.3 Interannual variability of ISM and teleco	nnec	tions	of t	he E	l Nií	ĭo	•	•	45
	3.3 Dynamics	•			•			•	•	52
	3.4 Summary	•						•	•	56
4 I	Indian summer monsoon variability during	g the	e mi	d-H	[olo	cen	e			58
	4.1 Annual cycle				•			•	•	59
	4.2 Mean state	•				•				60
	4.3 Interannual variability of ISM									61
	4.4 El-Niño southern oscillation and ISM									63

4.5 Possible dynamics	67
4.6 Summary	72
5 Simulating the Indian summer monsoon during Mid-Holocene	
and Last Millennium	74
5.1 The model, experiment setup and methodology	74
5.2 Validation of simulated mean summer monsoon rainfall and surface temperatures over India	80
	81
	82
5.2.3 Role of tropical Ocean-Atmospheric coupled processes or the lack thereof	84
5.3 Simulated circulation changes over India	85
5.3.1 Mid-Holocene	85
5.3.2 MWP and LIA	88
5.3.3 Possible mechanisms for the stronger mid-Holocene summer monsoon .	90
5.4 The mid-Holocene ISM response to changes in orbital forcings	91
5.4.1 Simulated rainfall and surface temperature	93
5.4.2 Simulated circulation changes over India	94
5.5 Potential role of concurrent ENSO	95
5.6 Summary	97
6 Conclusions and scope for future studies	99
References	105
Plagiarism Report	120

Acknowledgements

During my thesis work, I have been supported, encouraged, and motivated by many people. It is my pleasure to convey wholehearted gratitude to all of them

This work would not have been possible without the support and guidance of individuals at the University of Hyderabad at Hyderabad. First and foremost, I am sincerely grateful to my supervisor **Prof. Karumuri Ashok**. His knowledge, motivation as a teacher, and his integral view on high-quality research have made a deep impression on me. He has always motivated and taught me to work hard, think, critically evaluate my work, develop a scientific temperament, and importance of using every opportunity. I am indebted to him for his patient guidance and support, which helped me to overcome difficulties throughout my PhD work. I also acknowledge my coauthor **Dr. Supriyo Chakraborty**, Scientist F, Indian Institute of Tropical Meteorology, Pune for continuous encouragement and support throughout my PhD duration. I also acknowledge the contributions of Late **Prof. Rengaswamy Ramesh**, NISER Bhubaneswar during my first reseach article.

I am grateful to my PhD doctoral committee members, **Dr. S. Maqbool Ahmed**, Principal Scientific Officer and Head of Central Instruments Laboratory, UoH, **Dr. S. Sri Lakshmi**, Assistant Professor, CEOAS and **Dr. Vijay P. Kanawade**, Assistant Professor, CEOAS, UoH, for their valuable suggestions/comments, encouragement, and thought-provoking questions which greatly enhanced the quality of my research. Thank you also to **Dr. Sachin Dinkar Ghude** for mentoring me during my master's dissertation work.

I am also grateful to **Prof. K. S. Krishna**, Head of the department, CEOAS, UoH, and former Head of the department **Prof. M. Jayananda**, for the facilities made available to me for my research work. Special thanks to **Prof. V. Chakravarthi** and **Prof. A. C. Narayana** for their constant encouragement since my masters days here in University. I also sincerely thank the other faculty of CEOAS, **Dr. T. Devleena Mani**, **Dr. M. Ismaiel**, and **Dr. Aliba Ao** for their encouragement. I want to express my immense gratitude to **Prof. Ulrich Cubasch**, Institut für Meteorologie, Freie Universität Berlin, Germany for giving me an opportunity to work with him, for guiding me, providing me with all the necessary facilities and hosting me there under ERASMUS+ Worldwide fellowship. I would like to express my heartfelt thanks to **Dr. Esther Brady**, Project Scientist, Climate & Global Dynamics Lab, NCAR for her help in model installation and technical support.

I gratefully acknowledge the Council of Scientific and Industrial Research, and National Fellowship for Higher Education of ST Students for funding me during my PhD. I also acknowledge University of Hyderabad, Institut für Meteorologie, Freie Universität Berlin, Germany, and ERASMUS+ for giving me a fellowship for carryout a part of my research work at Institut für Meteorologie under the ERASMUS+ Worldwide student exchange program. I am gratefull to all the ERASMUS+ Worldwide members, interview panel from both University of Hyderabad and Freie Universität Berlin who supported me. I would also like to acknowledge the

support given by various funding agencies and coordinators of the conference/workshop i had attended during my PhD.

I thank my lab-mates, **Feba Francis**, **Hemadri Bhusan Amat**, **Vikas Kumar Kushwaha**, **Dr. Yagnesh Raghava Yakkala**, **Boyaj Alugula**, **S. Bidyabati**, **D. Govardhan**, and my senior **Dr. Pawan Kumar Gautam** for sharing ideas, constructive criticisms, long not so boring discussions, and enjoying the PhD days together at the CEOAS. Few of them actually helped me financially and emotionally during my PhD. I would like to extend my warm thanks to all my other research scholars non-teaching staff of the CEOAS. Apart from them thanks to my **Bachelors** and **Masters** friends, my **ERASMUS**+ colleagues, **Basketball Cricket** Teammates.

I thank and acnowledge various Climate observational, reanalysis and simulation data repositories for providing the access to the datasets. I also thank and acnowledge various data analyzation tools GrADS, ferret, NCL, CDO, NCO and python. With out these dataset archives and data analyzation tools completing this would have been next to impossible.

Throughout this process the support of my family has been vital. I sincerely thank each of them: my parents, **Ramu Tejavath** and **Satyavathi Tejavath** for teaching me to work hard, to show compassion and supporting me financially (although it is their job i should acknowledge it here); my sister **Yasoda Bhukya** and her husband (brother in law) **Naresh Kumar Bhukya** for supporting me; my crazy little niece **Lithika Sai Rathod** for making me laugh; thanks to all the other family members.

Last but not least, thank you to myself, for my patience, positive attitude, assurance, humor, and love towards myself. A choice I took one day made me write this one today.

Thank you all...! Charan Teja Tejavath

List of Publications:

Thesis related research papers published in peer-reviewed journals

- 1. **Tejavath. C. T.,** Ashok. K., Chakraborty S., Ramesh. R. (2019) A PMIP3 narrative of modulation of ENSO teleconnections to the Indian summer monsoon by background changes in the Last Millennium. Climate Dynamics. https://doi.org/10.1007/s00382-019-04718-z (I.F 4.4)
- 2. **Tejavath. C.T.**, Pankaj. U., Ashok. K., (2019) The past climate of the Indian region as seen from the modeling world. Current Science. Prof. R Ramesh Memorial Volume.(I.F. 0.75)
- 3. **Tejavath, C. T.**, Ashok K and Chakraborty S. The Importance of the Orbital Parameters for the Indian Summer Monsoon During the Mid-Holocene, as Deciphered From Atmospheric Model Experiments. Front. Earth Sci. 9:631310. (2021) doi: 10.3389/feart.2021.631310 (I.F. 2.6)

Other research papers published in peer-reviewed journal

- **1.** Ashok. K., Feba. F., **Tejavath. C. T.** (2019) The Indian summer monsoon rainfall and ENSO. MAUSAM. (I.F 0.57)
- 2. Amat, H.B., Pradhan, M., **Tejavath, C.T.** Avijit Dey, Suryachandra A. Rao, A. K. Sahai & Karumuri Ashok. Value addition to forecasting: towards Kharif rice crop predictability through local climate variations associated with Indo-Pacific climate drivers. Theor Appl Climatol (2021). https://doi.org/10.1007/s00704-021-03572-6 (I.F.2.88)
- **3.** Feba F, D. Govardhan, **Tejavath C.T.,** and Karumuri Ashok. ENSO Modoki teleconnections toIndian summer monsoonrainfall—A review (Book chapter, Title: Indian Summer Monsoon Variability: El Niño-teleconnections and beyond for Elsevier).
- **4.** Ashok. K., Soraisam. B., **Tejavath. C. T.**, & Ulrich Cubasch. The summer monsoon over the northeast India, the wettest region in the world, during the last millennium. (In review with International Journal of Climatology).

Papers presented in the International/National conference/seminars:

International

- Virtual Presentation on "The role of the orbital parameters in the Indian monsoon during the MidHolocene, as deciphered from atmospheric model experiments" PMIP2020 Nanjing Conference, 26-30 October 2020.
- 2. Oral Presentation titled "The ENSO teleconnections to the Indian summer monsoon climate through the Last Millennium as simulated by the PMIP3" in 1st PMIP4 conference held at *Stockholm (Sweden) during 25th 29th September 2017.*
- 3. Presented a poster titled "The Indian Summer Monsoon Climate During Last Millennium, As Simulated by the PMIP3" in CLIVAR-2016, held at *Qingdao (China) during* 18th 25th *September,* 2016.

National

- 1. Virtual Presentation on "The role of the orbital parameters in the Indian monsoon during the MidHolocene, as deciphered from atmospheric model experiments" International Virtual Conference on Earth's Changing Climate: Past, Present & Future; 15-17 October 2020.
- 2. Attended a conference on "International Workshop on Representation of Physical Processes in Weather and Climate Models, 13th 16th February 2017 Indian Institute of Tropical Meteorology, Pune, India.
- 3. Presented a poster "The Indian Summer Monsoon During Last Millennium" in Tropmet-2016, held at *Bhubaneswar*, *Odisha*, 18th- 21st *December*, 2016.
- 4. Attended a two-week workshop, "Extreme Weather and Climate Variability: Observation, Understanding, Prediction" 23rd 31st December 2016, Indian Institute Technology, Bhubaneswar, India.
- 5. Attended a two-week workshop on International Training course on "Indian Ocean Dynamics: From the Large scale Circulation to Small scale Eddies and Fronts" 16th 27th November 2015, INCOIS, Hyderabad.

List of Abbreviations

AAISMR : Area-averaged Indian summer monsoon rainfall

AAISMT : Area-averaged Indian boreal summer monsoon temperatures

AATASG : Area-averaged global boreal summer monsoon temperatures

AGCM : Atmospheric General Circulation Model

BCC : Beijing Climate Center Climate System Model (BCC-CSM1-1)

BP : Before Present BoB : Bay of Bengal

CAM5 : Community Atmospheric Model Version 5
CCSM4 : Community Climate System Model Ver 4

CE : Common Era

CESM1.2.0 : Community Earth System Model Version 1.2.0

CMAP : CPC Merged Analysis of Precipitation

CMIP5 : Coupled model Intercomparison Project phase 5

CMR : Core Monsoon Region

CNRM : Centre National de Recherches Météorologiques Climate Model Ver 5

(CNRM-CM5)

CPC : Climate Prediction Center
CRU : Climatic Research Unit

CSIRO : Commonwealth Scientific and Industrial Research Organisation climate

model (CSIRO-Mk3L-1-2 & CSIRO-Mk3-6-0)

ECMWF : European Centre for Medium-Range Weather Forecasts

ELP^{MH} : El Niño type SSTs in the tropical Pacific Ocean during MH

ELPI^{MH} : La Niña type SSTs in the tropical Indo-Pacific Ocean during MH

ENSO : El Niño - Southern Oscillation

ESC : Eurasian Snow Cover

FS2 : Flexible Global Ocean-Atmosphere-Land system model, Spectral Ver 2:

(FGOALS-s2)

GCM : General Circulation Model

GHG : Greenhouse Gases

GISS : NASA Goddard Institute for Space Studies E2-R Model (GISS-E2-R)

GPCP : Global Precipitation Climatology Project

HADCM3 : Hadley Centre Coupled Model version 3 (HadCM3)

HadISST : Hadley Centre's Monthly Sea Ice and Sea Surface Temperature

HCC & HES : Hadley Centre Global Environment Model Ver 2

(HadGEM2-CC & HadGEM2-CC)

HS : Historical simulations
IAV : Interannual Variability

IGBP : International Geosphere and Biosphere Programme

IMD : Indian Meteorological Department

IOD : Indian Ocean Dipole

IPSL : Institut Pierre Simon Laplace Model CM5A-LR (IPSL-CM5A-LR)

ISM : Indian summer monsoon

ISMR : Indian summer monsoon rainfall

ISMT : Indian summer monsoon surface temperatures (ISMST)

ITCZ : Intertropical Convergence Zone

JJAS : June to September months

LGM : Last Glacial Maximum

LIA : Little Ice Age

LM : Last Millennium

LNP^{MH} : La Niña type SSTs in the tropical Pacific Ocean during MH

LNPI^{MH} : El Niño type SSTs in the tropical Indo-Pacific Ocean during MH

MADA : Monsoon Asia Drought Atlas

MCA : Medieval Climate Anomaly

MH : Mid-Holocene

MIROC : University of Tokyo, National Institute for Environmental Studies, and Japan

Agency for Marine-Earth Science and Technology Earth System Model

(MIROC-ESM)

MMM : Multi-model Mean

MPI : Max-Planck-Institute Earth System Model (MPI-ESM-P)

MRI : Meteorological Research Institute CGCM Ver 3 (MRI-CGCM3)

MWP : Medieval Warm Period

NCAR : National Center for Atmospheric Research

NCEP : National Centre for Environmental Prediction

NCL : NCAR Command Language

ONI : Oceanic Niño Index

PAGES : Past Global Changes

PDO : Pacific Decadal Oscillation

PDSI : Palmer Drought Severity Index

PMIP2 : Paleo-Model Intercomparison Project 2

PMIP3 : Paleo-Model Intercomparison Project 3

SKT : Skin Temperature

SST : Sea surface temperatures

TEJ : Tropical Easterly Jet

TS-IPCC : Technical Summary - Intergovernmental Panel on Climate Change

TTG : Tropospheric Temperature Gradient

WCRP : World Climate Research Programme

List of Figures

Figure No.	Figure caption	Page
Figure 1.1	The area-average climatological monthly rainfall over the Indian region as a percentage of annual rainfall. The gridded rain gauge-based gridded rainfall data at 1° x 1° resolution from the India Meteorological Department (Rajeevan et al., 2005) for the 1960-1990 were used to generate the figure.	No. 2
Figure 1.2	Seasonal (JJAS) mean SST based on the HadISST (Rayner et al., 2003; Shaded; Units - °C), mean rainfall (Arkin et al., 2003; Contours; Units - mm/day) and 850 hPa winds (m/s) based on NCEP Reanalysis 2 (Kanamitsu et al., 2002) in the Indian Ocean during summer monsoon.	3
Figure 1.3	(a) The mean JJAS monsoon rainfall over India (Units - mm/day). (b) The percentage (%) JJAS monsoon rainfall over India. We have used the high resolution (0.25° x 0.25° resolution) gridded rainfall provided by IMD (Pai et al., 2014) over the period of 1901 to 2009.	5
Figure 1.4	The interannual variations of JJAS rainfall over India using the (Pai et al., 2014) over the period of 1901 to 2018. Overlaid by the ENSO events calculated by using the NINO3.4 Index from the HadISST (Rayner et al., 2003) for the same period.	5
Figure 1.5	A schematic diagram representing (a) the normal conditions and anomalous conditions (b) the El Niño, and (c) the La Niña in the tropical Pacific. This image is obtained from Ashok et al., (2009).	8
Figure 1.6	Simultaneous linear anomaly correlations between the NINO3.4 index and local rainfall over India for the summer monsoon season (June-September; JJAS) for the period of 1901 – 2013. The NINO3.4 Index calculated using the HadISST (Rayner et al., 2003) and rain gauge observations-based 0.25°X0.25° Gridded data Pai et al., (2014) has been used.	10
Figure 2.1	11-year running mean of simulated surface air temperature (°C) obtained by area-averaging (a) globally (b) over India (65°E-95°E; 10°N-30°N); the corresponding temperature anomalies (°C) are shown in panels (c) and (d), respectively.	27
Figure 2.2	(a) 11-year running mean of simulated, and observed, area-averaged ISMR (mm/day) during the 1901–2005, and (b) corresponding anomalies (mm/day).	27
Figure 2.3	Historical area-averaged mean monthly raiinfall (mm/day) during CE 1901-2005 from IMD observations and model simulations.	28
Figure 2.4	Historical JJAS seasonal spatial average of ISMR (Shaded; mm/day), overlaid by surface pressure (Contours; hPa), and wind vectors (m/s) plot of observational and model simulations during CE 1979-2005.	30
Figure 2.5	Correlations from historical data between the NINO3.4 and (a) AAISMR, (b) AAISMT over India of respective model simulations (red line represents the 0.05 significance level from a 2-tailed Student's t-test, yellow and greenrepresent the corresponding correlation values from observations) lines.	31

Figure 3.1	Comparisons of simulated area-averaged climatological cycle for the LM (CE 0850-1849) period by individual PMIP3 models (grey lines), and that of the MMM (black line) over the Indian land region (65°E–95°E; 10°N–30°N) for (a) rainfall and, (b) surface temperature. Seasonal cycle of, latitudinally (over 10°N to 30°N) averaged of MMM (c) rainfall and (d) surface temperature, over the Indian region for the LM.	34
Figure 3.2	Spatial distributions of the simulated summer monsoon (a) rainfall (mm/day) and (b) surface temperature during the LM.	35
Figure 3.3	101-year running mean of simulated surface air temperature (K) obtained by area-averaging (a) globally (b) over India.	37
Figure 3.4	101-year running mean anomalies of near surface air temperature (kelvin) obtained by area-averaging (a) globally, (b) over the Indian Region; The MWP, and LIA period are shown in red and blue boxes, respectively.	38
Figure 3.5	(a) 101-year running mean anomalies of ISMR (mm/day); The MWP & LIA period are shown in red and blue boxes, respectively. (b) Liner trend lines of the area-averaged ISMR during LM, as simulated by the nine PMIP3 models.	39
Figure 3.6	Comparisons of simulated area-averaged climatological cycle for the MWP (CE 1000-1199) and LIA (CE 1550-1749) period for MMM (black line) and PMIP3 models (grey lines) of (a) rainfall during MWP, (b) rainfall during LIA, (c) surface temperature during MWP, and (d) surface temperature during LIA over the Indian land region (65°E–95°E; 10°N–30°N). Spatial distribution of the latitudinal (10°N to 30°N) averaged seasonal cycle of simulated (e) rainfall during MWP, (f) rainfall during LIA, (g) surface temperature during MWP, and (h) surface temperature during LIA of the Indian region for MWP and LIA of the MMM.	42
Figure 3.7	Spatial distributions of the simulated summer monsoon (a) rainfall (mm/day) and (b) surface temperature during the MWP and LIA time periods.	43
Figure 3.8	Spatial distributions of the simulated summer monsoon rainfall (mm/day) during the MWP and LIA compared to the LM-mean. The descriptor string above each panel indicates the name of the model and the periods over which difference is calculated.	44
Figure 3.9	Spatial distributions of the simulated summer monsoon surface temperatures (kelvin) during the MWP and LIA compared to the LM-mean. The descriptor string above each panel indicates the name of the model and the periods over which difference is calculated.	44
Figure 3.10	Simulated correlations, for each model, during MWP (blue bars) and LIA (red bars) between the NINO3.4 index and (a) AAISMR, and (b) AAISMST. Yellow line shows the significant value at 0.05 level from a 2-tailed Student's t-test.	46
Figure 3.11	Figure 3.11: Distributions of simulated differences in the time-averaged JJAS Sea Surface Temperatures (SSTs; °C; contours), Statistically significant temperatures at 90% from two-tailed Student's t-test for the SST areshown in grey shading. Differences in simulated 1000 hPa winds (m/s) are also shown. The descriptor string above each panel indicates the name of the model and the periods over which the difference is calculated. In the top panel, for example shows the MMM	48

Figure 3.12	Scatter plots showing simulated NINO3.4 index (°C) on the X-Axis and simulated area-averaged ISMR (mm/day) on Y-Axis during both MWP and LIA. The last descriptor string in each panel indicates the name of the model and the period.	51
Figure 3.13	Distributions of simulated 850 hPa differences in the time-averaged JJAS velocity potential ' χ 850' (m2 s-1) differences. The descriptor string above each panel indicates the name of the model and the periods over which the difference is calculated. The top left panel, for example shows the excess of mean JJAS χ 850 as compared to that for the LM, as simulated by the GISS model. Statistical significance at 80% confidence level from Student's t-test is showed in contours.	53
Figure 3.14	The composite spatial distribution of 90% statistically significant (a) rainfall anomalies (absolute) (b) surface temperature (absolute). Calculated using two sample Student's t-test.	54
Figure 3.15	The MMM distributions of simulated differences (from the LM mean) in the 850 hPa for JJAS season specific humidity for (a) MWP and (b) for LIA. Statistically significancat specific humidity differences at 95% significance level from two-tailed Student's t-test are marked with hatched region. Panels (c), (d), (e) and (f) show the distributions of JJAS season simulated zonal and meridional for 90% statistically significant moisture transport at 850 hPa from two-tailed Student's t-test in shaded. The descriptor string above each panel indicates the name of the model and the periods over which the difference is calculated.	55
Figure 4.1	Comparisons of simulated area-averaged climatological cycle, for the MH (CE 0850-1849) period (a) rainfall and (b) surface temperature over the Indian land region (65°E–95°E; 10°N–30°N). MMM is shown as (black line) and PMIP3 models in grey lines.	59
Figure 4.2	Spatial distribution of the latitudinal (10°N to 30°N) averaged seasonal cycle of simulated (a) rainfall (mm/day) and (b) surface temperature (K) of the Indian region for MH for the MMM.	60
Figure 4.3	Spatial distributions of the simulated mean summer monsoon (a) rainfall (mm/day) and (b) surface temperature (K) during the MH.	60
Figure 4.4	Spatial distributions of the simulated summer monsoon rainfall (mm/day) during the MH compared to the HS period. The descriptor string above each panel indicates the name of the model and the periods over which difference is calculated.	61
Figure 4.5	Spatial distributions of the simulated summer monsoon surface temperatures (kelvin) during the MH compared to the Hs period. The descriptor string above each panel indicates the name of the model and the periods over which difference is calculated.	62
Figure 4.6	Standard deviations of simulated Indian summer monsoon rainfall (ISMR; blue bars) and Indian summer monsoon surface temperatures (ISMT; red bars) for the MH period.	62

MWP-LM means MMM model simulated SST(°C) difference during MWP from

Figure 4.7	Simulated correlations, for each model, during MH of NINO3 index (light green bars) and NINO3.4 index (light red bars) between the (a) Area averaged ISMR, and (b) Area averaged ISMST. Black line shows the significant value at 0.05 level and Red line show the significant value at 0.10 level from a 2-tailed Student's t-test.	63
Figure 4.8	Simultaneous linear correlation between the JJAS NINO3.4 index with summer monsoon rainfall for MH period. Hatching indicates significant correlation values at 0.05 significance level from a 2-tailed Student's t-test.	65
Figure 4.9	Same as Fig. 4.8 but for simultaneous linear correlation between the JJAS NINO3.4 index with monsoon surface temperatures for MH period.	66
Figure 4.10	Simulated regressions, for each model, during both MH and HS periods between Area averaged ISMR and (a) NINO3 index, (b) NINO3.4 index.	67
Figure 4.11	Spatial distributions of simulated summer monsoon (a) rainfall (mm/day) (b) surface temperature (°C) (c) sea surface temperatures (°C), and (d) sea level pressure (hPa), overlaid by the summer monsoon winds (m/s) at 850 hPa difference in the between MH and HS. Statistical significance at 80% confidence level from Student's t-test is showed in hatched region.	69
Figure 4.12	Distributions of simulated summer monsoon velocity potential ' χ ' (m 2 s -1) and overlaid by summer monsoon winds (m/s) differences between MH and HS periods (a) at 850 hPa and (b) at 100 hPa. Panel (c) show Distributions of simulated differences in the summer monsoon vorticity at 500 hPa. Statistical significance at 90% confidence level from Student's t-test is showed in hatched region.	70
Figure 4.13	Spatial distribution of the simulated 850 hPa differences in the summer monsoon (a) Specific humidity (g/kg) and (b) Moisture Flux Convergence (X 10-5 g/(kg-s)). Statistical significance at 80% confidence level from Student's t-test is showed in hatched region.	71
Figure 5.1	Mean JJAS sea surface temperatures ($^{\circ}$ C) used in the control simulations for MH, MWP, LIA, and HS periods.	77
Figure 5.2	The sea surface temperature (°C) anomalies imposed in these SST sensitivity experiments for the MH period over tropical Indo-Pacific oceans (a) El Niño (b) La Niña.	78
Figure 5.3	Comparisons of PMIP3/CMIP5 CCSM4 simulated area-averaged climatological cycle of rainfall and surface temperature with AGCM simulation rainfall and surface temperatures, with the observational rainfall and surface temperatures respectively. (a) for rainfall; (b) for surface temperature for HS; The are calculated over the Indian land region (66.5°E–101.5°E; 6.5°N–39.5°N). IMD rainfall climatology calculated from CE 1901-2009, SKT climatology calculated from CE 1901-2009, Climate Prediction Center (CPC) Global Land Surface Air Temperature data from CE 1948-2020.	80
Figure 5.4	Comparison between the area-averaged seasonal cycle of Mid-Holocene (MH) and Historical period, (a) is for the simulated rainfall and (b) is for the simulated surface temperature over Indian land region. Spatial distributions of the simulated summer monsoon rainfall (mm/day); (c) and surface temperature (°C); (d) for MH	81

with the difference to HS. The dotted region represents a statistically s	significant
region at a 95% confidence level from a two-tailed Student's t-test.	

Figure 5.5 Comparison between the area-averaged seasonal cycle of Medieval Warm Period (MWP) and Little Ice Age (LIA) period, (a) is for the simulated rainfall, and (b) is for the simulated surface temperature over Indian land region. Spatial distributions 83 of the simulated summer monsoon rainfall (mm/day) (c) and surface temperature (°C); (d) for MWP with the difference to LIA. Hatched region represents a statistically significant region at an 80% confidence level from the two-tailed Student's t-test. Figure 5.6 Comparisons of PMIP3/CMIP5 CCSM4 simulated area-averaged climatological cycle of rainfall and surface temperature with AGCM simulation rainfall and surface temperatures, respectively. (a), (b), (c), and (d) for rainfall; (e), (f), (g), (h) for surface temperature for past climate periods; The are calculated over the Indian 85 land region (66.5°E–101.5°E; 6.5°N–39.5°N). The legend string of each panel indicates the name of the type of the simulation and the period over which the difference is calculated. Figure 5.7 (a) Spatial distribution of the simulated surface temperature (°C) difference in the time-averaged JJAS between MH and HS. (b) Spatial distribution of the simulated 86 sea level pressure (hPa) and overlaid by the monsoon winds (m/s) at 850 hPa difference in the time-averaged JJAS between MH and HS. Figure 5.8 (a) spatial distribution of the simulated 850 hPa differences in the time-averaged JJAS velocity potential ' χ 850 ' (m² s⁻¹; Shaded), and overlaid by the mean monsoon winds (m/s; Vectors) for MH period relative to that for the HS. Panels (b) show spatial distributions of simulated 600 hPa differences in the time-averaged 87 JJAS Moisture Flux Convergence (10⁻⁵ g/(kg-s)). Panel (c) shows spatial distributions of simulated 500 hPa relative vorticity (X 10⁻⁵ S⁻¹) for the MH period relative to that for the HS. Hatched region represents a statistically significant region at a 95% confidence level from the two-tailed Student's t-test. Spatial distribution of simulated pre-monsoon (March, April, and May) surface Figure 5.9 88 temperatures (°C) difference between the MH and HS. (a) spatial distribution of the simulated 850 hPa differences in the time-averaged Figure 5.10 JJAS velocity potential ' χ 850 ' (m² s⁻¹; Shaded), and overlaid by the mean monsoon winds (m/s; Vectors) for MWP period relative to that for the LIA. Panels (b) show spatial distributions of simulated 600 hPa differences in the time-89 averaged JJAS Moisture Flux Convergence (10⁻⁵ g/(kg-s)). Panel (c) shows spatial distributions of simulated 500 hPa relative vorticity (X 10⁻⁵ S⁻¹) for the MWP period relative to that for the LIA. Hatched region represents a statistically significant region at a 95% confidence level from the two-tailed Student's t-test. Figure 5.11 Simulated insolation difference (W/m2) between Mid-Holocene and HS (present-90 day). Averaged over all the longitudes (0°E to 360°E). Simulated insolation difference (W/m2) between (a) MH sensitivity experiment Figure 5.12 with HS orbital parameters to MH control simulation (b) MH sensitivity 92 experiment with 8.2 kyr BP orbital parameters to MH control simulation and (c)

MH sensitivity experiment with LGM orbital parameters to MH control

simulation. Averaged over all the longitudes (0°E to 360°E).

- Figure 5.13 Comparison between the area-averaged seasonal cycle of Mid-Holocene (MH) simulations, (a) is for the simulated rainfall, and (b) is for the simulated surface temperature over the Indian land region. Here, MH(0) is MH Control simulations; MH(1) is MH simulation with HS orbital values; MH(2) is MH simulation with 8.2 kyr BP orbital values; MH(3) is MH simulation with LGM orbital values.
- Figure 5.14 Spatial distribution of the simulated 850 hPa differences in the time-averaged JJAS velocity potential ' χ 850 ' (m² s¹; Shaded), and overlaid by the mean monsoon winds (m/s; Vectors) for MH sensitivity experiments relative to that for the MH control simulation. (a) MH sensitivity experiment with HS orbital parameters to MH control simulation and (c) MH sensitivity experiment with LGM orbital parameters to MH control simulation.
- Figure 5.15 Comparision between the area-averaged seasonal cycle of AGCM sea-surface temperature (SST) sensitivity experiments. From Panel (a) CLIM(MH) MH Control simulations, ELP(MH) MH simulation with El Niño type SSTs in the tropical Pacific Ocean, LNP(MH) MH simulation with La Niña type SSTs in the tropical Indo-Pacific Ocean, LNPI(MH) MH simulation with La Niña type SSTs in the tropical Indo-Pacific Ocean.

List of Tables

Table No.	Table caption	Page No.
Table 2.1	CMIP5 Historical simulations with their temporal span and acronyms of the models used.	21
Table 2.2	PMIP3 Last Millennium simulations with their temporal span and acronyms of the models used.	22
Table 2.3	PMIP3 Mid-Holocene simulations with their temporal span and acronyms of the models used.	23
Table 2.4	Interannual standard deviations of observational and historical simulations of near air-surface temperature (°C), which are area-averaged (June-September) globally (AATASG) and over the Indian region (AAIMST), respectively. Also shown in this table are, the the area-averaged Indian summer monsoon rainfall (mm/day; AAISMR) and NINO3.4 index from observations and and historical simulations.	29
Table 2.5	Number of simulated strong (events whose magnitude is above one standard deviation) ENSO events after CE 1950.	29
Table 3.1	Boreal summer interannual standard deviations of near air area-averaged (June-September) surface temperature (oC) over the globe (AATASG) and that over India (AAIMST), and that of ISM Rainfall (AAISMR, in mm/day) and NINO3.4 Index(oC), as simulated by CMIP5/PMIP3 Last Millennium models (here A: CE 0850-1849; B: CE 0850-1349; C: CE 1100-1599 and D: CE 1350-1849).	36
Table 3.2	Correlations between NINO3.4 and area-averaged Indian Summer Monsoon surface temperatures (AAISMST) during the Last Millennium, as simulated by CMIP5 models (Significant correlation values are shown in bold and are significant at less than 0.05 level from 2-tailed student's t-test).	40
Table 3.3	Correlation between NINO3.4 and area-averaged Indian Summer Monsoon Rainfall (AAIMSR) during Last Millennium, as simulated by CMIP5/PMIP3 models (Significant correlation values are shown in bold (italic) and are significant at less than 0.05 (0.10) level from 2-tailed student's t-test).	41
Table 3.4	Simulated boreal summer (June-September) interannual standard deviation (oC) for area-averaged near air surface temperature over Global region (AATASG) and Indian region (AAIMST), area-averaged Indian summer monsoon rainfall (AAISMR) and NINO3.4 Index during MWP (CE 1000-1199) and LIA (CE 1550-1749) of CMIP5/PMIP3 models.	45
Table 3.5	Frequency table of simulated El Niños and La Niñas during MWP (CE 1000-1199) and LIA (CE 1550-1749).	47
Table 3.6	Categorization of El Niños and La Niñas as as per the normalized strength of the NINO3.4 index. 'σ)ofthesimulatedarea-averaged globalsurface' represents the standard deviation of the NINO3.4 index.	47

Table 3.7	Percentages of 'strong' (a) El Niños with positive (EL+) and negative (EL-) area- averaged ISMR anomalies, and (b) La Niñas with positive (LN +) and negative (LN-) area-averaged ISMR anomalies during both MWP and LIA.	49
Table 4.1	Orbital parameters of the different climatic periods.	58
Table 4.2	Boreal summer interannual standard deviations of NINO3 Index(°C) and NINO3.4 Index (°C), as simulated by CMIP5/PMIP3 MH and HS simulations.	64
Table 5.1	Summary of boundary conditions used in different climate periods	76
Table 5.2	Linear approximation of the orbital parameters. https://wiki.lsce.ipsl.fr/pmip3/doku.php/pmip3:design:lm:final .	76
Table 5.3	Orbital parameters of the different climatic periods.	76
Table 5.4	Brief list of Simulation carried out in this chapter.	79

Abstract

In this thesis, I investigated the Indian summer monsoon and its variability during the Mid-Holocene (\approx 6000 year before present) and Last Millennium (CE 0850-1849) from the modelling perspective using and available past climate simulations as well as by carrying out few simulations atmospheric general circulation.

Using nine model simulations from the Paleo-Model Intercomparison Project 3 (PMIP3), we studied simulated mean Indian summer (June-September) climate and its variability during the Last Millennium (LM; CE0850-1849) with emphasis on the Medieval Warm Period (MWP; CE 1000-1199) and Little Ice Age (LIA; CE 1550-1749), after validation of the simulated 'current day (CE 1850-2005)' climate and trends. We find that the simulated above (below) mean-LM summer temperatures during the MWP (LIA) are associated with relatively higher (lower) moisture, and relatively higher (lower) number of concurrent El Niños (La Niñas). Importantly, the models simulate higher (lower) Indian summer monsoon rainfall (ISMR) during the MWP (LIA) compared to the LM-mean, notwithstanding a strong simulated negative correlation between NINO3.4 index and the area-averaged ISMR. Interestingly, the percentage of the simulated strong El Niños (La Niñas) associated with negative (positive) ISMR anomalies is higher (lower) in the LIA (MWP). This nonlinearity is explained by the simulated background climate changes, as follows. Distribution of simulated anomalous 850 hPa boreal summer velocity potential during MWP in models indicates, relative to the mean LM conditions, a zone of anomalous convergence in the central tropical Pacific flanked by two zones of divergence, i.e. a westward shift in the Walker circulation. The anomalous divergence centre in the west during the MWP also extends into the equatorial eastern Indian Ocean, triggering in an anomalous convergence zone over India and relatively higher moisture transport therein and therefore excess rainfall during the MWP as compared to the LM-mean, and hence a relative weakening in the El Niño impact.

Using twelve model simulations from the Paleo-Model Intercomparison Project 3 (PMIP3), we studied the variability of ISM during MH. Our results based on multi-model analysis broadly suggest that during the Mid-Holocene (MH, ≈6 kyr BP) ISM was stronger than that the present day. The simulated ENSO-ISM correlation values also suggest that their association was weaker during the MH and received more summer rainfall than LM and HS. The ENSO variance is also lower during MH than other time periods. From the simulated velocity potential at 850 hPa, we can conjecture qualitatively, notwithstanding the inter-model spread, a relatively higher convergence (divergence) over the Indian region during MH compared to the Historical time period (CE 1901-1999). This kind of change in the large-scale circulation patterns over Indian region resulted in relatively more ISMR during MH.

Using the CESM1 atmospheric general circulation model, we carried-out multiple ensemble AGCM simulations for the Mid-Holocene (MH; \approx 6 kyr BP), Medieval Warm Period (MWP; \approx 1 kyr BP), Little Ice Age (LIA; \approx 0.35 kyr BP), and Historical (HS; \approx CE 2000) periods. We used the PMIP3/ CMIP5 boundary conditions for this purpose. Our simulations indicate that the ISM during the MH was stronger compared to HS and the rainfall is higher, in agreement with several proxy studies. The experiments also suggest that the MWP received higher ISM rainfall (ISMR) relative to the LIA, in agreement with the results from the PMIP3 models. Relatively northward migration of the ITCZ over the Indian region and strengthening of the neighboring subtropical high over the northwestern Pacific, both associated with stronger insolation associated with the obliquity and precision during the MH, seem to be the main reason for a wetter Indian summer monsoon during the MH.

Chapter 1

Introduction

This chapter introduces the known general information about the Indian summer monsoon (ISM) and the El Niño Southern Oscillation and the teleconnections between them during the current and past periods. I particularly focus on the ISM variability during the mid-Holocene (~6000 yr BP) and the Last Millennium (~1000 yr BP) periods. With this, we set the stage for problems in the context of the research carried out so far, which will be addressed in the following chapters of the thesis. Note that the term 'period' in this thesis has not been used from the geological terminology, but just in the general sense. The same applies to any other similar terminology used to represent the span of time. The chapter is divided as follows.

1.1 The current day Indian summer monsoon

The Indian monsoon system is a complex, large-scale system comprising of distinct seasonal circulation features and precipitation patterns. Monsoon is an Arabic term believed to have been derived from the Arabic/Persian word 'Mausam', alluding to a seasonal reversal of winds. Ramage (1971) defined a few characteristics of monsoon regions, mainly based on the kinematic consideration of the winds. The Indian monsoon system can be divided into two parts depending on the direction from where the surface winds blow or the season in which it occurs, e.g., the southwest monsoon or the summer monsoon occurring during June to September, and the north-east monsoon or the winter monsoon occurring during October to December. However, the importance of monsoon, particularly in the Indian subcontinent, stems from the copious rainfall it brings (Rao, 1976), which is the lifeline for many of the monsoon-dependent economies in the region. The three

criteria of Ramage, which were not discussed here, mainly talk about seasonal reversal, persistence, sufficient strength. A critical component missing from the definition is the rainfall, which is crucial for societal purposes but plays a significant role in monsoonal dynamics and variability (Rao, 1976). Consequently, in this thesis, I focus on the summer monsoon because it contributes to the significant annual total rainfall over India. Any changes in the usual seasonal rainfall or occurrence of extreme events, such as droughts and floods, etc., would disrupt the livelihood of 1.5 billion people, economy, and agriculture of India (e.g., Parthasarathy et al., 1988; Parthasarathy et al., 1992; Gadgil, 1996; Webster et al., 1998; Kumar et al., 2004; Amat and Ashok, 2018, Ashok et al., 2019).

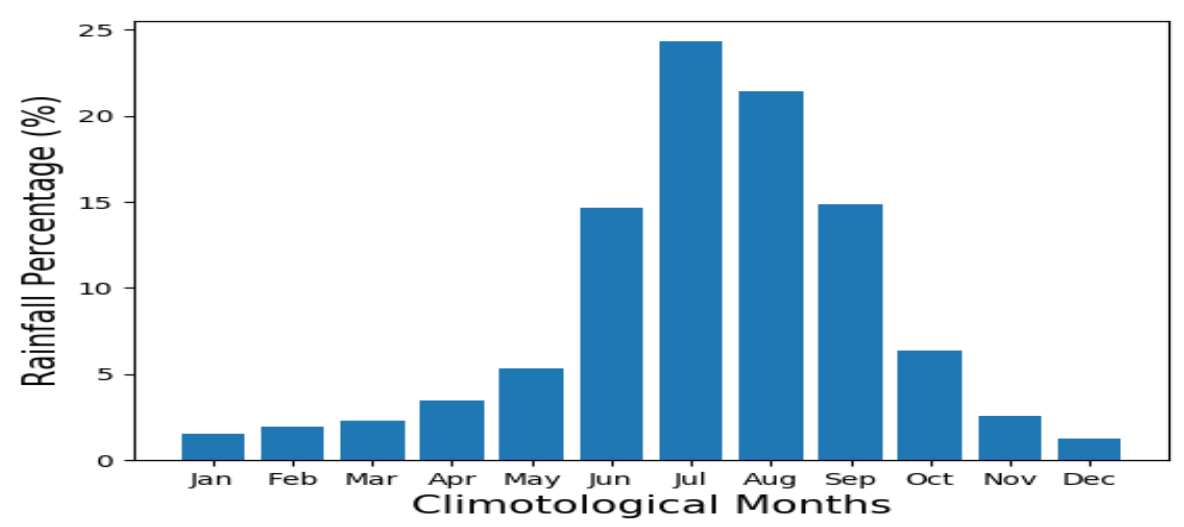


Figure 1.1: The area-average climatological monthly rainfall over the Indian region as a percentage of annual rainfall. The gridded rain gauge-based gridded rainfall data at 1° x 1° resolution from the India Meteorological Department (Rajeevan et al., 2005) for the 1960-1990 were used to generate the figure.

The Indian Summer Monsoon (ISM) has been the focus of considerable attention for a long time. Agriculturists have revered, and seafaring traders and sailors depended on the ISM for centuries. The scientific interest in the ISM probably mat have started with Henry Blandford and Sir Gilbert Walker with their early attempts at ISM observations and prediction (Blandford, 1884,1886;

Walker, 1923, 1924, 1928). The Indian Meteorological Department (IMD) has been studying for over 100 years now and predicting it since last 2-3 decades. The ISM is often defined by June through September rainfall (ISMR) based on the summer monsoon onset and withdrawal (e.g. Rao et al., 1976). The average area-averaged Indian summer monsoon rainfall, occurring over June-September, is estimated to be 890 mm (Pattanaik, Chapter 2, Meteorological Monographs, 2012). Indian region receives roughly 75% of its annual average precipitation from the ISM during these months (**Figure 1.1**).

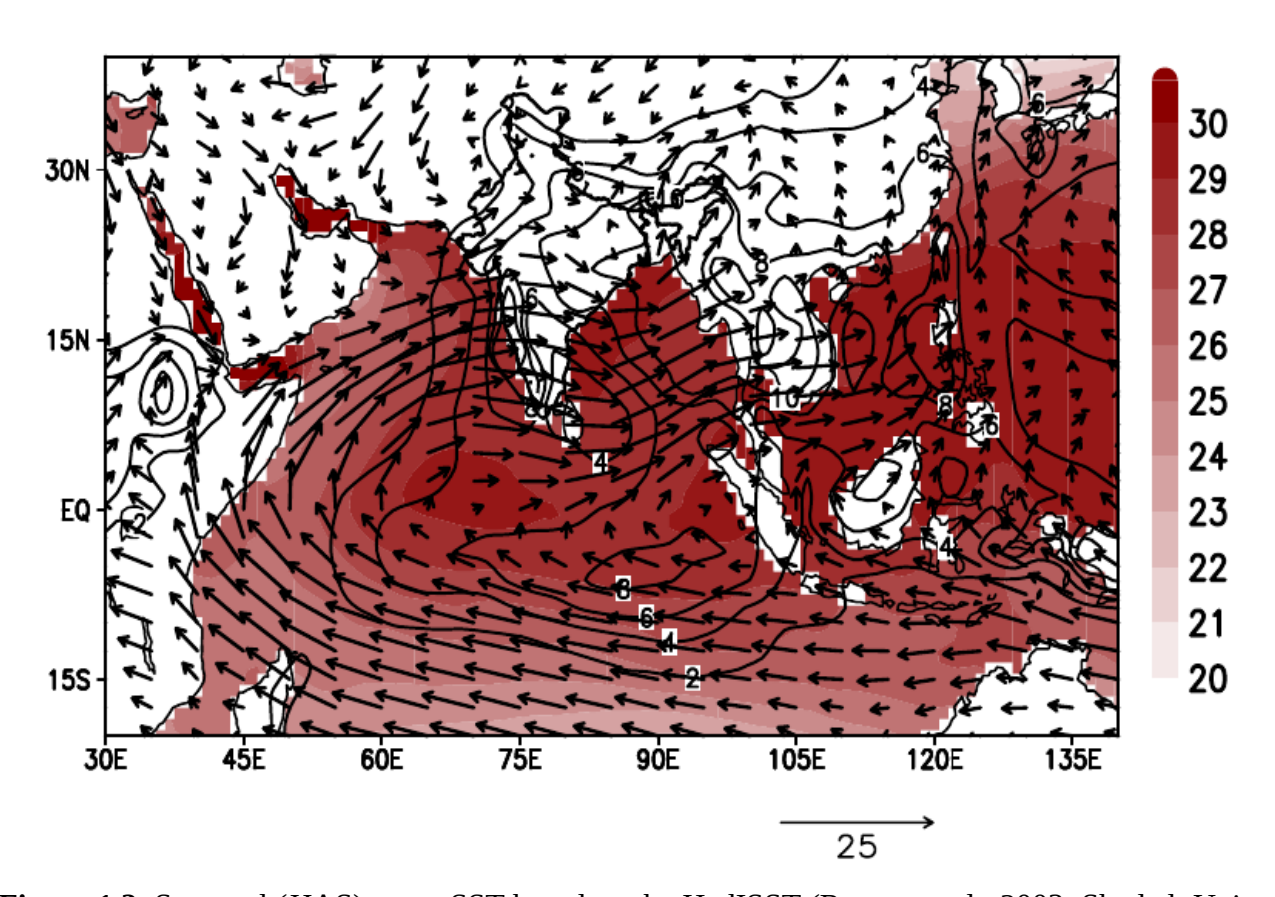


Figure 1.2: Seasonal (JJAS) mean SST based on the HadISST (Rayner et al., 2003; Shaded; Units - °C), mean rainfall (Adler et al., 2003; Contours; Units - mm/day) and 850 hPa winds (m/s) based on NCEP Reanalysis 2 (Kanamitsu et al., 2002) in the Indian Ocean during summer monsoon.

The southwesterly summer monsoon winds flow in two branches (**Figure 1.2**). One branch directly blows over to the Indian subcontinent through the Western Ghats. The other branch enters the Bay of Bengal and goes over to India's central parts, featuring the monsoon trough (e.g., Rao, 1976; Gadgil, 2018). The monsoon trough (region of low pressure) extends in the northwest direction from the head Bay of Bengal to northwestern India. The southwest monsoon's first rains occur over the state of Kerala in India sometime between late May to early June, and when they do, the 'onset' of monsoon is said to have occurred. The onset of ISM is also associated with the northward shift of the Sub Tropical Jet (Yin, 1949). The onset is suggested to be dependent on various other factors, like the warming of the Eurasian region by diabatic heating (Murakami and Ding, 1982) or the dynamical influences of the Tibetan Plateau (Yanai et al., 1992; Yanai et al., 2006). From June to September, ISM remains over India as a stationary wave (Goswami and Shukla, 1984). ISM rainfall shows significant spatial variability (Figure 1.3), with the highest rainfall along the western coast of India, due to the orographic effects and over the head of the Bay of Bengal with a northwest-ward stretch along the monsoon trough. This north-westward stretching region is called the Monsoon Zone (Sikka and Gadgil, 1980). These rains last for one season, with maximum rainfall during July-August (Rao, 1976) and withdraw from the subcontinent towards the end of September. Given the importance of summer monsoon rainfall, it is essential to understand its space-time variations. Several publications and reports have provided a collated and detailed description of the mean monsoonal features and variability. Rao (1976), Pant and Kumar (1997), and the Monsoon Monograph series (Tyagi et al., 2012) provide excellent summaries of all these aspects.

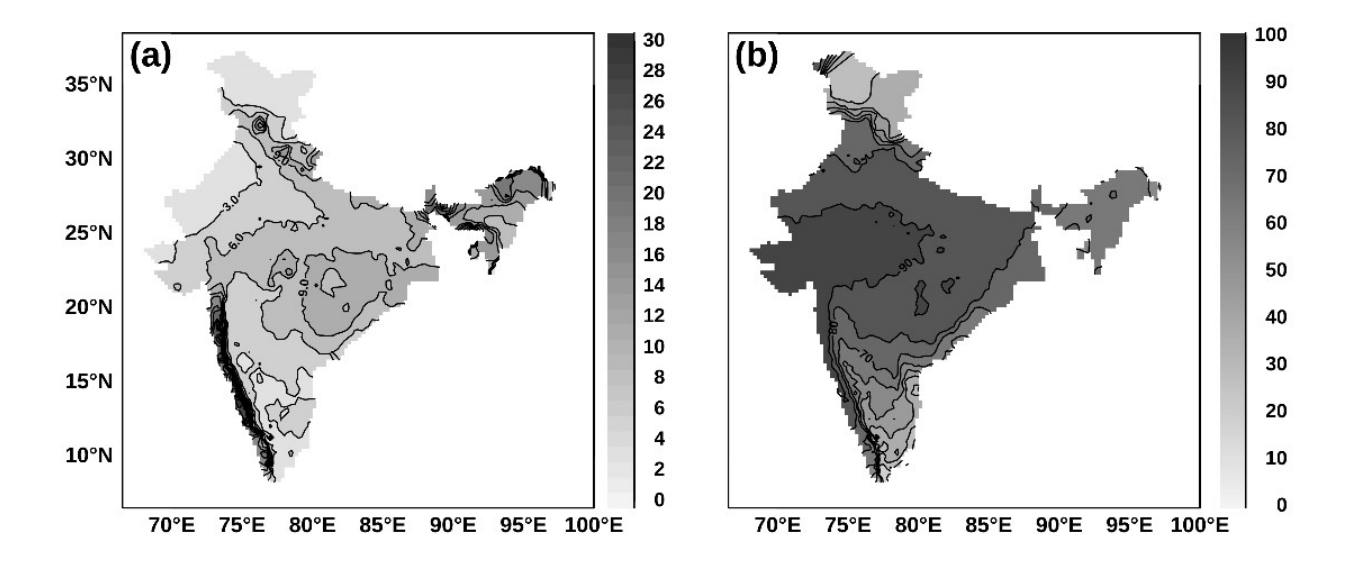


Figure 1.3: (**a**) The mean JJAS monsoon rainfall over India (Units - mm/day). (**b**) The percentage (%) JJAS monsoon rainfall over India. We have used the high resolution (0.25° x 0.25° resolution) gridded rainfall provided by IMD (Pai et al., 2014) over the period of 1901 to 2009.

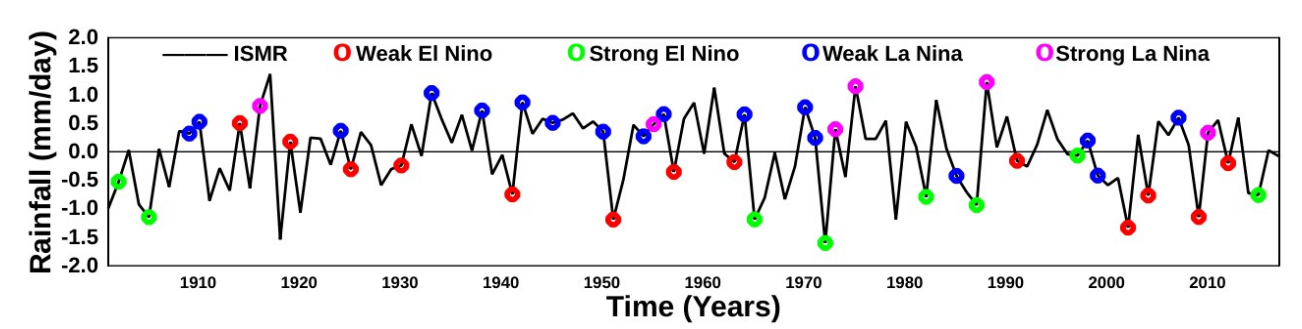


Figure 1.4: The interannual variations of JJAS rainfall over India using the (Pai et al., 2014) over the period of 1901 to 2018. Overlaid by the ENSO events calculated by using the NINO3.4 Index from the HadISST (Rayner et al., 2003) for the same period.

A study by Guhathakurta and Rajeevan (2008) using the India Meteorological Department (IMD) ground-based observational data for the period of 1901-2000 shows that the ISMR is relatively stable and hasn't shown any noticeable overall trend. Still, the extreme events are suggested to have increased (Goswami et al., 2006). However, recent studies demonstrate a weakening of the summer monsoon rainfall in several states with a weakening trend in monsoons (e.g., Guhatakurtha and Rajeevan 2006; Krishnan et al., 2012). Roxy et al. (2015) show a

decreasing trend in ISMR over the central-east northern regions of the Indian subcontinent and south of the Western Ghats region using the IMD and CRU observed rainfall datasets from 1901 to 2012. Further, the maximum surface temperatures for the pre-monsoon months (April and May) over India show a multi-decadal increase during the 1950~2010 period (Ross et al., 2018). There are numerous studies on the interannual variability (IAV) of ISM, which use the modern instrumental data for the Indian region (e.g., Rajeevan et al., 2006; Pai et al., 2014; Kothawale et al., 2017; refer to these studies for further references). The interannual variability of an area-averaged ISM rainfall index is shown in **Figure 1.4**. It has a 10% standard deviation, in agreement with earlier studies such as Gadgil, 2003.

1.2 The El Niño - Southern Oscillation

A periodic fluctuation in the sea surface temperatures (El Niño) and the overlying atmospheric air pressure (Southern Oscillation) between the equatorial eastern and western Pacific Ocean known as the El Niño and the Southern Oscillation (Bjerkenes, 1969), also known as El Niño Southern Oscillation (ENSO). El Niño (La Niña) means "The Little Boy (The Little Girl)," or "Christ Child" in Spanish and is termed because it peaks around December, which coincides with the Christmas. For various reasons, in some years, we find large-scale anomalous warming (cooling) in the tropical eastern Pacific Ocean, associated with anomalous cooling (warming) in the tropical western Pacific, causing widespread global-scale effects. These anomalous conditions are usually seasonally phase-locked from boreal spring through ensuing boreal winter when it peaks, commonly referred to as an El Niño.

The exact initiation of ENSO warm and cold events is not fully understood. The normal conditions in the tropical Pacific are trade winds from either hemisphere converge in the equator's

vicinity and blow from east to west (**Figure 1.5a**). They accompany a shallow thermocline, cool SST and high sea level pressure in the eastern equatorial Pacific, a deep thermocline, warm SST, and low sea level pressure in the western equatorial Pacific. During an El Niño event (**Figure 1.5b**), favourable sea surface temperature (SST) anomaly in the eastern equatorial Pacific reduces the east-west thermal gradient, the easterly trade winds converging across the equatorial Pacific weaken also results in weakening the Walker circulation (Gill, 1980; Lindzen and Nigam, 1987). The weaker trade winds further enhance the warming by giving positive ocean-atmosphere feedbacks. This phenomenon slows the ocean current that draws surface water away from the western coast of South America and reduces the upwelling of cold, nutrient-rich water from the deeper ocean, flattening out the thermocline and allowing warm surface water build in the eastern part of the basin. Conversely, a cold phase (**Figure 1.5c**), with cooler than usual SST anomalies in the equatorial eastern pacific strengthens the trade winds and the Walker circulation - The La Niña (Philander, 1985, 1990).

To a significant extent, ENSO is a self-sustaining because of the positive ocean-atmospheric feedback. The Rossby waves generated in the eastern Pacific propagate to the west and reflect from the western boundary returns as Kelvin wave and reverses the phase of ENSO known as the delayed oscillator theory (Zebiak and Cane, 1987; Suarez and Schopf, 1988; Battisti and Hirst, 1989). The divergence by Sverdrup transport discharges the equatorial heat content, which gets recharged by climatological upwelling. This is known as the recharge-discharge oscillator theory (Jin, 1997a). Another hypothesis is that off-equatorial SST anomalies induce equatorial easterly wind anomalies (off-equatorial anomalous anticyclones), causing upwelling and subsequent cooling. This mechanism is called the western Pacific oscillator mechanism (Weisberg and Wang, 1997; Wang et al., 1999). External land heating and interaction with the previously coupled anomalies play a role (Masumoto and Yamagata, 1991).

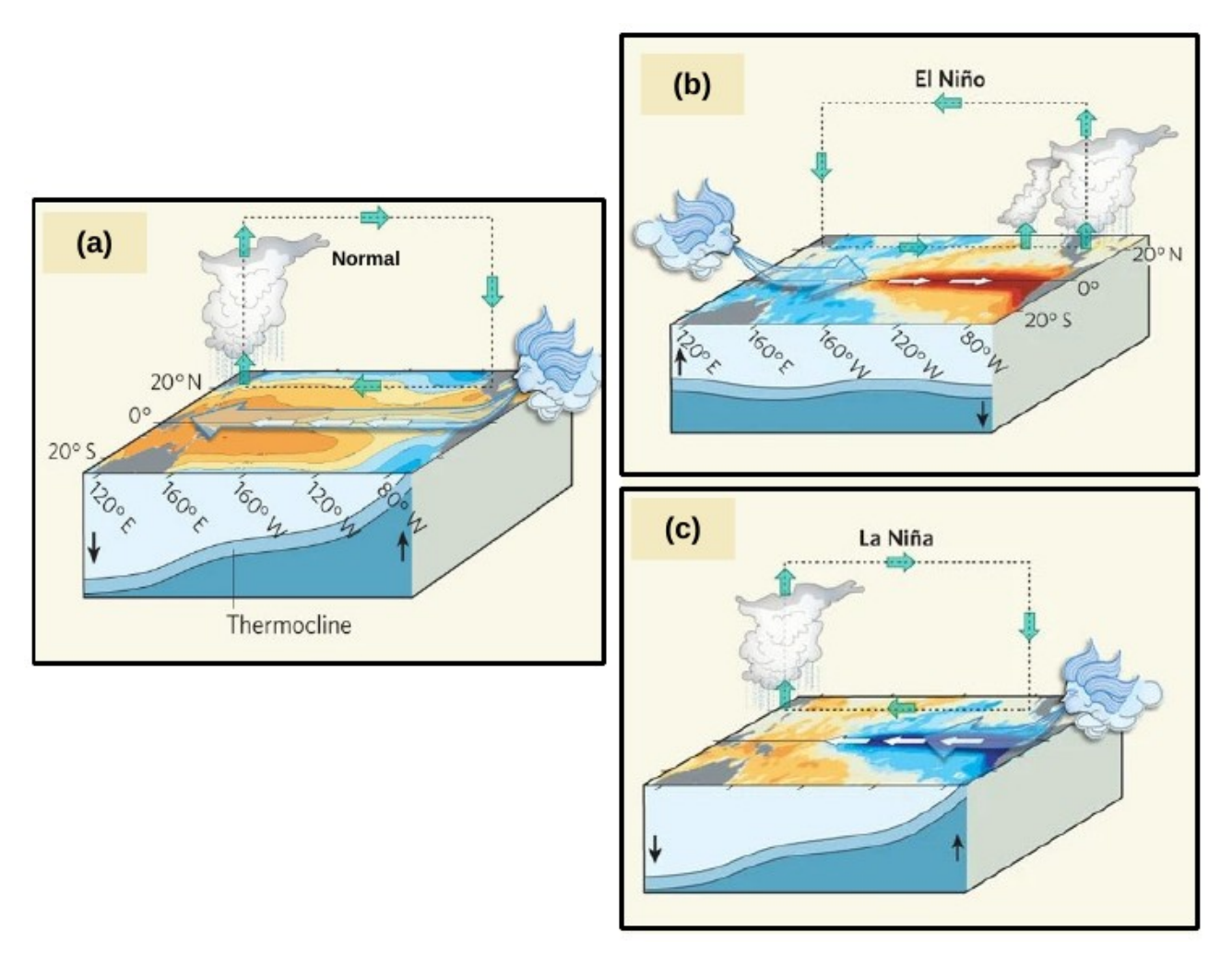


Figure 1.5: A schematic diagram representing (**a**) the normal conditions and anomalous conditions (**b**) the El Niño, and (**c**) the La Niña in the tropical Pacific. This image is obtained from Ashok et al., (2009).

In addition to the well-known canonical El Niño, a new type of El Niño with anomalous warming in the central tropical pacific flanked by the anomalous cooling of SST on both sides, have been occurring with increased frequency since the mid-1970s (Ashok et al., 2007; Kao and Yu, 2009; Kug et al., 2009; Marathe et al., 2015) are named as the El Niño Modoki, and also referred to as Central Pacific El Niño in literature. The Modoki definition is more stringent, and stipulates that the anomalous warming should persist for three consecutive seasons, thereby distinguishing the signal from the transniño signal, which is part of the evolution of a canonical ENSO event

(Stepaniak and Trenberth, 2001). The heat source location has relevance in defining domain and type of its impacts (e.g. Matsuno, 1966; Gill, 1980; Keshavamurty, 1982; Soman and Slingo, 1997).

Several indices are used to monitor the ENSO events; most of them are based on the SST anomalies averaged across a given region. The NINO3 index, NINO3.4 index and its five month running mean referred to as the Oceanic Niño Index (ONI) are the most commonly used indices to define the El Niño and the La Niña events. The NINO3.4 index is calculated using the area-averaged anomalies of equatorial SSTs across the Pacific from about the dateline to the South American coast (5°N-5°S, 170°W-120°W).

1.3 ENSO impacts on the Indian summer monsoon and associated mechanisms

The ENSO is one of ISM's primary drivers, accounting for about 40% of its interannual variability (Sikka, 1980; Keshavamurty, 1982; Shukla and Paolina, 1983; Rasmussen and Carpenter, 1983). The earliest research on interannual variability (IAV) of the Indian summer monsoon (ISM) led to the eventual discovery of two crucial climatic drivers, the El Niño-Southern Oscillation (ENSO; Walker et al., 1918) and Himalayan/Eurasian snow cover (ESC; Blanford et al., 1884. Contributions from various Sea Surface Temperature (SST) anomalies, significantly the tropical pacific, affect the ISM resulting in a prominent interannual variability (**Figure 1.4**).

In **Figure 1.6**, we show the simultaneous linear correlations between the NINO3.4 index and local rainfall anomalies over India for the summer monsoon months of June-September (JJAS), which in general shows that most of the correlations are negative over the Indian sub-continent region, implying that the anomalously warm conditions during boreal summer over the eastern tropical pacific can result in anomalously deficit rainfall over India during summer monsoon

season. Simply put, the ENSO phases of El Niño and La Niña are commonly linked to anomalous weakening and strengthening of the ISM, respectively.

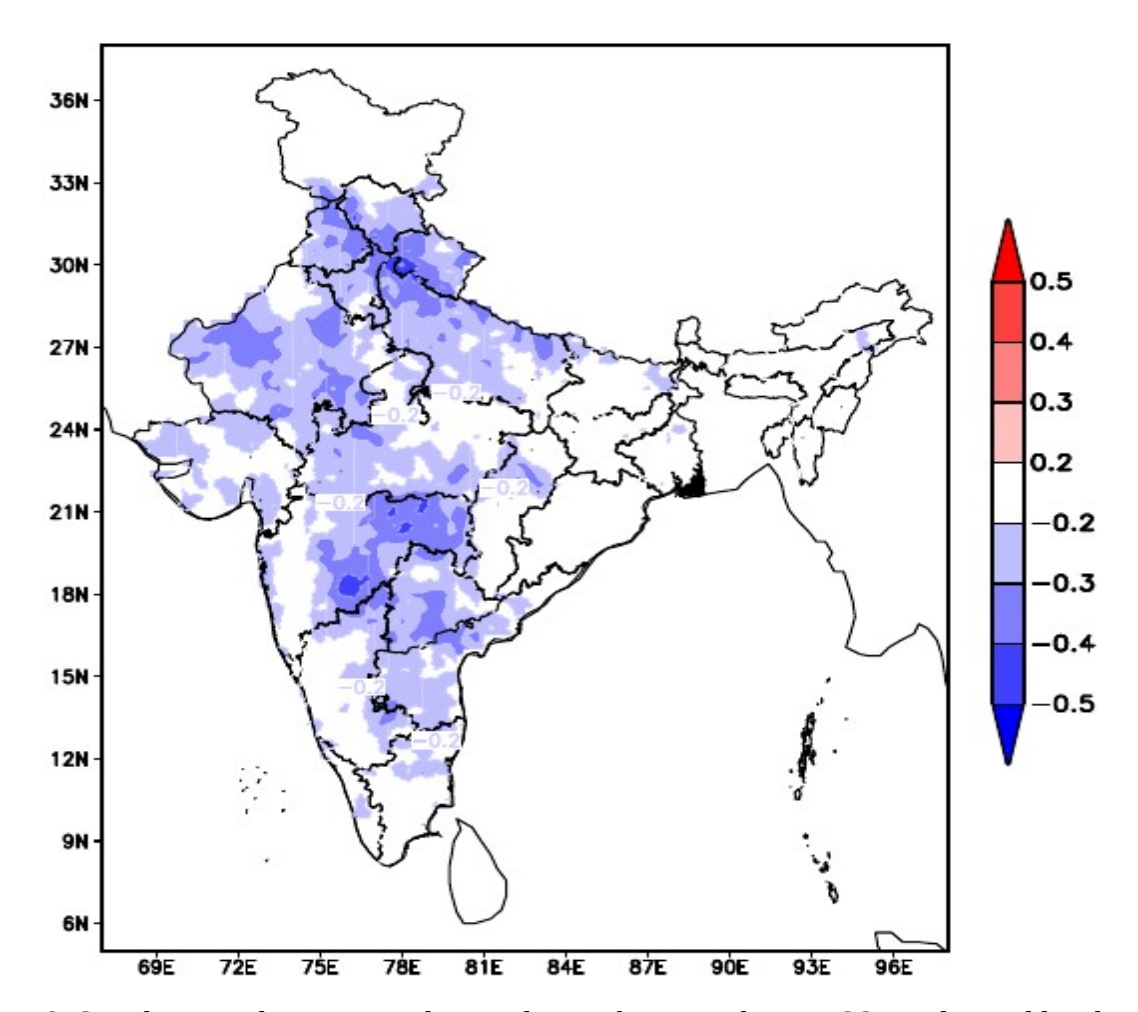


Figure 1.6: Simultaneous linear anomaly correlations between the NINO3.4 index and local rainfall over India for the summer monsoon season (June-September; JJAS) for the period of 1901 – 2013. The NINO3.4 Index calculated using the HadISST (Rayner et al., 2003) and rain gauge observations-based 0.25°X0.25° Gridded data Pai et al., (2014) has been used.

Several mechanisms have been proposed to explain the ENSO impact on the ISM. The tropical pacific SSTs primarily affect the Indian summer monsoon region through the Walker circulation changes. Few studies like Keshavamurty (1982); Palmer et al. (1992); Shukla and Wallace (1983); Navarra et al. (1999); Soman and Slingo (1997); Dai and Wigley, 2000; Ashok et al. (2004), etc. suggest that eastward (westward) shift of Walker Circulation changes the large scale

circulation resulting in the decreased (increased) equatorial divergence over the tropical Indian Ocean during El Niño (La Niña) years. The anomalous convergence in the tropical Indian Ocean results in the cross-equatorial meridional circulation modulation into the Indian region. This causes an anomalous divergence over the Indian region and thereby a drier (wetter) than normal ISM. Ju and Slingo (1995) suggested another mechanism that weak ISM years are associated with increased upper-level westerlies associated with the shift in the mean latitudinal position of the subtropical westerly jet over northern India influenced by Pacific SST anomalies. AGCM studies by Krishnan et al. (1998) indicate that, in addition to the Walker circulation changes by ENSO and Hadley cell modulations, the anomalous ENSO divergent forcing over the tropical Pacific Ocean acts as a potential source for Rossby wave dispersion. Furthermore, Krishnan et al. (2009) suggest that meridionally propagating Rossby waves, which results from the El Niño forcing region, interact with the subtropical westerlies and generate anomalous quasi-stationary highs and lows in the subtropics and extratropics over West Asia, Pakistan, and northwest India during drought years co-occurring with El Niños (Lau and Nath, 2000).

On another note, Kumar et al. (1999) found that the ENSO-ISM teleconnections are weakening since the late 1990s, particularly for 1997, a year of a major El Niño. Kumar et al. (1999) suggested that this weakening was owing to anthropogenic warming. Various other reasons such as the frequent occurrence of Indian Ocean dipole (IOD; Saji et al., 1999; Webster et al., 1999; Murtugudde et al., 2000) events (e.g., Ashok et al., 2001; 2004), decadal variations in monsoon (Kriplani and Kulkarni 1999), varying phases of the Pacific decadal oscillation that affect the interannual teleconnections of ENSO (Krishnamurthy and Goswami, 2000; Krishnam and Sugi, 2003; Krishnamurthy and Krishnamurthy, 2014a; Feba et al., 2018, simply etc.) have also been suggested. Another argument is that this apparent weakening of the ENSO-Monsoon relationship may be due to statistical sampling (Gershunov et al. 2001). Further details can be found in Ashok

and Saji (2007); Ashok et al. (2019). A study by Krishnamurthy and Krishnamurthy (2014) proposes that the PDO modulates the ISM-ENSO relationship by enhancing (counteracting) ENSO effects when in (out of) phase. Sreejith et al. (2015) claim that the reason for the recent monsoon-ENSO weakening is the change in air-sea coupled interactions over the tropical Indian Ocean. A shift in the mean ISM winds, with a cyclone-like intensification over the northwestern Pacific, is seen in recent decades (Mujumdar et al., 2012; Feba et al., 2018). Feba et al. (2018) suggest that this decadal cyclonic intensification opposes the anomalous anticyclonic signature associated with the canonical El Niños (Lau and Nath, 2000) and therefore 'disconnects' the impact of the El Niño through this pathway. Interestingly, Feba et al. (2018) also find a simultaneous strengthening of cross-equatorial winds over the equatorial Indian Ocean in recent decades in association with the weakening of ISM-ENSO links.

In the next sub-section, I espouse on the available information from the literature on monsoon climate and its variability over the Indian region during mid-Holocene, with a focus on the last millennium. The literature survey is mainly based on proxy-based studies and the few available modelling studies

1.4 Indian summer monsoon during the Mid-Holocene and Last Millennium

1.4.1 Proxy-data based studies

1.4.1.1 The Mid-Holocene

The Holocene period (from the last ≈12 kyr BP to the present) has been known for its abrupt changes in the solar forcing (e.g., Steinhilber et al., 2009, and the references therein). The consequent climate variability within the period has even been claimed to have resulted in several disruptions of human civilization (Mayewski et al., 2004). Few available proxy-based records from the Indian subcontinent and Arabian sea suggest centennial to millennial timescale variability in the

ISMR during the Holocene (Sarkar et al., 2000; Fleitmann et al., 2007; Ramesh et al., 2010; Dixit et al., 2014b; Dutt et al., 2015; Nakamura et al., 2015).

A study by Band et al. (2018), which analyses oxygen isotope ratios of stalagmite records from the Kotumsar cave in central India, shows that beginning of the mid-Holocene from 8.5 kyr BP to 6.5 kyr BP declining summer monsoon rainfall in central India associated with the decreasing insolation which is in agreement with previous coarser-resolution ISM reconstructions. They also report that the summer monsoon rainfall gradually increased from 6.5 kyr BP to 5.6 kyr BP. A Study by Jalihal et al. (2019) shows that on orbital timescales, solar insolation plays a significant role in changing the precipitation patterns also suggests that surface energy and vertical stability are also important. Another study by Band et al. (2018) shows the increased frequency of the ENSO events and changing North Atlantic teleconnections played a vital role in MH ISM variability.

Proxy-based past climate studies by Staubwasser et al. (2003), Dixit et al. (2018), and Dutt et al. (2018) suggest during 4.2 kyr BP ISM intensity weakened, and it might have triggered the end of the Indus valley civilization. Studies by Berkelhammer et al. (2012), using a speleothem stable isotope record from northeast India, and Giosan et al. (2012) based on fluvial morphodynamics from the Sindh region in Pakistan suggest weakened ISM activity during the 4 kyr BP. Another proxy-based study by Ali et al. (2018) shows that the ISM was stable at around 3 kyr BP, with few enhanced ISM periods around 2.8 kyr BP, 2.1 kyr BP, and the medieval warm period (≃1 kyr BP). A study by Rawat et al. (2015) reports that the ISM strengthened from 6.7 kyr BP to 3.3 kyr BP, which contradicts Ali et al. (2018). Sinha et al. (2018) show that the abrupt changes in the ISM during 2.8 kyr BP coincides with the North Atlantic cold event linked with the low solar activity during that period. Sandeep et al. (2017), in a proxy-based study, claim that the ISM was steady from 3 kyr BP to the present. A multiple proxy reconstructions study by Gill et al. (2016) shows

enhanced La Niña conditions during 10 kyr BP with the concurrent higher ISMR. Gill et al. also claim that, till 2 kyr BP, eastern equatorial Pacific was gradually warming up. Interestingly, other proxy-based studies by several other researchers indicate a 'suppressed' ENSO activity during MH (e.g., Moy et al., 2002; Abram et al., 2007; Lu et al., 2018), which is also suggested by the PMIP2 model simulations (An et al., 2013). This suppressed ENSO activity is attributed to basin-wide cooling activity and the weakened air-sea interactions with reduced precipitation (An et al., 2013). On the other hand, model experiments by Phipps et al. (2010) suggest that the El Niño activity during 8 kyr BP is due to changes in the Asian monsoon, which in turn is controlled by solar insolation changes.

1.4.1.2 The Last Millennium

Many publications pointed out that significant centennial climate variations have been observed during the last two millennia (PAGES 2k Consortium, 2013; TS-IPCC13). Studies based on proxy-data identify two significant climatic periods in the last millennium (LM), i.e., Common Era (CE) 0850–1849. These two periods widely known as (1) the Medieval Warm Period (MWP; CE 950–1350; a relatively warmer period), roughly followed by (2) the Little Ice Age (LIA; CE 1500–1850; a relatively cooler period), (e.g., Lamb 1965; Grove 1988; Graham et al. 2010; Mann et al. 2009). The MWP is also known as the Medieval Climate Anomaly (MCA). There is a lot of heterogeneity between the warmer MWP and cooler LIA) events in terms of region, timing, duration, and magnitude (e.g. Stocker et al., 2013; Dixit and Tandon 2016). Reconstructions from various proxy-based data suggest that the temperatures during the MWP in some regions are as warm as the mid-twentieth century (Stocker et al., 2013). In contrast, some other regions, such as the extratropics, southern hemisphere land regions, were as warm as the late-twentieth-century (Stocker et al., 2013). As can be seen, these studies do not report the conditions at a regional scale.

For example, there aren't modeling-based studies that have reported on the temperature conditions over the Indian region, and the proxy-based studies for India are also rather few), and detailed below.

A recent review study by Dixit and Tandon, (2016) suggests that the climatic optimums like MWP and LIA effects are well reflected in the Indian summer monsoon rainfall (ISMR). It also suggests that they exhibit heterogeneity in terms of timing, duration, and magnitude. Proxy records suggest that during the LM, the ISMR was higher during the MWP and relatively weaker during the LIA (Yadava et al. 2005). Few proxy-data studies show that increased ISMR during the MWP is suggested to be associated with the ENSO, which has been modulated by solar forcing variations (Berkelhammer et al. 2010; Emile-Geay et al. 2007). Interestingly, few other paleoclimate reconstruction studies by Overpeck et al. (1996), Sinha et al. (2007) suggest that ISM was stronger. Studies by Sanwal et al. (2013), Polanski et al. (2014) suggest wetter ISM during MWP. A study by Rehfeld et al. (2013) suggested that warm and wet ISM during the MWP is because of an earlier onset of the summer monsoon felicitated by the earlier retreat of the Tibetan High. A speleothembased past climate reconstruction by Sinha et al. (2007, 2011) suggests a severe weakening of ISM during the LIA. It is associated with multi-year to decades-long droughts, particularly between the thirteenth and seventeenth centuries. A study using the Monsoon Asia Drought Atlas (MADA) by Cook et al. (2010) report that most parts of India, particularly the western part of the Indian subcontinent, experienced wide-spread and persistent mega-droughts during LM, but the longevity and the periods of these droughts varied across region to region. Interestingly, the four major Asian mega-droughts of the LM coincides with the LIA period also suggest that they were associated with El Niño events. Apart from these studies by Sanwal et al. (2013) and Ali et al. (2018), ISM was stronger and wetter during LIA.

A study using both the MADA and reconstructed PDSI by Ummenhofer et al. (2013) suggests that droughts in South Asia are mostly coincident with phases of Indo-Pacific drivers with a significantly enhanced South Asian monsoon. Another study using coral oxygen isotopic record from the equatorial Pacific ocean by Chakraborty et al. (2012) shows that tropospheric temperature (TT) gradient related to ENSO (e.g., Goswami et al., 2006) played a vital role in driving the ISM climate variability of during the LM. Apart from these, on longer time scales, thermodynamic effect and changes in land conditions, and shorter time scale, local and remote SST patterns and external boundary conditions can be important for monsoonal variations (Sinha et al. 2015).

1.4.2 Modelling based studies

There are very few past climate studies available from a modeling perspective for the Indian region. A study by Liu et al. (2003) using the coupled model simulations show that enhancement of the South Asian monsoon during the early Holocene is attributed to the insolation changes in agreement with the studies by Braconnot et al. (2007a and 2007b), Zheng et al. (2008), Bosmans et al. (2012) and Marzin et al. (2013). A study by Zhao et al. (2005) using the multiple model simulations shows that changes in the insolation during the MH affected the ISM retreat through the dipole patterns in the late summer SST patterns of the northwest Indian Ocean. Another study by Polanski et al. (2012) using both proxy-based and regional atmospheric model show that monsoon intensity during MH is strongly influenced. A study by Kumar et al. (2018) using a single PMIP3 simulation of CSIRO and proxy-based datasets shows that the area-averaged mean annual precipitation cycle of the Indian subcontinent did not change much in MH, MWP, and Historical periods.

A 1000-year control simulation using a single coupled model (MRI-CGCM2.2) carried out by Kitoh et al. (2007) shows a robust ENSO-ISM relationship during LM. Another modeling study by Fallah and Cubasch (2015) using CMIP5/PMIP3 simulations show that Asian megadroughts during the last millennium are mostly linked with the El Niño-events. Studies by Polanski et al. (2013, 2014) using both model and proxy-based datasets show MWP and LIA climate events had the same driving mechanisms. Polanski et al. (2014) also show the more rainfall has been observed over the Arabian Sea and India during MWP and observed less rainfall over these regions during LIA. Interestingly, the greenhouse gas concentrations are not very much different in the early-Holocene, and LM except for the last 175-years (Phipps et al., 2010). Notably, there has not been any multi-model comparative studies bringing out the similarities and differences.

1.5 Objectives and Scope of the study

The variability of ISM during the LM and MH has been a relatively less studied field, particularly from the modeling perspective. Whatever the little work been carried out in this field is by employing the single GCMs (Kitoh et al. 2007; Prasad et al. 2014). From this perspective, it is interesting to look at the Indian summer monsoon variability using the available multiple model simulations during the LM and MH periods. The available multiple PMIP3 model simulations (detailed information in Chapter 2) provide a measure of inter-model spread to study Indian summer monsoon conditions during the LM and MH. Such a study would explore the capability of these coupled models in capturing the past climate variability on the regional scale, specifically during LM and MH. For example, suppose that the models are in qualitative agreement with any climate statistic. In that case, the model agreement confirms the veracity of the indication from the proxybased studies, its validity, or plausibility of the occurrence of an associated climatic phenomenon in the real world, as the case may be. Therefore, carrying out an analysis using multi-model

simulations will provide a detailed view of the relevant climate period complementing the available knowledge from proxy-data studies. Furthermore, such a study using the multi-model simulations would serve as a benchmark for addressing climate variability of more extended periods relevant to the ISM. Keeping all these in mind, it will be interesting to understand the ISM variability during LM and MH using various coupled model simulations. In addition, carrying out targeted sensitivity experiments to isolate the causal mechanism will also contribute to the knowledge and information.

In this regard, I have designed the following objectives to understand the ISM variability during the MH and LM.

- 1. Understanding the seasonal cycles of surface temperature and rainfall over India during the Mid-Holocene and Last Millennium using the available coupled model simulations.
- 2. Understanding the ENSO and Indian summer monsoon relations during the Mid-Holocene and Last Millennium.
- 3. Simulating the Indian summer monsoon climate during the Mid-Holocene and Last Millennium using an AGCM.
- 4. Identifying the role of external forcings (Orbital forcing) on Indian summer monsoon during the Mid-Holocene.

1.6 Summary

In this chapter, I have presented up to dated summary of the research on the ENSO-Indian summer monsoon rainfall mainly during the MH and LM, and some other useful background information. The critical gaps have been identified, based on which a list of objectives to be achieved in the thesis have been set. In Chapter 2, I provide a description of different datasets and

analysis techniques used in the thesis. The Chapter 3, Chapter 4, and Chapter 5 address Objectives 1 to 4, respectively. In the last chapter, I present a summary of the results in light of the objectives, and briefly discuss the future scope.

Chapter 2

Datasets and methodology

In this chapter, the datasets and statistical techniques that are common to several subsequent chapters are described. Any specific datasets and analysis techniques used in a certain chapter will be discussed in the respective chapter.

2.1 Datasets

I have mainly used the CMIP5 Historical simulations and PMIP3 Mid-Holocene and Last Millennium simulations in this thesis. The PMIP3 MH, LM and CMIP5 HS datasets have been downloaded from https://cera-www.dkrz.de/WDCC/ui/cerasearch/. In addition, the IMD gridded rainfall datasets and NCEP reanalysis datasets have been used to validate the historical simulations for (CE 1901-2005) the period. The models that are able to simulate the observed mean climate as well as other statistics are also deemed to have similar fidelity in simulating the past climate.

2.1.1 CMIP5 Historical simulations

It is indeed a challenging prospect to validate the simulated Indian summer monsoon features from the PMIP3 simulations for the Last Millennium (LM) and Mid-Holocene (MH) periods, given the sparse and scanty observations. Fortunately, the corresponding model simulations of the CMIP5 vintage for the historical period (CE 1850-2005), i.e. the current day climate, can be validated using various observed/reanalysed gridded datasets, keeping in mind the uncertainties associated with such datasets during the pre-satellite period.

Therefore, in this study, we start by exploring the fidelity of simulated Indian summer monsoon climate from historical simulations (HS), which that the CE 1850-2005 period during which instrumental observations are available. Specifically, for the LM, the criteria we adopt for validation of the historical model simulations are, the ability of the models to reproduce the observed trends in surface temperature and rainfall over India during the summer monsoon season, and to simulate the observed negative correlation between the ISMR and the concurrent NINO3.4 Index.

Table 2.1 CMIP5 Historical simulations with their temporal span and acronyms of the models used.

S No	CMIP5 Models	Atmosphere's	Temporal coverage	Acronyms
		horizontal		
		resolution		
1	BCC-CSM1-1	128x64	CE 1850-2005	BCC
2	CCSM4	288x192	CE 1850-2005	CCSM4
3	IPSL-CM5A-LR	96x96	CE 1850-2005	IPSL
4	MPI-ESM-P	192x96	CE 1850-2005	MPI
5	GISS-E2-R	144x90	CE 1850-2005	GISS
6	FGOALS-s2	128x108	CE 1850-2005	FS2
7	HadCM3	96x72	CE 1860-2005	HADCM3
8	CSIRO-Mk3L-1-2	64x56	CE 1850-2005	CSIRO1
9	HadGEM2-CC	192x145	CE 1860-2005	HCC
10	HadGEM2-ES	192x145	CE 1860-2005	HES
11	MRI-CGCM3	320x160	CE 1850-2005	MRI
12	MIROC-ESM	128x64	CE 1850-2005	MIROC
13	CNRM-CM5	256x128	CE 1850-2005	CNRM
14	CSIRO-Mk3-6-0	192x96	CE 1850-2005	CSIRO2

As outlined by Taylor et al. (2012), for the HS, the models were forced with observed atmospheric composition changes with natural and anthropogenic aerosols or their precursors, natural sources of short-lived species, and time-evolving land cover. The brief details and the acronyms of the HS model simulations, are presented in **Table 2.1**. We evaluate the fidelity of the monsoon simulations of the HS by comparing various simulated monsoon statistics with those of the corresponding observations-based gridded Indian summer monsoon rainfall datasets as well as

various other reanalysed climate datasets. Details of the various observational/reanalysed data sets used for the validation of the HS are present in **Section 2.1.4**.

2.1.2 PMIP3 Last Millennium simulations

It may be noted that this exercise is primarily carried out for nine available CMIP5 models for which the PMIP3 simulation outputs for the LM period are available. The LM simulations are available for the CE 0850–1849 period (LM), under the class termed as 'past1000' (henceforth referred to as p1000). The LM simulation results were obtained by forcing the models with well-mixed greenhouse gases, changes in volcanic aerosols, land use, and solar irradiance changes (Taylor et al. 2012; Schmidt et al. 2011; Schmidt et al. 2012).

The nine model simulation outputs used for the LM period, they are: BCC-CSM1-1, CCSM4, CSIRO-Mk3L-1-2, FGOALS-s2, GISS-E2-R, HadCM3, IPSL-CM5A-LR, MPI-ESM-P, and MRI-CGCM3. The brief details such as the resolutions and the acronyms of the LM model simulations, are presented in **Table 2.2**.

Table 2.2 PMIP3 Last Millennium simulations with their temporal span and acronyms of the models used.

S No	CMIP5 Models	Atmosphere's	Temporal coverage	Acronyms
		horizontal		
		resolution		
1	BCC-CSM1-1	128x64	CE 0850-1850	BCC
2	CCSM4	288x192	CE 0850-1850	CCSM4
3	IPSL-CM5A-LR	96x96	CE 0850-1850	IPSL
4	MPI-ESM-P	192x96	CE 0850-1849	MPI
5	GISS-E2-R	144x90	CE 0850-1850	GISS
6	FGOALS-s2	128x108	CE 0850-1850	FS2
7	HadCM3	96x72	CE 0850-1850	HADCM3
8	CSIRO-Mk3L-1-2	64x56	CE 0850-1850	CSIRO
9	MRI-CGCM3	320x160	CE 0850-1850	MRI

2.1.3 PMIP3 Mid-Holocene simulations

For the MH analysis, we primarily used the available twelve PMIP3 MH simulation outputs for which the CMIP5 HS simulations are available. These simulations were generated with orbital parameters and atmospheric concentrations of well-mixed greenhouse gases for the period (Taylor et al. 2012; Schmidt et al. 2011; Schmidt et al. 2012).

Table 2.3 PMIP3 Mid-Holocene simulations with their temporal span and acronyms of the models used.

S. No.	Model	midHolocene (length in years)	Atmosphere's horizontal resolution	Acronyms
1	BCC-CSM1-1	100	128x64	BCC
2	CCSM4	301	288x192	CCSM4
3	CNRM-CM5	200	256x128	CNRM
4	CSIRO-Mk3-6-0	100	192x96	CSIRO
5	FGOALS-s2	100	128x108	FS2
6	GISS-E2-R	100	144x90	GISS
7	HadGEM2-CC	35	192x145	HCC
8	HadGEM2-ES	102	192x145	HES
9	IPSL-CM5A-LR	500	96x96	IPSL
10	MIROC-ESM	100	128x64	MIROC
11	MPI-ESM-P	100	192x96	MPI
12	MRI-CGCM3	100	320x160	MRI

The twelve model simulation outputs used for the MH period, are: BCC-CSM1-1, CCSM4, CNRM-CM5, CSIRO-Mk3-6-0, FGOALS-s2, GISS-E2-R, HadGEM2-CC, HadGEM2-ES, IPSL-CM5A-LR, MIROC-ESM, MPI-ESM-P, and MRI-CGCM3. The brief details and the acronyms of the MH model simulations, are presented in **Table 2.3**.

2.1.4 Observational and Reanalysis datasets

We have used various observational and reanalysis climate datasets for the validation of the HS. The datasets are, the Hadley Centre Interpolated sea surface temperature (HadISST; Titchner and Rayner, 2014) for the CE 1870–2014 period, the ERA-20CM sea surface temperature (SST) and skin temperature (SKT) datasets (Hersbach et al. 2015) for the CE 1900 to 2010 period. Using two SST datasets throws light on any uncertainties associated with the data quality therein. We also use the Climate Prediction Center (CPC) Global Land Surface Air Temperature data (Fan and van den Dool, 2004) datasets. The India Meteorological Department (IMD) gridded rainfall datasets for CE 1901–2009 period (Rajeevan et al. 2006), available at 1.0° latitude × 1.0° longitude resolution and covering the land region bound by 66.5°E–101.5°E; 6.5°N–39.5°N. The Global Precipitation Climatology Project Version 2 (GPCP; Adler et al. 2003) and CPC Merged Analysis of Precipitation (CMAP; Xie et al. 1997) have also been used. The multi-level NCEP/NCAR Reanalysis version 1 datasets of horizontal winds available for the 1948–2009 period (Kalnay et al. 1996) have been analysed for the validation of the model-simulation circulations.

2.2 Methodology

For uniformity, all the simulated precipitation and near air surface temperature data sets were re-gridded to 2.0° latitude × 2.0° longitude resolution grids. As mentioned above, the historical simulations from the individual models are validated by comparing various climate statistics with the corresponding climate statistics from observed and reanalysed datasets for the CE 1901–2005 period. As is the practice, the various reanalysis datasets are deemed to represent the 'observations', particularly the large scale circulation and pressure.

To represent the ENSO variability, we compute the well-known NINO3 index, which is defined as the area-averaged SST anomaly over the region bounded by 150°W-90°W; 5°S-5°N and also NINO3.4 index, which is defined as the area-averaged SST anomaly over the region bounded by 170°W-120°W; 5°S-5°N. A representative Indian summer monsoon rainfall (ISMR) index, which we designate as the AAISMR, is obtained by area-averaging the mean June-through-September (JJAS) rainfall over the land region bounded by 65°E–95°E; 10°N–30°N. The area-averaged temperature for the Indian region is also obtained by averaging the surface temperature over this region (AAISMT).

To check the ENSO-ISM relationship and its variability during LM and MH, we calculate the monthly anomalies of surface temperature and precipitation from their respective climatological monthly means. The seasonal anomalies are averages of the constituent monthly anomalies. The seasonal anomalies of any parameter, such as, say, the JJAS temperature, for each model have been obtained by subtracting the climatological values of respective simulation of the individual seasonal values. Linear correlation analysis and standard deviation methods are used to compare the ENSO-ISMR relationship across various periods.

We also carry out trend analysis, the significance of which has been evaluated through the Mann-Kendall test. The statistical significance of linear correlation, and that of the partial correlation, has been evaluated using a 2-tailed Student's t-test. Further, while ascertaining the statistical significance of correlation differences from the MWP to LIA, we employ a bootstrapping test with 1000 simulations. For this, we use the bootstrapping subroutine "bootstrap_correl", a freely available NCL package from NCAR. This routine takes the two input time series (the model-simulated ISMR & NINO3.4 SSTA for MWP, for example, in our case) for which the correlations need to be obtained. Based on these input series, it generates 1000 timeseries pairs randomly, and

computes correlations between each pair. After that, the correlations are ordered as per magnitude. The fifth highest correlation, for example, gives us the 0.005 significance level (i.e. 99.5% confidence level) for the correlations, and so on. In case of correlation differences between two simulations, such as the MWP & LIA simulations by the same model, the differences of correlations are ordered as per magnitude to mark the significant threshold values.

We have analyzed the simulated fields of velocity potential (which represent divergence), vorticity and moisture flux convergence. The moisture flux convergence has been computed as the sum of moisture convergence and moisture advection (Banacos and Schultz, 2005). The fields of velocity potential, vorticity, and moisture convergence have been computed from the simulated outputs of horizontal winds and moisture through the application of spherical harmonics using various NCL routines. The details can be found at https://www.ncl.ucar.edu/Applications/wind.shtml.

2.3 Validation of the CMIP5 Historical simulations

Figure 2.1a, shows the 11-year running mean of near-surface air temperatures averaged over the globe, from the nine models of the HS, and Figure 2.1b over Indian region. Figure 2.1c and 2.1d show the corresponding time series of anomalies. It is seen from Figure 2.1c and 2.1d that all the models simulate the observed increasing temperature trend for the CE 1901-2005 period reasonably, notwithstanding an inter-model spread. Further, we find that the observed as well as simulated trends are significantly above the respective interannual standard deviations (Figure 2.1). Figure 2.1d suggests that the surface temperatures over India have also continued to rise till the end of the twentieth century, which agrees with a study based on station observations (Revadekar et al. 2012). Several recent studies suggest a decreasing trend in Indian summer monsoon rainfall (e.g. Goswami et al., 2006; Guhathakurtha et al. 2007; Krishnan et al. 2016; Sano et al. 2011) in recent

decades. **Figure 2.2a** shows the observed and simulated AAISMR. The corresponding AAISMR anomalies are presented in **Figure 2.2b**. We find a relatively higher inter-model spread in the AAISMR when compared to the corresponding surface temperatures (**Figure 2.1b, 2.1d**).

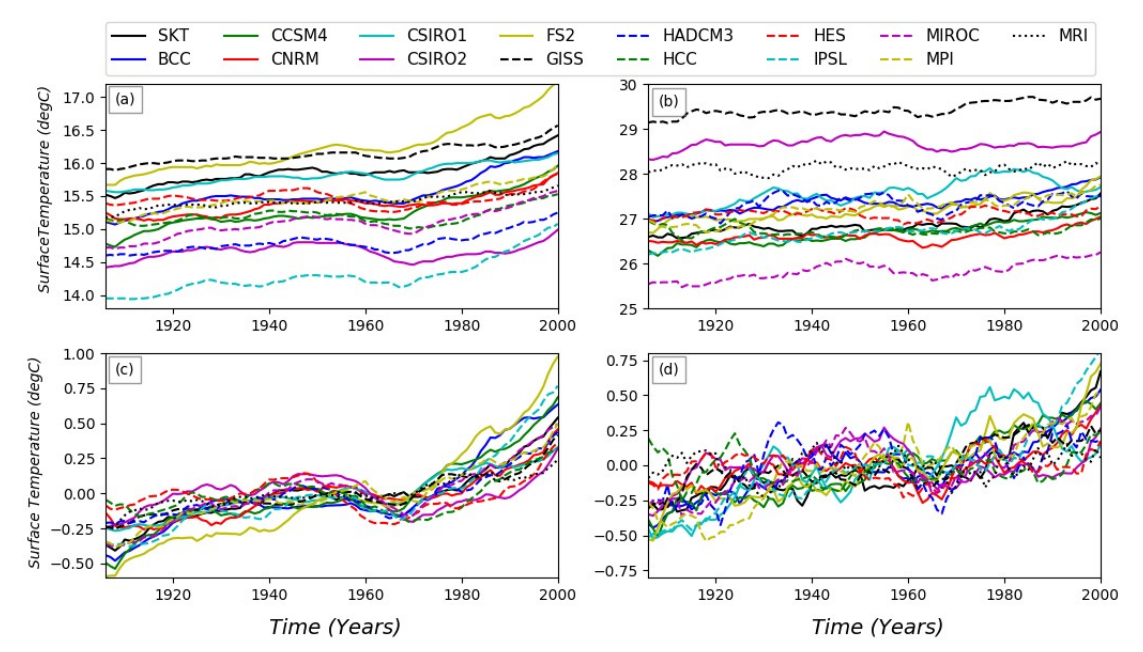


Figure 2.1: 11-year running mean of simulated surface air temperature (°C) obtained by area-averaging (**a**) globally (**b**) over India (65°E-95°E; 10°N-30°N); the corresponding temperature anomalies (°C) are shown in panels (**c**) and (**d**), respectively.

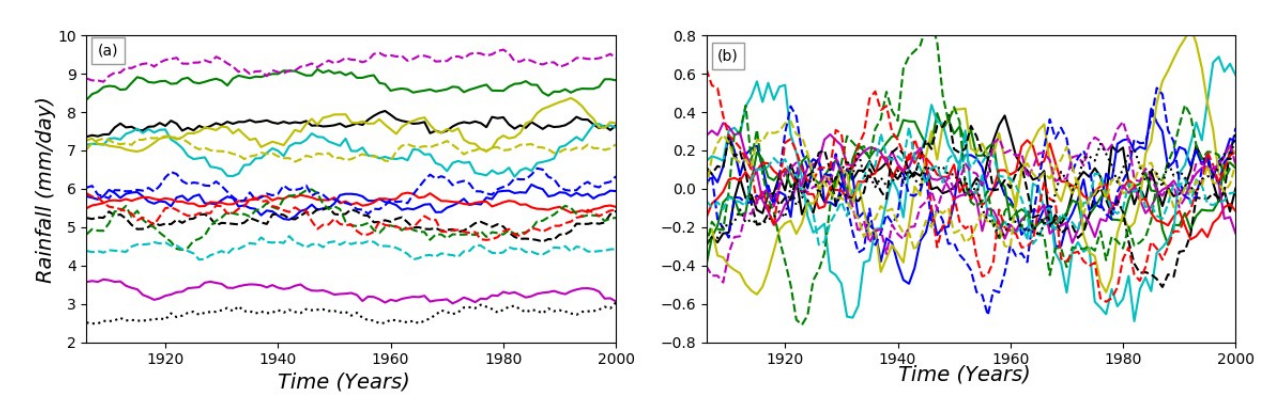


Figure 2.2: (**a**) 11-year running mean of simulated, and observed, area-averaged ISMR (mm/day) during the 1901–2005, and (**b**) corresponding anomalies (mm/day).

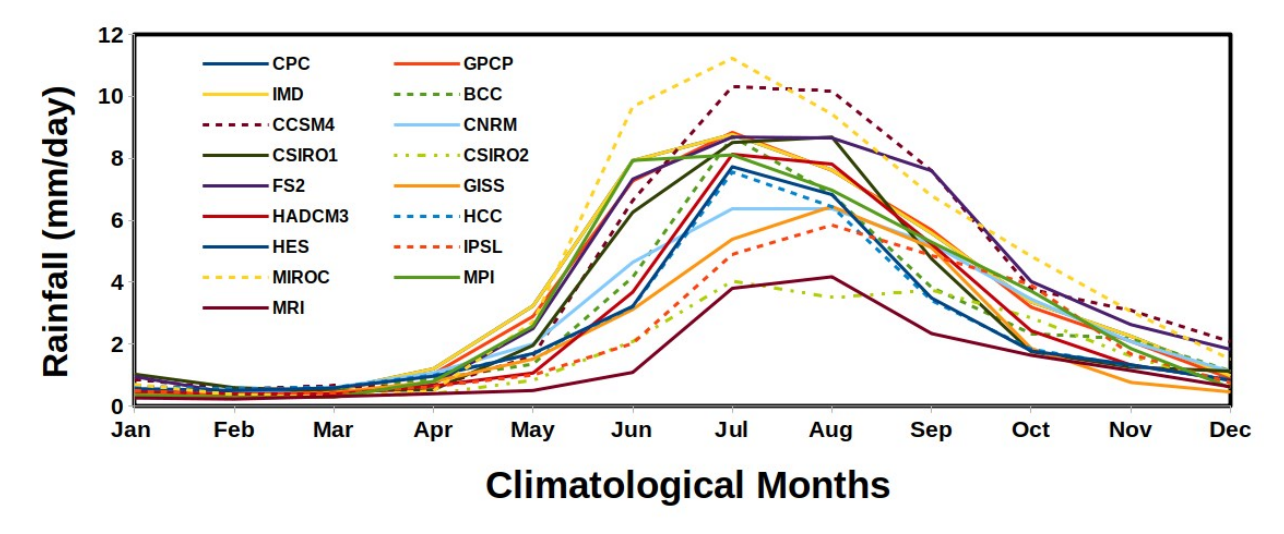


Figure 2.3: Historical area-averaged mean monthly raiinfall (mm/day) during CE 1901-2005 from IMD observations and model simulations.

We show the area-averaged climatological seasonal cycle of the Indian rainfall during CE 1901–2005 in Figure 2.3, and mean climatological distributions (CE 1979–2005) of the observed and Indian summer monsoon rainfall as well as that from the model simulations in Figure 2.4. From Figures 2.3, it is evident that all the models except CCSM4 and MIROC show a dry bias comparing to the IMD. There is a large inter-model spread, which is mainly because of the systematic bias in the models (e.g. Jourdain et al., 2013; Sharmila et al., 2015; Jain et al., 2019). Although, the CMIP5 models have inter-model spread, all the models are able to capture the ISM characteristics well in comparision with the observational and reanalysis data (Figure 2.4). The interannual standard deviation for these the area-averaged rainfall and temperature over India during JJAS, from observations as well as from the individual model simulations, are presented in Table 2.4. We find that simulated standard deviations from various models fall within ± 20% range of observations. On a different note, an increase in warm ENSO events, be them canonical or Modoki types (e.g. Ashok et al. 2007; Marathe et al., 2021), has been observed in the late twentieth century with an increase in global temperature (e.g. Collin 2000; Cai et al. 2015). The models are

able to reproduce this trend qualitatively to a reasonable extent, as seen by the higher number of simulated warm events, represented by the positive NINO3.4 index (**Table 2.5**).

Table 2.4 Interannual standard deviations of observational and historical simulations of near airsurface temperature (°C), which are area-averaged (June-September) globally (AATASG) and over the Indian region (AAIMST), respectively. Also shown in this table are, the the area-averaged Indian summer monsoon rainfall (mm/day; AAISMR) and NINO3.4 index from observations and and historical simulations.

S No	Models/			Variables	
	Observations	AATASG (°C)	AAISMT (°C)	NINO3.4 Index	AAISMR (mm/day)
		, ,	, ,	(°C)	, , ,
1	SST_HADI	NA	NA	0.60	0.69 (RF_IMD)
2	SST_ECMWF	0.27 (SKT)	0.42 (SKT)	0.70	0.53
					(PRECIP_NOAA)
3	BCC	0.33	0.36	0.76	0.77
4	CCSM4	0.35	0.43	0.80	0.60
5	GISS	0.20	0.34	0.52	0.68
6	HADCM3	0.22	0.52	0.71	0.82
7	IPSL	0.36	0.47	0.71	0.59
8	MPI	0.26	0.48	0.74	0.57
9	CSIRO1	0.20	0.48	0.50	0.96
10	MRI	0.16	0.38	0.50	0.48
11	FS2	0.49	0.44	1.19	0.83
12	CNRM	0.24	0.31	0.83	0.4
13	HCC	0.18	0.34	0.68	0.91
14	HES	0.19	0.34	0.64	0.87
15	MIROC	0.27	0.41	0.43	0.56
16	CSIRO2	0.2	0.33	0.68	0.5

Table 2.5 Number of simulated strong (events whose magnitude is above one standard deviation) ENSO events after CE 1950.

S.No	Model	El Niños	La Niñas	S.No	Model	El Niños	La Niñas
1	BCC	11	8	8	MPI	10	6
2	CCSM4	15	6	9	FS2	14	8
3	GISS	12	8	10	CSIRO1	12	10
4	HADCM3	12	8	11	MRI	11	7
5	IPSL	16	7	12	HES	7	11
6	CSIRO2	6	10	13	MIROC	16	3
7	HCC	13	10	14	CNRM	10	9

The fact that the ENSO is a major driver of interannual variability of the Indian summer climate is evidenced by the negative correlation of -0.5 (**Figure 2.5a**) between the AAISMR and NINO3.4 index derived from the HadISST for the period CE 1901–2005. The correlation is statistically significant at 0.01 level from a 2-tailed Student's t-test. Note that, the analogous correlation obtained by using the NINO3.4 index from the ECMWF SST data sets is -0.57. The simulated NINO3.4-AAISMR correlations from the HS are presented in **Figure 2.5a**. Seven out of the nine models simulate the negative correlations with a range of -0.21 to -0.51, which are statistically significant at the 0.05 significance level from a 2-tailed Student's t-test. The CCSM4 and FGOALS-s2 models simulate weaker but negative correlation coefficients of -0.12 (significant at 0.2 level) and - 0.1, respectively.

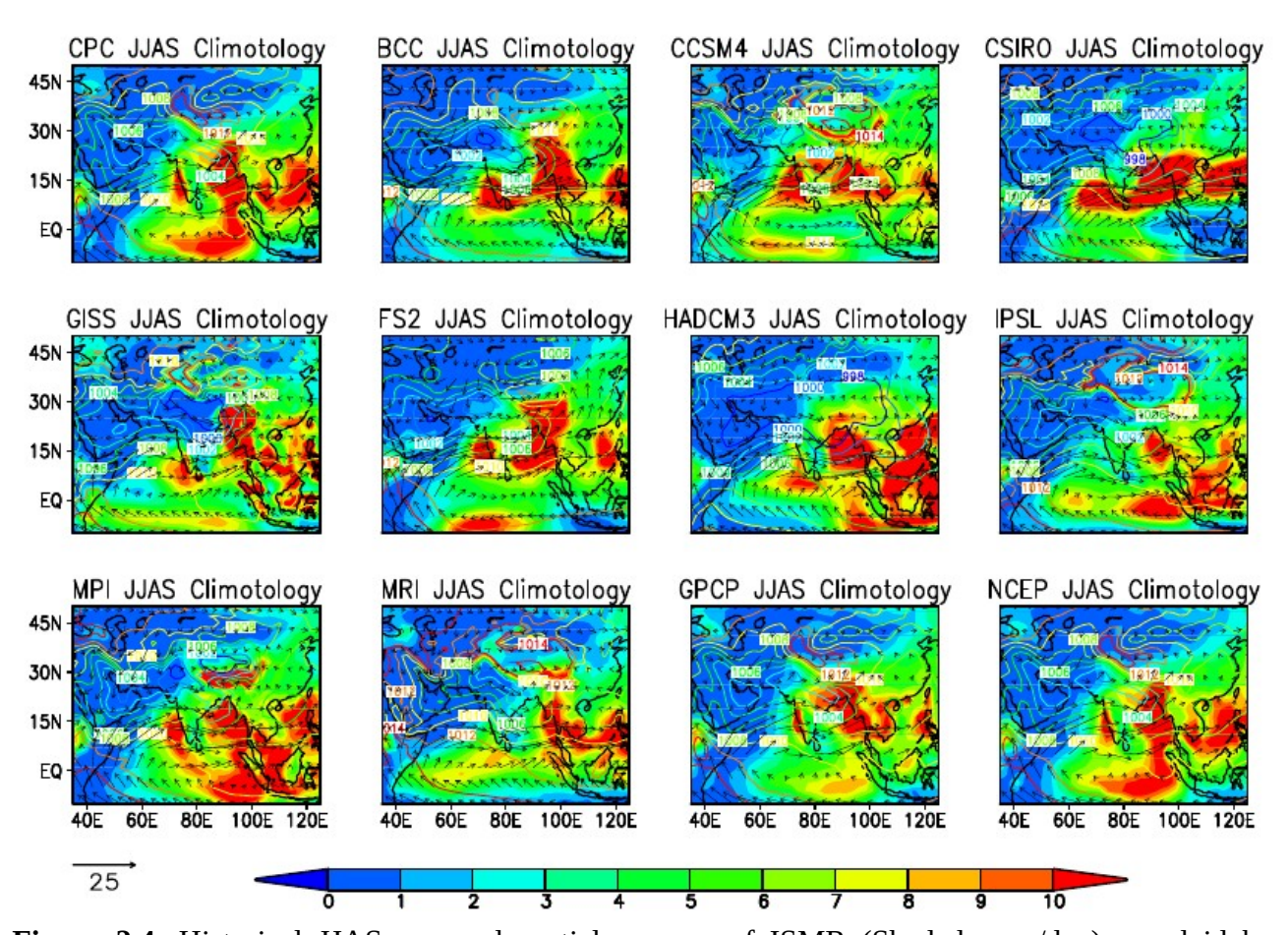


Figure 2.4: Historical JJAS seasonal spatial average of ISMR (Shaded; mm/day), overlaid by surface pressure (Contours; hPa), and wind vectors (m/s) plot of observational and model simulations during CE 1979-2005.

The AAISMT (CE 1901-2005) from the NCEP reanalysis yields moderate correlation coefficients of 0.34 and 0.38 with the concurrent NINO3.4 index from HadISST and that from the ECMWF SST datasets, respectively. Both values are statistically significant at 0.05 level from a 2-tailed Student's t-test. Corresponding correlations of all the models are statistically significant at 0.05 level from a 2-tailed test, though they vary over a wide range of values varying from 0.19 to 0.74 (**Figure 2.5b**).

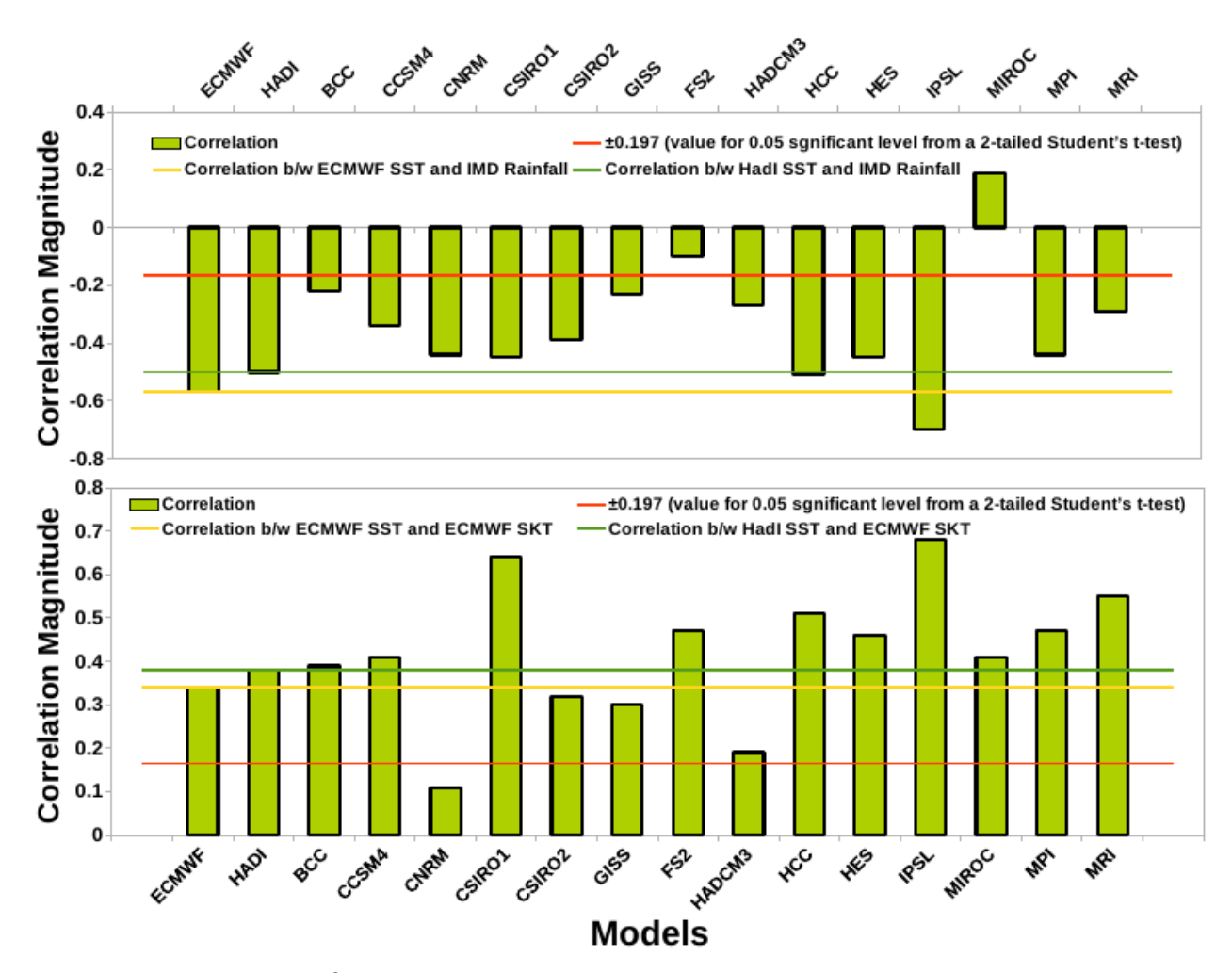


Figure 2.5: Correlations from historical data between the NINO3.4 and (**a**) AAISMR, (**b**) area-averaged near-surface air temperature over India of respective model simulations (red line represents the 0.05 significance level from a 2-tailed Student's t-test, yellow and greenrepresent the corresponding correlation values from observations) lines.

2.4 Summary

In summary, In this chapter, I have in detail talked about the various CMIP5 Historical, PMIP3 Last Millennium and Mid-Holocene simulations used in this study. Also, I have briefly discussed about the various Observational and Reanalysis datasets used in validating the CMIP5 Historical simulations. Apart from the datasets used in this study, I have also in detail explained the various analysis techniques used in this thesis.

Based on the criterion mentioned above, nine model simulations, namely BCC-CSM1-1, IPSL-CM5A-LR, MPI-ESM-P, GISS-E2-R, CCSM4, HadCM3, CSIRO-Mk3L-1-2, MRI-CGCM3 and FGOALS-s2 simulations, have been found suitable to be used for further analysis to understand the monsoon variability during the LM. Also, twelve model simulations, namely BCC-CSM1-1, IPSL-CM5A-LR, MPI-ESM-P, GISS-E2-R, CCSM4, MRI-CGCM3, CNRM-CM5, CSIRO-Mk3-6-0, HadGEM2-CC, HadGEM2-ES, MIROC-ESM and FGOALS-s2 model simulations to be used for further analysis to understand the monsoon variability during the MH.

Chapter 3

Indian summer monsoon variability during the Last

Millennium

In this chapter, we discuss in detail about the Indian summer monsoon variability, i.e., mean state, seasonal cycle, ENSO-ISM relationship, and dynamics involved during the Last Millennium (LM; CE 850-1849) using the paleoclimate modeling intercomparison project phase 3 (PMIP3) coupled model simulations. We mainly focus on the Medieval Warm Period (MWP) and Little Ice Age (LIA) of the LM, compared to the LM-mean conditions. We consider the two hundred consecutive warmest (coldest) common years across the models as the simulated MWP (LIA) period. Thus, the MWP and LIA periods for the models are chosen as the CE 1000–1199 and CE 1550–1749 against the CE 0950–1350 and CE 1500–1850 from the proxy-observations, respectively against, respectively. We should also keep in mind that the temporal and spatial signatures of the MWP and LIA varied from region to region, at least in terms of magnitude. As discussed in Chapter 2, for this analysis, we use simulations from the nine model.

3.1 Last Millennium analysis

3.1.1 Annual cycle

We present the evolution of the area-averaged seasonal cycle of simulated rainfall and surface temperature for the Indian region for the Last Millennium (LM) in **Figure 3.1 from** for the multi-model mean (MMM). From **Figure 3.1**, it is evident that the MMM of the seasonal cycle

evolution is similar to those seen in the historical periods, with highest rainfall occurring during June to September, the season of the summer monsoon rainfall (**Figure 3.1a**).

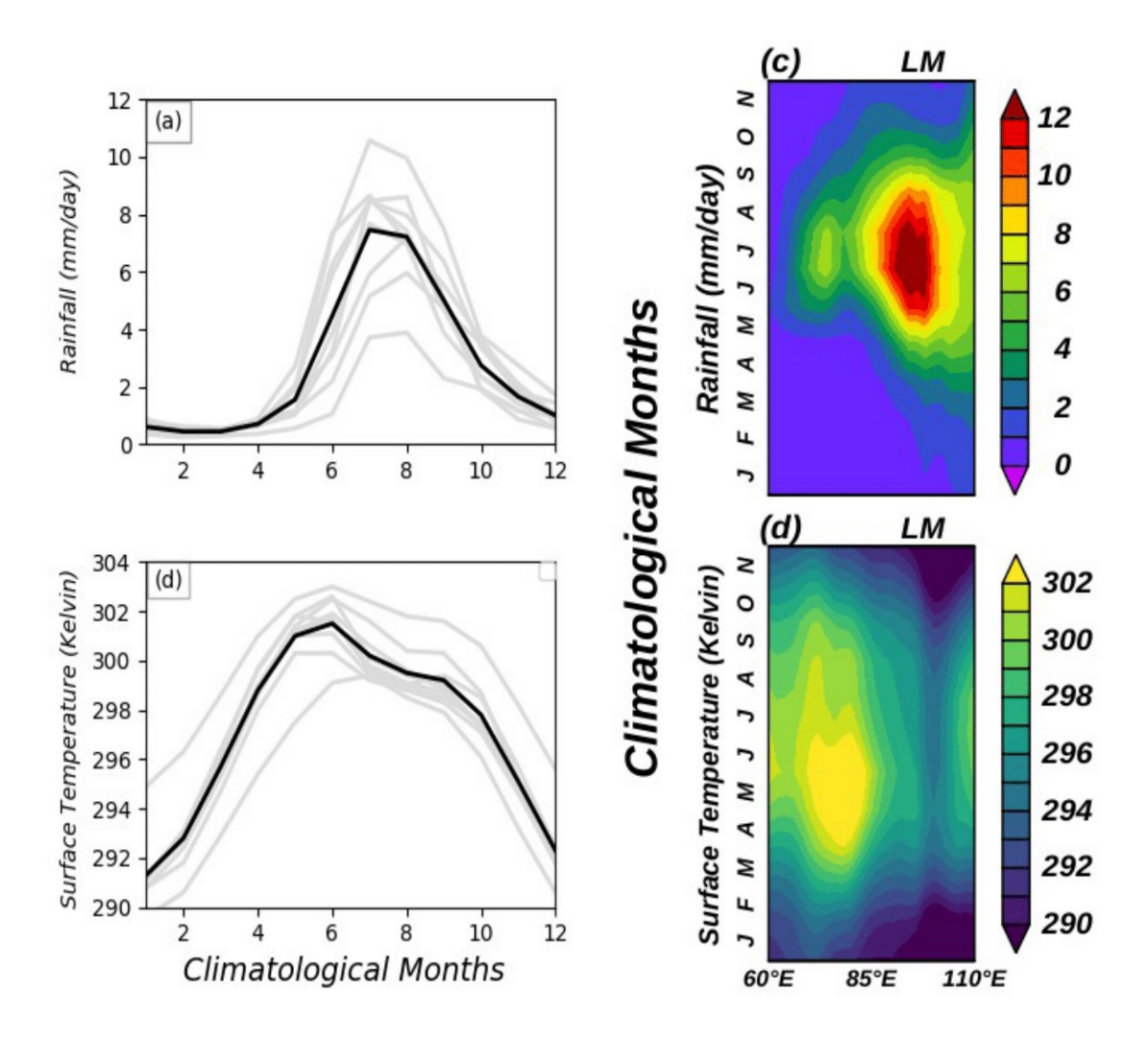


Figure 3.1: Comparisons of simulated area-averaged climatological cycle for the LM (CE 0850-1849) period by individual PMIP3 models (grey lines), and that of the MMM (black line) over the Indian land region (65°E–95°E; 10°N–30°N) for (a) rainfall and, (b) surface temperature. Seasonal cycle of, latitudinally (over 10°N to 30°N) averaged of MMM (c) rainfall and (d) surface temperature, over the Indian region for the LM.

We also show the spatial distribution of the latitudinally (10°N to 30°N) averaged seasonal cycle of simulated rainfall and surface temperature for the Indian region over the LM for the MMM in **Figure 3.1**. From the figure, we see that during the summer monsoon months, the Eastern Indian

region receives more rainfall than the western Indian region, and during the pre-summer monsoon months, the central Indian region is warmer compared to the other parts of the Indian region in LM.

3.1.2 Mean state

In **Figure 3.2**, we present the mean state of spatial distributions of simulated rainfall and surface temperatures of the LM period for the summer monsoon months of June to September (JJAS) for the MMM. Figure 3.2, we can see that western ghats and northeastern Indian regions are receiving more rainfall (**Figure 3.2a**) and central to northern Indian regions are warmer compared to the rest of the Indian regions (**Figure 3.2b**). The rainfall pattern is consistent with the surface temperatures over the Indian land region.

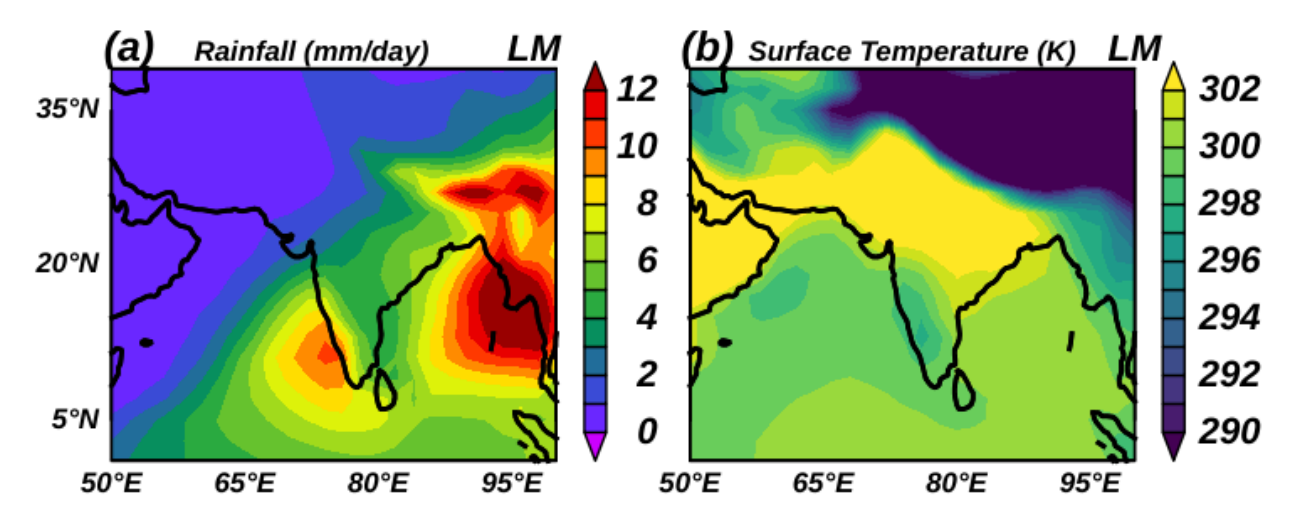


Figure 3.2: Spatial distributions of the simulated summer monsoon (a) rainfall (mm/day) and (b) surface temperature during the LM.

3.1.3 Simulated interannual variability of ISM

To ascertain that there is a reasonable agreement among the PMIP3 LM simulations, we present the JJAS multi-model standard deviations (σ) of the simulated area-averaged global surface

temperatures, area-averaged Indian summer monsoon surface temperatures (AAISMST), area-averaged Indian summer monsoon rainfall (AAISMR), and the NINO3.4 index for the whole period (i.e., 0850-1849) as well as three overlapping 500-year sub-periods, namely, CE 850 to1349, CE 1100 to 1599, and CE 1350 to 1849 in **Table 3.1**. The simulated statistics for all these variables from the individual PMIP3 LM models fall within the range of \pm 1 σ of the corresponding statistic (**Table 3.1**) in general, except the standard deviations of the simulated NINO3.4 index from the FGOALS-s2 model. This shows that the simulated variabilities across the PMIP3 LM model simulations are, in general, in reasonable agreement with one another.

Table 3.1: Boreal summer interannual standard deviations of near air area-averaged (June-September) surface temperature (°C) over the globe (AATASG) and that over India (AAIMST), and that of ISM Rainfall (AAISMR, in mm/day) and NINO3.4 Index(°C), as simulated by CMIP5/PMIP3 Last Millennium models (here A: CE 0850-1849; B: CE 0850-1349; C: CE 1100-1599 and D: CE 1350-1849).

S. No	Models	Variables							
			AAGST(°C)			AAISMST (°C)			
		A	В	С	D	A	В	С	D
1	BCC	0.13	0.13	0.13	0.11	0.29	0.30	0.29	0.28
2	CCSM4	0.25	0.25	0.27	0.21	0.38	0.40	0.40	0.37
3	GISS	0.19	0.18	0.16	0.18	0.35	0.33	0.35	0.36
4	HADCM3	0.20	0.19	0.19	0.20	0.46	0.33	0.46	0.49
5	IPSL	0.19	0.20	0.20	0.18	0.39	0.41	0.41	0.37
6	MPI	0.20	0.20	0.21	0.20	0.42	0.41	0.44	0.42
7	CSIRO	0.16	0.15	0.16	0.16	0.41	0.39	0.41	0.43
8	MRI	0.13	0.13	0.14	0.12	0.38	0.37	0.39	0.38
9	FS2	0.26	0.25	0.21	0.18	0.39	0.40	0.40	0.36
	_								
					V	ariables			
S. No	Models	1	AAISMR	(mm/da	y)		NINO	3.4 Index ((°C)
		A	В	С	D	A	В	С	D
1	BCC	0.76	0.74	0.75	0.77	0.65	0.65	0.64	0.65
2	CCSM4	0.62	0.59	0.60	0.64	0.73	0.75	0.74	0.72
3	GISS	0.70	0.70	0.71	0.69	0.45	0.43	0.45	0.46
4	HADCM3	0.76	0.73	0.74	0.78	0.63	0.60	0.62	0.60
5	IPSL	0.54	0.55	0.56	0.53	0.60	0.60	0.62	0.60
6	MPI	0.60	0.61	0.60	0.69	0.59	0.60	0.63	0.58
7	CSIRO	0.81	0.78	0.82	0.84	0.49	0.49	0.50	0.48
8	MRI	0.46	0.45	0.48	0.46	0.48	0.48	0.50	0.48
9	FS2	0.75	0.76	0.76	0.74	1.14	1.15	1.15	1.11

We show the 101-year running mean of area-averaged globally simulated surface temperature for the JJAS season during LM, i.e., from CE 0850–1849 in Figure 3.3a, and a similar one representing the surface temperature over the Indian subcontinent in Figure 3.3b. The 101-year running mean window has been applied to identify the long term changes in the surface temperature variability. We see a coherent evolution in time among the simulated surface temperatures, but with a spread across the models. To visualize the evolution of surface temperatures more clearly bereft of the systematic biases, we calculate the 101-year running mean of temporal anomalies of the global region (Figure 3.4a) and for the Indian region (Figure 3.4b). As we mentioned earlier, we see a relatively more coherent inter-model evolution in the anomalous surface temperatures for the global region (Figure 3.4a) as well as over the Indian region (Figure 3.4b). Qualitatively, the evolutions are similar. Notably, while there are fluctuations in surface temperature during LM, we see all the models showing a warming signal during the MWP and cooling during the LIA. This is in general agreement with the earlier studies (e.g., Fig. 1B of TS-IPCC13).

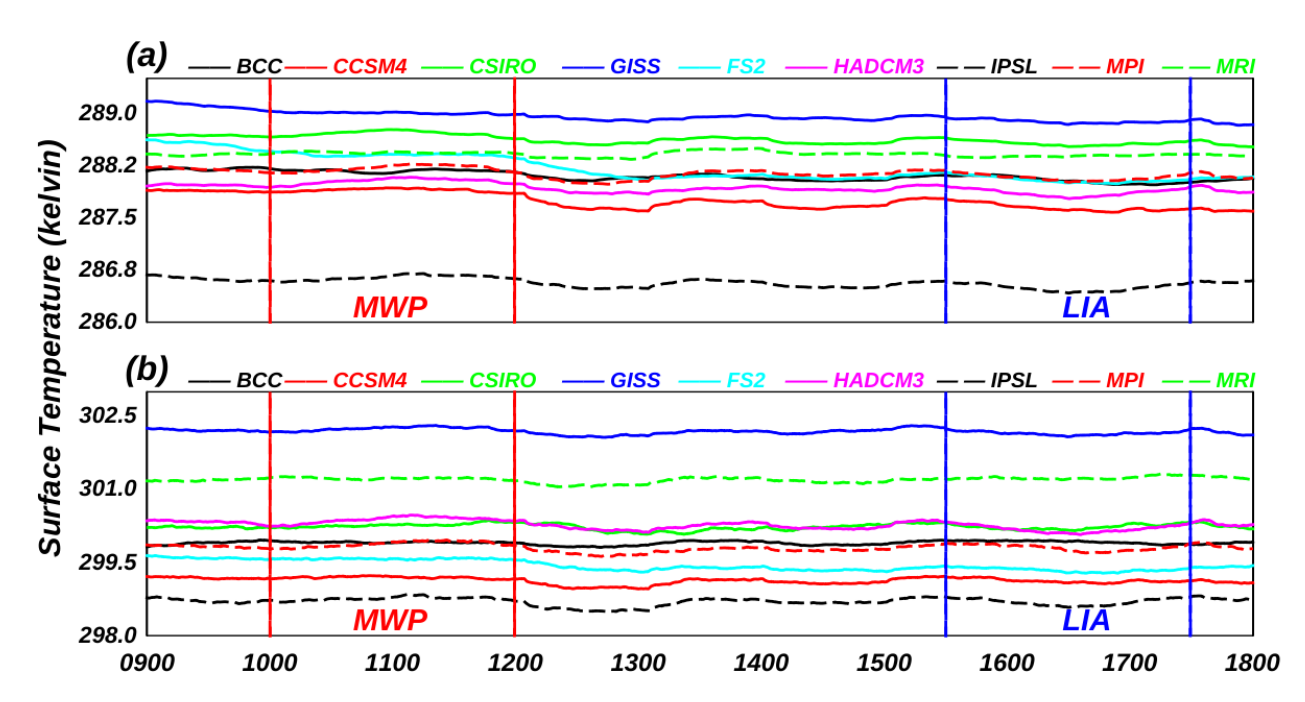


Figure 3.3: 101-year running mean of simulated surface air temperature (K) obtained by area-averaging (**a**) globally (**b**) over India.

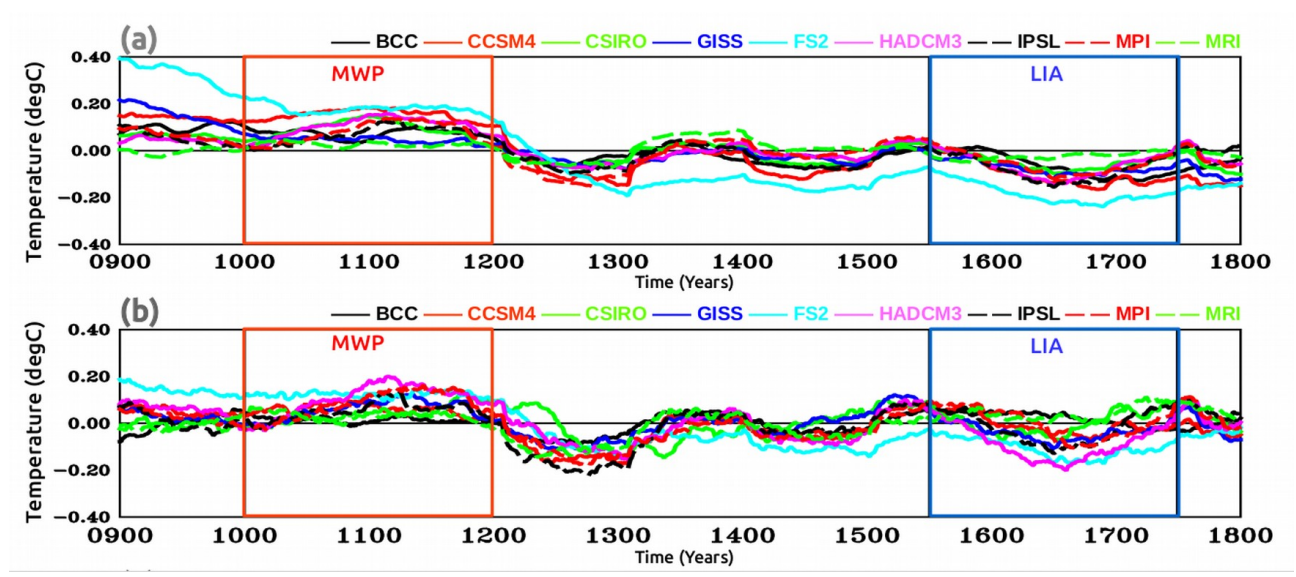


Figure 3.4: 101-year running mean anomalies of near surface air temperature (kelvin) obtained by area-averaging (**a**) globally, (**b**) over the Indian Region; The MWP, and LIA period are shown in red and blue boxes, respectively.

Interestingly, in addition to these two well-known epochs, we see a few more warm and cold climatic periods, but with a shorter duration. **Figure 3.3b** and **Figure 3.4b** also show that the intermodel spread in the anomalies of surface temperature over the Indian region is relatively less as compared to the corresponding anomalies of global surface temperatures. In comparison, as seen in **Figures 3.3b** and **3.4b**, from the simulated temperature response during the MWP and LIA over the Indian region, is relatively more coherent across the models, and its evolution qualitatively agrees with available proxy records (Yadava et al. 2005; Ramesh et al. 2010; Thamban et al. 2007).

We see a sharp cooling around year CE 1250 in the global and Indian summer monsoon temperature across all the models (**Figures 3.3a, b**), which is coincident with an intense volcanic event, identified as Samalas volcanic eruption (Sigl et al. 2015, Vidal et al. 2016; Gao et al. 2008). In this context, it is worth noting that other volcanic eruptions resulted in potentially decades-long cooling episodes (Liu et al., 2016; Sigl et al., 2015; Iles et al., 2014). Such a signal is apparent from a few proxy records (e.g., Fig. 1 TS5 of TS-IPCC13). Also evident is that all the modeled

temperatures have apparently entered a cooling phase from this point, showing that they respon well to the volcanic forcing imposed.

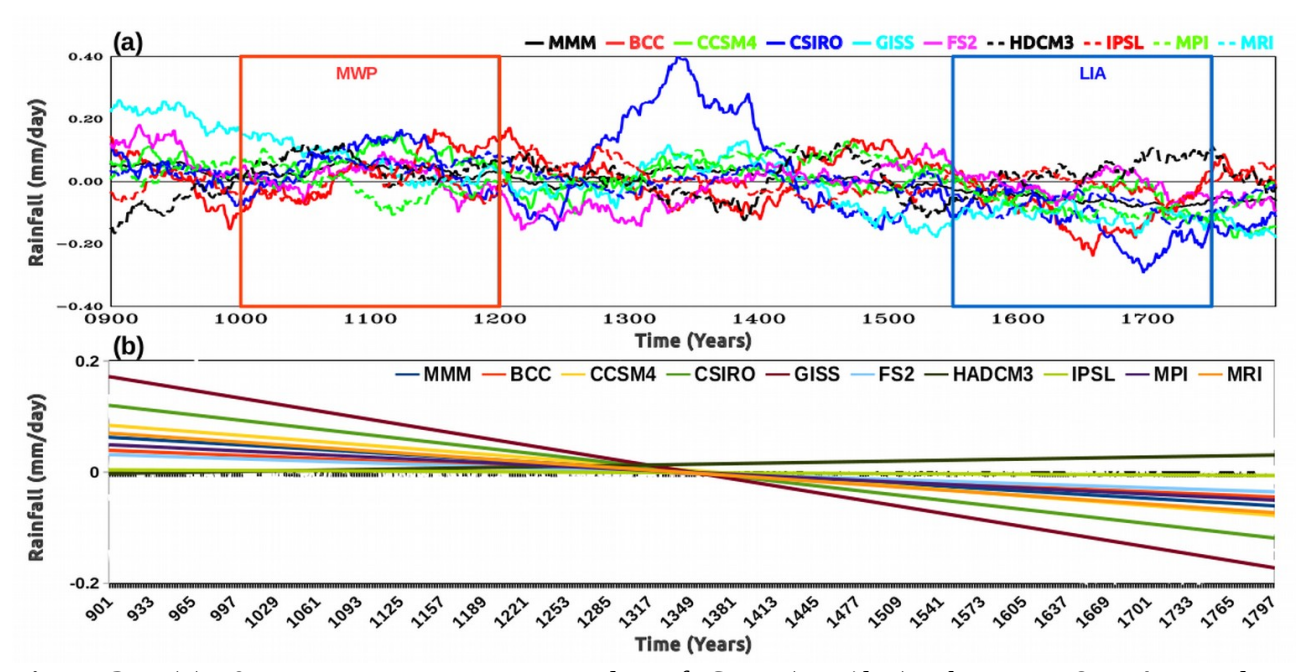


Figure 3.5: (a) 101-year running mean anomalies of ISMR (mm/day); The MWP & LIA period are shown in red and blue boxes, respectively. (b) Liner trend lines of the area-averaged ISMR during LM, as simulated by the nine PMIP3 models.

We show the 101-year running means of the simulated area-averaged Indian summer monsoon rainfall (AAISMR) anomalies in **Figure 3.5a**. We carry out a linear trend analysis of the same, which is presented in **Figure 3.5b**. **Figure 3.5b** shows a moderate decreasing trend of AAISMR in four models throughout the LM, and they are statistically significant at a 0.10 level. This decreasing trend is in agreement with several proxy records (e.g., Fig. 8 of Ramesh et al., 2010). Four other models also simulate a weak decreasing trend. Only the HadCM3 simulates a moderate increasing trend. The time series of the MMM AAISMR also shows a long-term decreasing trend throughout the LM. **Figure 3.5a** shows that the simulated MWP climate is marked by relatively higher ISMR compared to the LM-mean conditions, and the LIA by a relatively low ISMR.

3.1.4 El Niño-Southern oscillation and ISM

The simulated concurrent anomaly correlation coefficients between the AAISMST and NINO3.4 index for the whole LM period and those overlapping 500-year periods of LM, i.e., the first, middle, and the last 500-year chunks, are presented in **Table 3.2**. We also computed similar concurrent animaly correlations between AAISMR and NINO3.4 index, which are presented in **Table 3.3**. In general, these simulated AAISMR-NINO3.4 correlations are negative, while the corresponding AAISMST-NINO3.4 concurrent correlations are positive. Most of these correlation coefficients are statistically significant at 0.05 level from a 2-tailed Student's t-test, suggesting that ENSO has been consistently influencing the Indian summer monsoon climate throughout the LM, just as for the historical period.

Table 3.2: Correlations between NINO3.4 and area-averaged Indian Summer Monsoon surface temperatures (AAISMST) during the Last Millennium, as simulated by CMIP5 models (Significant correlation values are shown in **bold** and are significant at less than 0.05 level from 2-tailed student's t-test).

S No	Models	CE 0850-1849	CE 0850-1349	CE 1100-1599	CE 1350-1849
1	BCC	0.26	0.29	0.23	0.23
2	CCSM4	0.31	0.36	0.39	0.26
3	GISS	0.38	0.31	0.38	0.43
4	HADCM3	0.30	0.31	0.30	0.28
5	IPSL	0.59	0.61	0.58	0.58
6	MPI	0.47	0.48	0.49	0.47
7	FS2	0.41	0.44	0.37	0.35
8	CSIRO	0.55	0.53	0.61	0.56
9	MRI	0.47	0.46	0.51	0.47

A study by Whittenberg et al. (2009) using multi-century model simulation shows multi-decadal changes in the ENSO statistics. The consistent ENSO-monsoon links over a period of 1000-

year simulation across many models, as shown above, reconfirms that the ENSO is indeed an essential driver of the interannual Indian summer monsoon climate variability. However, we must be mindful that the above analysis only explores the association of an ENSO index with the (AAISMR), which may not necessarily apply to every local region of the Indian region.

Table 3.3: Correlation between NINO3.4 and area-averaged Indian Summer Monsoon Rainfall (AAIMSR) during Last Millennium, as simulated by CMIP5/PMIP3 models (Significant correlation values are shown in **bold** (*italic*) and are significant at less than 0.05 (0.10) level from 2-tailed student's t-test).

S No	Models	CE 0850-1849	CE 0850-1349	CE 1100-1599	CE 1350-1849
1	BCC	-0.32	-0.34	-0.30	-0.29
2	CCSM4	-0.12	-0.08	-0.11	-0.17
3	GISS	-0.28	-0.24	-0.33	-0.34
4	HADCM3	-0.39	-0.37	-0.37	-0.40
5	IPSL	-0.70	-0.74	-0.69	-0.66
6	MPI	-0.43	-0.43	-0.46	-0.44
7	FS2	-0.05	-0.07	-0.05	-0.03
8	CSIRO	-0.33	-0.31	-0.32	-0.34
9	MRI	-0.36	-0.32	-0.35	-0.39

Here, we are mainly interested in the ISM changes during the MWP and LIA periods compared to the LM-mean conditions. In the next section, we will discuss them.

3.2 MWP and LIA analysis

3.2.1 Annual cycle

Figure 3.6 presents the evolution of the area-averaged seasonal cycle of simulated rainfall and surface temperature for the Indian region for the MWP and LIA. We mainly show the seasonal cycle evolution for the multi-model mean (MMM). As shown in the **Figure 3.6**, seasonal cycle

evolution simulated by each model is similar to that for the historical period. However, the models show spread among them, and it is maximum during June to September.

Figure 3.6 shows the MMM spatial distribution of the latitudinal (10° N to 30° N) averaged seasonal cycle of simulated rainfall and surface temperature for the Indian region during MWP and LIA periods. We see that during the summer monsoon months, the eastern Indian region receives more rainfall than the western Indian region. During the pre-summer monsoon months, central Indian region is warmer compared to the other parts of the Indian region in MWP and LIA, just as for the historical period (**Figure 3.6**).

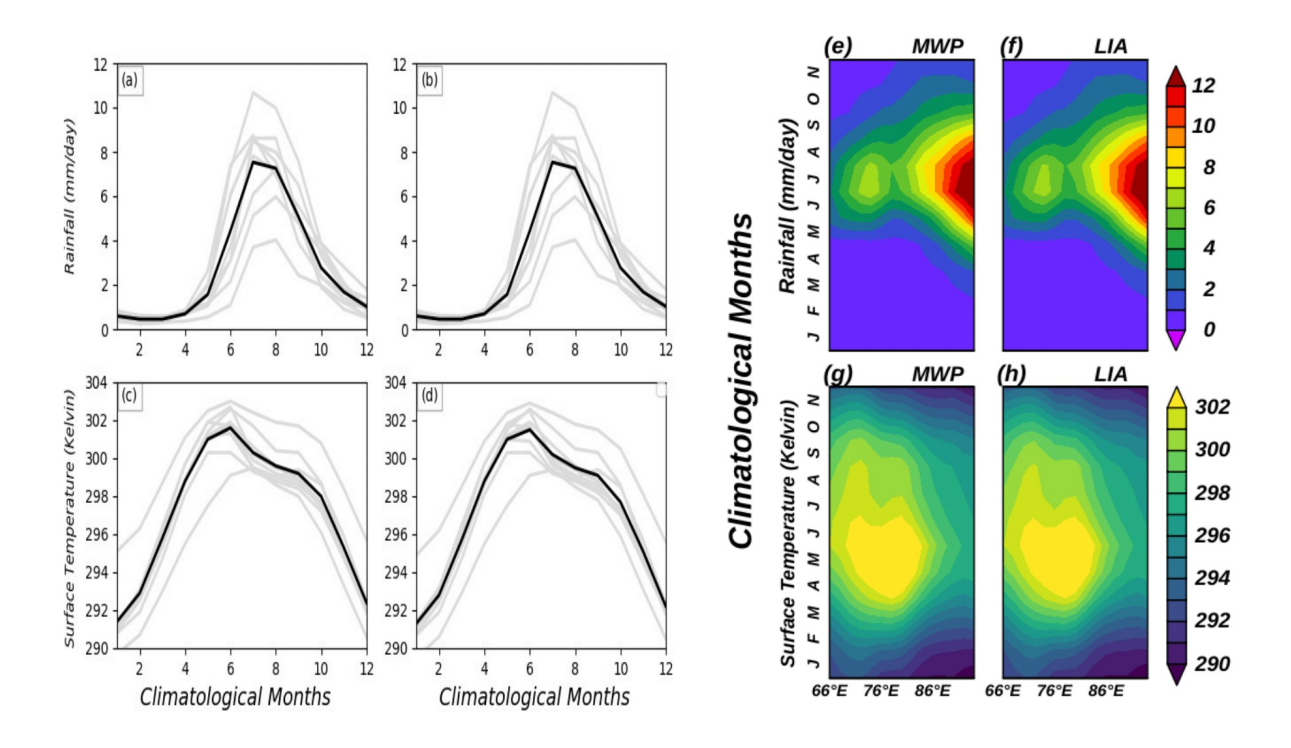


Figure 3.6: Comparisons of simulated area-averaged climatological cycle for the MWP (CE 1000-1199) and LIA (CE 1550-1749) period for MMM (black line) and PMIP3 models (grey lines) of (a) rainfall during MWP, (b) rainfall during LIA, (c) surface temperature during MWP, and (d) surface temperature during LIA over the Indian land region (65°E–95°E; 10°N–30°N). Spatial distribution of the latitudinal (10°N to 30°N) averaged seasonal cycle of simulated (e) rainfall during MWP, (f) rainfall during LIA, (g) surface temperature during MWP, and (h) surface temperature during LIA of the Indian region for MWP and LIA of the MMM.

3.2.2 Mean state

In **Figure 3.7**, we present the MMM mean state of spatial distributions of simulated rainfall and surface temperatures of MWP and LIA periods for the summer monsoon months of June to September (JJAS). **Figure 3.7** shows that western ghats and northeastern Indian regions are receiving more rainfall, and central to northern Indian regions are warmer compared to the rest of the Indian regions. The rainfall pattern is dynamically consistent with the surface temperatures over the Indian land region.

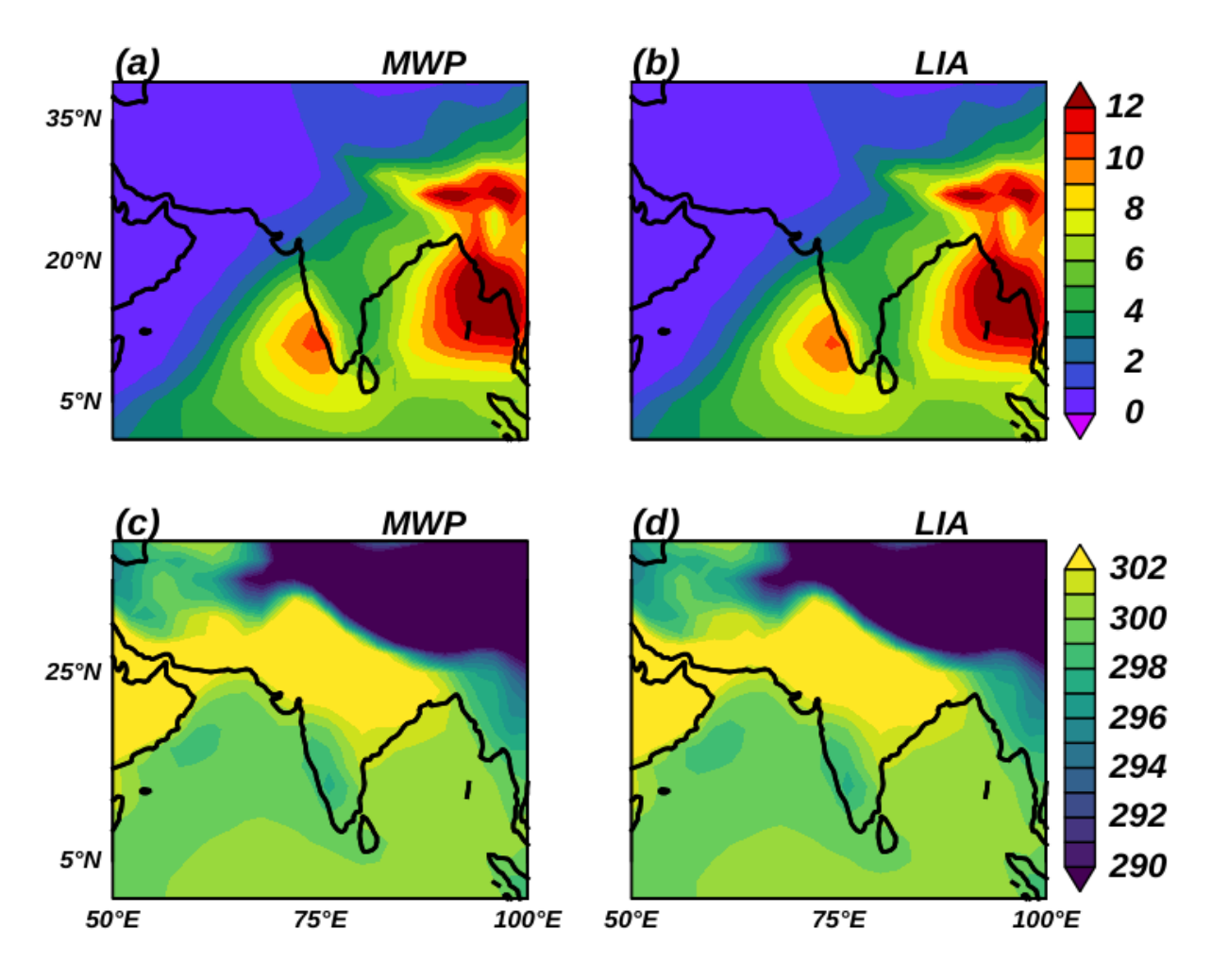


Figure 3.7: Spatial distributions of the simulated summer monsoon (**a**) rainfall (mm/day) and (**b**) surface temperature during the MWP and LIA time periods.

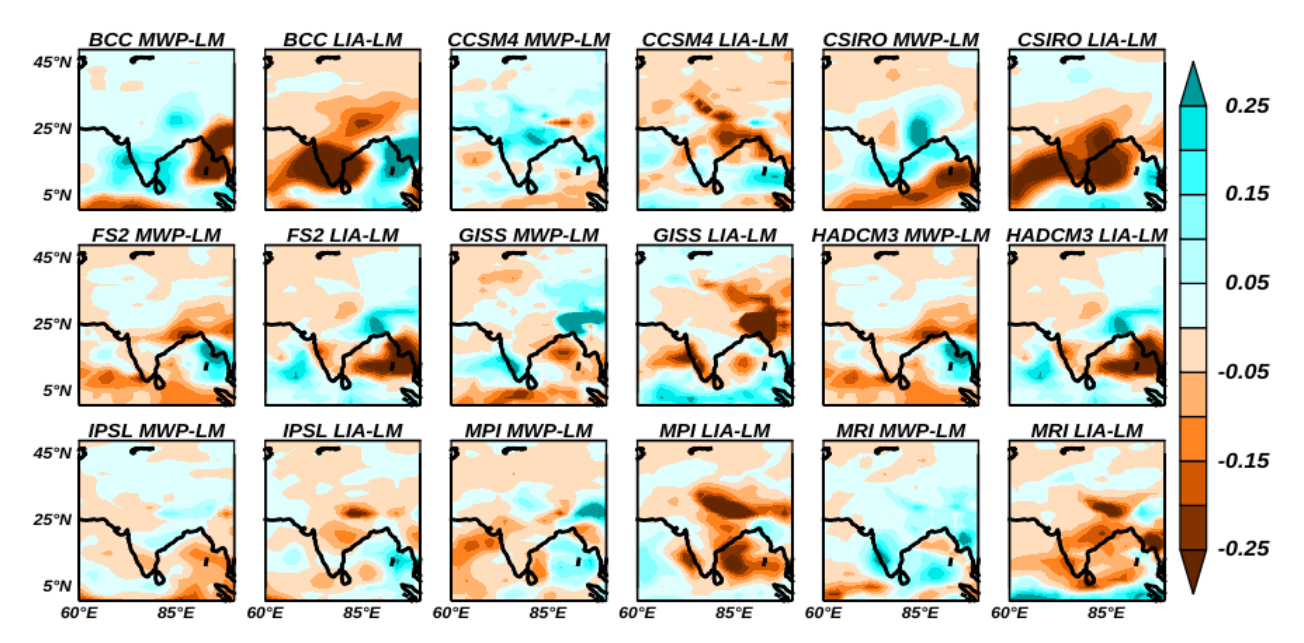


Figure 3.8: Spatial distributions of the simulated summer monsoon rainfall (mm/day) during the MWP and LIA compared to the LM-mean. The descriptor string above each panel indicates the name of the model and the periods over which difference is calculated.

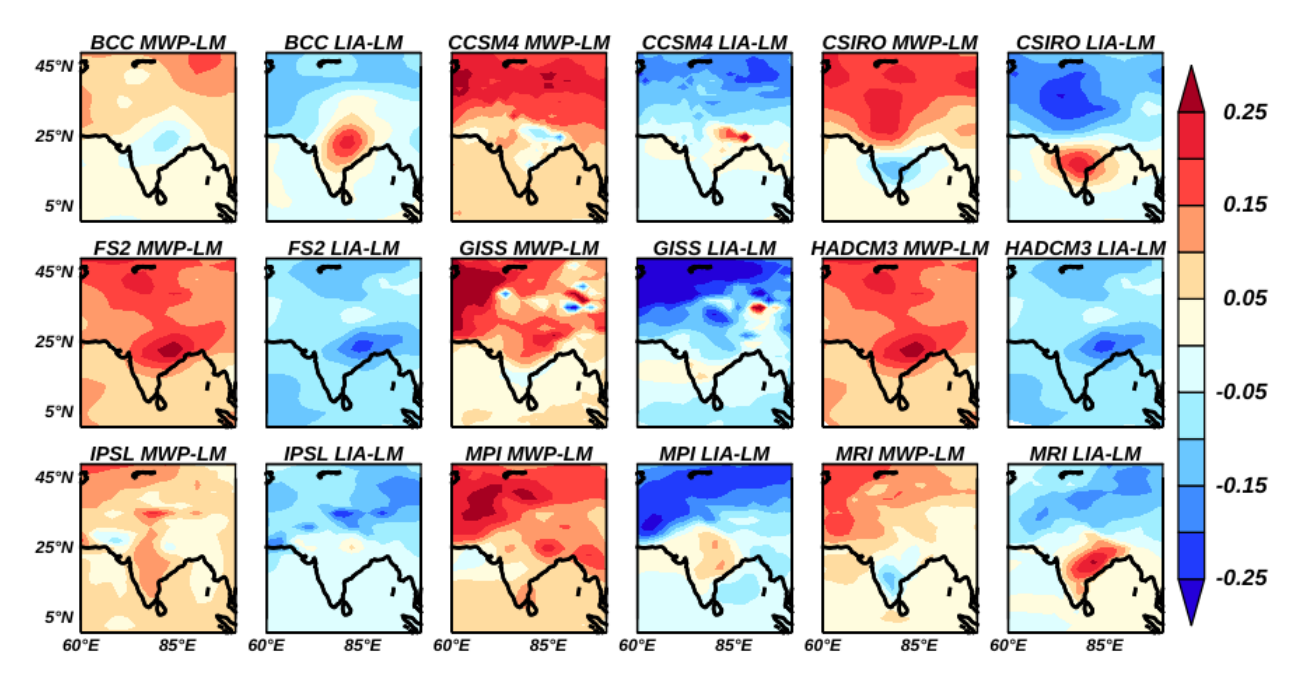


Figure 3.9: Spatial distributions of the simulated summer monsoon surface temperatures (kelvin) during the MWP and LIA compared to the LM-mean. The descriptor string above each panel indicates the name of the model and the periods over which difference is calculated.

We show spatial distributions of the simulated summer monsoon surface temperatures during the MWP and LIA climate periods relative to LM-mean in **Figure 3.8**. We found that six out

of nine model simulations show, in general, a warmer MWP and relatively cooler LIA compared to the LM-mean. It can also be seen from **Figure 3.8** that the simulated summer monsoon surface temperatures during the LIA are substantially less (i.e., cooler) than that for the MWP majority of the models. We also carried out a similar analysis for the summer monsoon rainfall and is present in **Figure 3.9**. From **Figure 3.9**, we see that six out of nine model simulations show, in general, a wetter MWP and drier LIA compared to the LM-mean. It can also be seen from **Figure 3.9** that the simulated summer monsoon rainfall during the LIA is substantially less than that for the MWP across most of the model simulations.

3.2.3 Interannual variability of ISM and teleconnections of the El Niño

Table 3.4: Simulated boreal summer (June-September) interannual standard deviation (°C) for area-averaged near air surface temperature over Global region (AATASG) and Indian region (AAIMST), area-averaged Indian summer monsoon rainfall (AAISMR) and NINO3.4 Index during MWP (CE 1000-1199) and LIA (CE 1550-1749) of CMIP5/PMIP3 models.

S	Models		Variables							
No		AATAS	G (°C)	AAIS	MT (°C)	AAISMR	(mm/day)	NINO3.4	NINO3.4 Index (°C)	
		MWP	LIA	MWP	LIA	MWP	LIA	MWP	LIA	
1	BCC	0.11	0.13	0.28	0.29	0.76	0.82	0.70	0.64	
2	CCSM4	0.13	0.17	0.33	0.32	0.53	0.60	0.73	0.72	
3	GISS	0.09	0.17	0.29	0.34	0.69	0.67	0.42	0.42	
4	HADCM 3	0.15	0.18	0.39	0.44	0.73	0.76	0.58	0.65	
5	IPSL	0.17	0.17	0.37	0.36	0.56	0.51	0.61	0.58	
6	MPI	0.13	0.17	0.37	0.40	0.67	0.60	0.58	0.58	
7	CSIRO	0.10	0.13	0.34	0.41	0.76	0.84	0.45	0.47	
8	MRI	0.10	0.10	0.35	0.35	0.44	0.43	0.47	0.46	
9	FS2	0.13	0.15	0.37	0.36	0.75	0.71	1.14	1.07	

We show the simulated interannual standard deviations of surface temperatures (for both global and Indian regions) for the summer monsoon months of JJAS during the MWP and LIA periods in **Table 3.4**. Similar standard deviations for the ISMR and the NINO3.4 index are also

present in **Table 3.4**. We found that, In five out of nine models, the amplitude of simulated NINO3.4 standard deviations during LIA are lower than those during the MWP, but only marginally so. Standard deviations of other variables across the MWP and LIA only differ marginally.

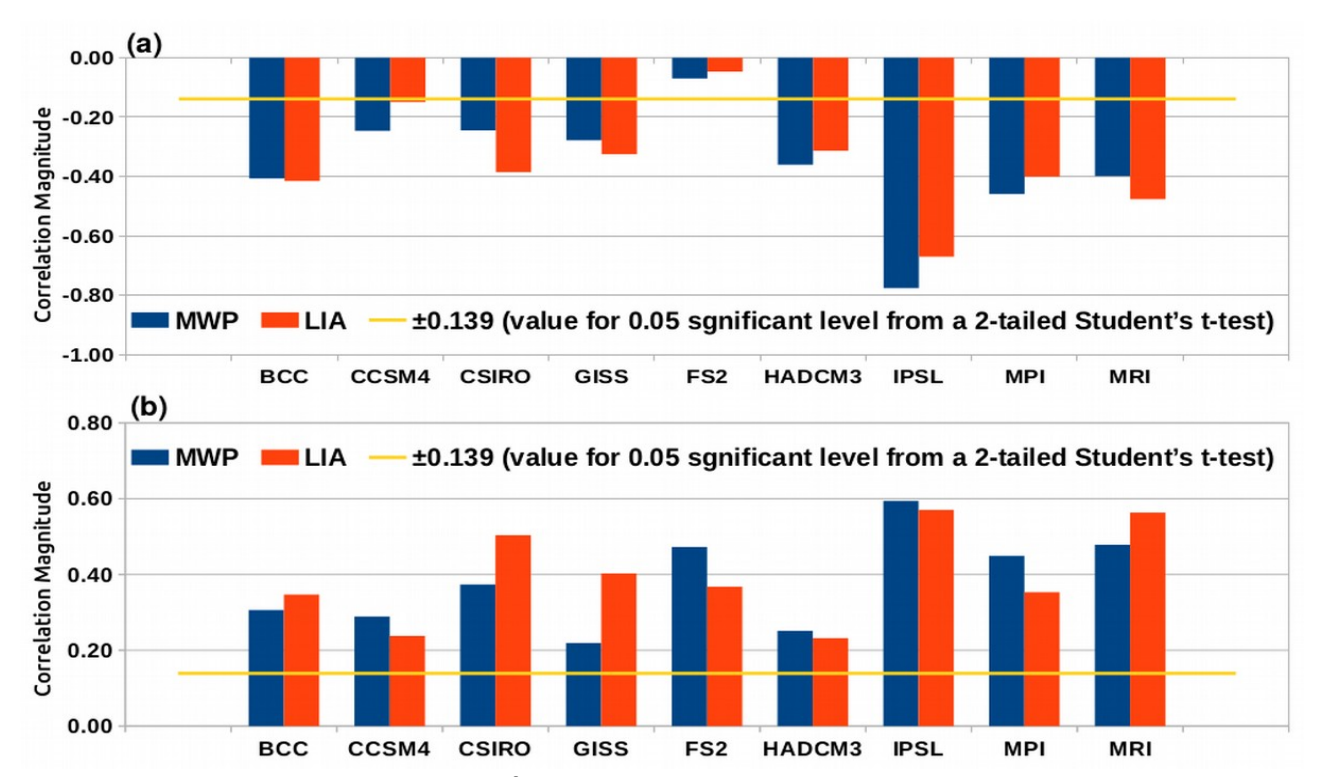


Figure 3.10: Simulated correlations, for each model, during MWP (blue bars) and LIA (red bars) between the NINO3.4 index and (a) AAISMR, and (b) AAISMST. Yellow line shows the significant value at 0.05 level from a 2-tailed Student's t-test.

We present the simulated concurrent correlation coefficients between the boreal summer NINO3.4 index with the area-averaged ISMR during the MWP and LIA periods from the individual models in **Figure 3.10a** and those with the corresponding area-averaged ISMST in the **Figure 3.10b**. The signs and magnitudes of all these simulated concurrent correlations are comparable to the correlations of the last century observational dataset and statistically significant at 0.10 level. The simulated area-averaged ISMR-NINO3.4 index correlations for both MWP and LIA periods, except for the FGOALS-s2 model, are statistically significant at 0.05 level from a 2-tailed Student's t-test. For the Indian region, the magnitudes of the correlations with the ENSO index are stronger in

the surface temperature than the rainfall (**Figure 3.10**). Interestingly, for five models out of the nine, the magnitudes of the correlation coefficients of the NINO3.4 index with the area-averaged ISMR are weaker in the LIA relative to the corresponding correlations over the MWP, and six models out of the nine, the magnitudes of the correlation coefficients of the NINO3.4 index with the area-averaged ISMST are weaker in the LIA relative to the corresponding correlations over the MWP.

Table 3.5: Frequency table of simulated El Niños and La Niñas during MWP (CE 1000-1199) and LIA (CE 1550-1749).

	GE 1880 17 18).								
S No	Models		MWP (CE)	LIA (CE 1550-1749)				
		Weak El	Strong	Weak La	Strong La	Weak El	Strong	Weak	Strong La
		Niños	El Niños	Niñas	Niñas	Niños	El Niños	La	Niñas
								Niñas	
1	BCC	47	33	20	36	41	29	31	35
2	CCSM4	25	45	21	24	37	27	29	29
3	GISS	32	42	25	30	34	28	23	41
4	HADCM3	38	41	35	23	26	23	31	34
5	IPSL	42	32	22	34	36	23	26	40
6	MPI	29	40	32	26	36	33	32	39
7	CSIRO	53	35	69	30	63	34	64	32
8	MRI	64	27	70	32	73	31	61	30
9	FS2	39	41	27	30	27	27	43	35

Table 3.6: Categorization of El Niños and La Niñas as as per the normalized strength of the NINO3.4 index. 'σ' represents the standard deviation of the NINO3.4 index.

S. No	El N	Niño Classification	La l	Niña Classification	
1	$0.5\sigma < 1\sigma$	Weak El Niño	$(-1\sigma) < 0.5\sigma$ Weak La Niña		
2	> 1σ	Strong El Niño	< (-1 _o)	Strong La Niña	

To explore ENSO-ISM relations during the MWP and LIA further, we calculate the simulated frequencies of 'strong' El Niños and La Niñas during the MWP and LIA periods of the individual models. While calculating and distinguishing the frequencies of the events, we catalogued them following a method: if any simulated ENSO event amplitude exceeds one standard deviation value, i.e., '10', we report it as a strong event see **Table 3.5** for details). The majority of PMIP3 models consistently simulates more number of strong El Niños during the MWP as

compared to the number of strong El Niños during the LIA. Interestingly, the majority of PMIP3 models consistently simulates more number of strong La Niñas during the LIA as compared to the number of strong La Niñas during the MWP, as shown in **Table 3.6**; this is statistically significant at 0.05 level from a two-tailed Student's t-test carried out for difference of means. Interestingly, at least six of the of the PMIP3 models (six) simulate more strong El Niños compared to strong La Niñas during the MWP (**Table 3.6**). On the other hand, the number of strong La Niñas is marginally more than that of strong El Niños in seven models during the LIA. This clearly shows that strong El Niños are more dominant in the tropical Pacific during MWP in most models, and 'strong' La Niñas are more dominant in the tropical Pacific during the LIA.

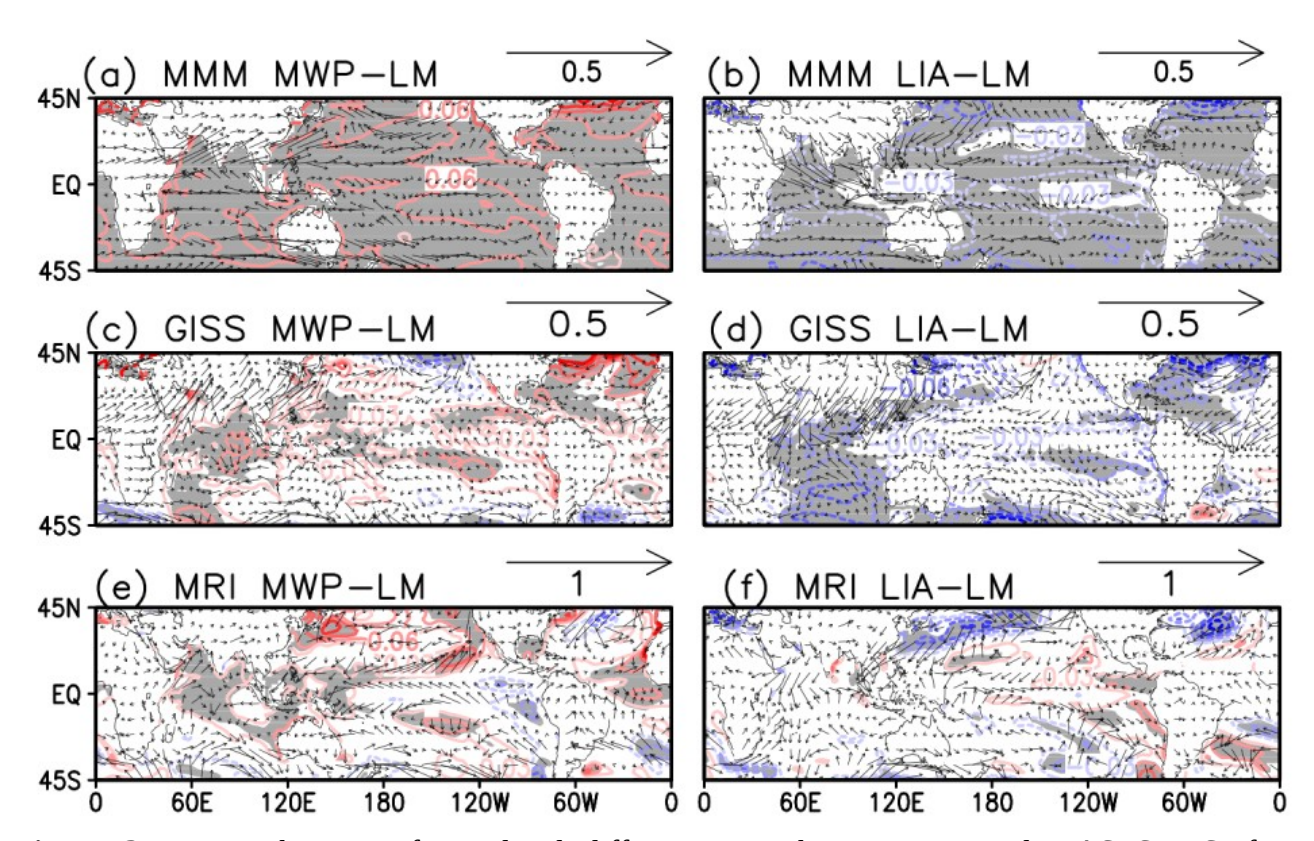


Figure 3.11: Distributions of simulated differences in the time-averaged JJAS Sea Surface Temperatures (SSTs; °C; contours), Statistically significant temperatures at 90% from two-tailed Student's t-test for the SST are shown in grey shading. Differences in simulated 1000 hPa winds (m/s) are also shown. The descriptor string above each panel indicates the name of the model and the periods over which the difference is calculated. In the top panel, for example shows the MMM MWP-LM means MMM model simulated SST(°C) difference during MWP from LM.

We also show in **Figure 3.11,** the simulated MMM SST differences of the MWP from that of the LM, along with the corresponding anomalous SST for the LIA relative to the LM, . It shows that the tropical SST was relatively warmer (cooler) during the MWP (LIA). The background changes in temperatures may modulate the relative strengths of El Niños and La Niñas (e.g., Federov & Philander 2000). This may be a possible cause for more strong El Niños in MWP and La Niñas in LIA. On the other hand, in the recent period, El Niños and La Niñas have been suggested to cause an anomalous increase and decrease in global temperature, respectively (e.g., Trenberth et al. 2002). It will be interesting to explore the cause-and-effect, but beyon the scope of the current study.

Table 3.7: Percentages of 'strong' (a) El Niños with positive (EL⁺) and negative (EL⁻) area-averaged ISMR anomalies, and (b) La Niñas with positive (LN⁺) and negative (LN⁻) area-averaged ISMR anomalies during both MWP and LIA.

dionaires during both wiver and Elizi.								
Models	MWP EL ⁺	LIA EL ⁺	MWP EL ⁻	LIA EL	MWP LN ⁺	LIA LN ⁺	MWP LN ⁻	LIA LN
BCC	30	10	70	90	75	68	25	31
CCSM4	33	44	67	55	71	55	29	45
GISS	29	21	79	78	56	58	43	41
HADCM3	49	22	51	78	69	76	30	23
IPSL	00	13	100	87	97	91	3	8
MPI	32	18	68	82	57	33	42	67
CSIRO	37	15	63	85	70	59	30	38
MRI	30	13	70	87	81	70	19	30
FS2	44	48	56	52	50	43	50	57
AVERAGE	32	23	69	77	70	62	30	38

Positive (+) = Positive anomalies of area-averaged ISMR (AAISMR) Negative (-) = Negative anomalies of area-averaged ISMR (AAISMR)

EL⁺⁽⁻⁾= Positive (Negative) AAISMR Anomalies associated with El Niños LN⁺⁽⁻⁾= Positive (Negative) AAISMR Anomalies associated with La Niñas

A study by Mann et al. 2005, using a Cane-Zebiak type of coupled model, suggests that La Niña-like conditions during the MWP period. In this context, it is pertinent to note several proxybased studies (Cobb et al. 2003; Graham et al. 2007; Mann et al. 2009) suggest either a weak ENSO variance or more La Niñas the MWP period. A study by Henke et al. (2017) using the precipitation proxy data compilation shows a propensity of more El Niño-like LIA than the MWP; however, as per Henke et al., the difference is not statistically significant and is not apparent in a proxy-derived temperature compilation. On the other hand, a study by Conroy et al. (2008) finds that their diatom record is not consistent with the SST interpretation with that of a coral record (Cobb et al. 2003). Specifically, while the diatom record suggests warmer SST in the eastern equatorial Pacific during some part of the medieval period, the coral derived SST indicates a cooling trend in the same location. Conroy et al. (2008) suggest a more heterogeneous SST in the region. Notably, Henke et al. (2017) claim that their result is insensitive to the choice of definition for the MWP and LIA. Therefore, a higher number of the PMIP3-simulated El Niños as compared to La Niñas in almost all the models during the MWP conforms to a good extent with the Conrov et al. (2008) observations and agrees reasonably well with the proxy-temperature analysis of Henke et al. (2017). Given this agreement across the models, which have a more detailed and fuller oceanic component as compared to simpler model used in Mann et al. (2005), the relevance of any positive skewness in ENSOs for global temperature during the MWP (as against the influence of external forcing) needs to be verified by doing some AGCM sensitivity experiments, which we plan to do in the near future. Despite the statistically significant correlations between the simulated AAISMR-NINO3.4 index, it will be interesting to explore any non-linearity in the association. When averaged over the nine models, the percentage of strong El Niño events with concurrent negative AAISMR anomalies (henceforth referred to as EL⁻) is about 69% and 77% during the MWP and LIA, respectively (**Table 3.7**; **Figure 3.12**). To be specific, five models simulate a significantly higher proportion of EL during the LIA (90%, 78%, 85%, 87%, and 82% of strong El Niños in LIA) as compared to

those in MWP (70%, 51%, 63%, 70% and 68% of El Niños in MWP). Other models simulate an almost equal number (up to a difference of 1%) of EL⁻. Thus, we can say that the simulated strong El Niños during the LIA tend to be more 'efficient' as compared to those in MWP in causing negative ISMR anomalies. On the other hand, it is evident from **Table 3.7**, the model-averaged percentage of strong La Niñas with positive AAISMR anomalies (referred to as LN⁺) shows a higher percentage during MWP (70%) than that during the LIA (62%). Five models simulate significantly higher numbers of LN⁺, among all La Niñas during MWP (75%, 71%, 97%, 57%, 70%, 81% and 50%) as compared to those in LIA (68%, 55%, 91%, 33%, 59%, 70% and 43%). One model simulates an almost equal number of LN⁺.

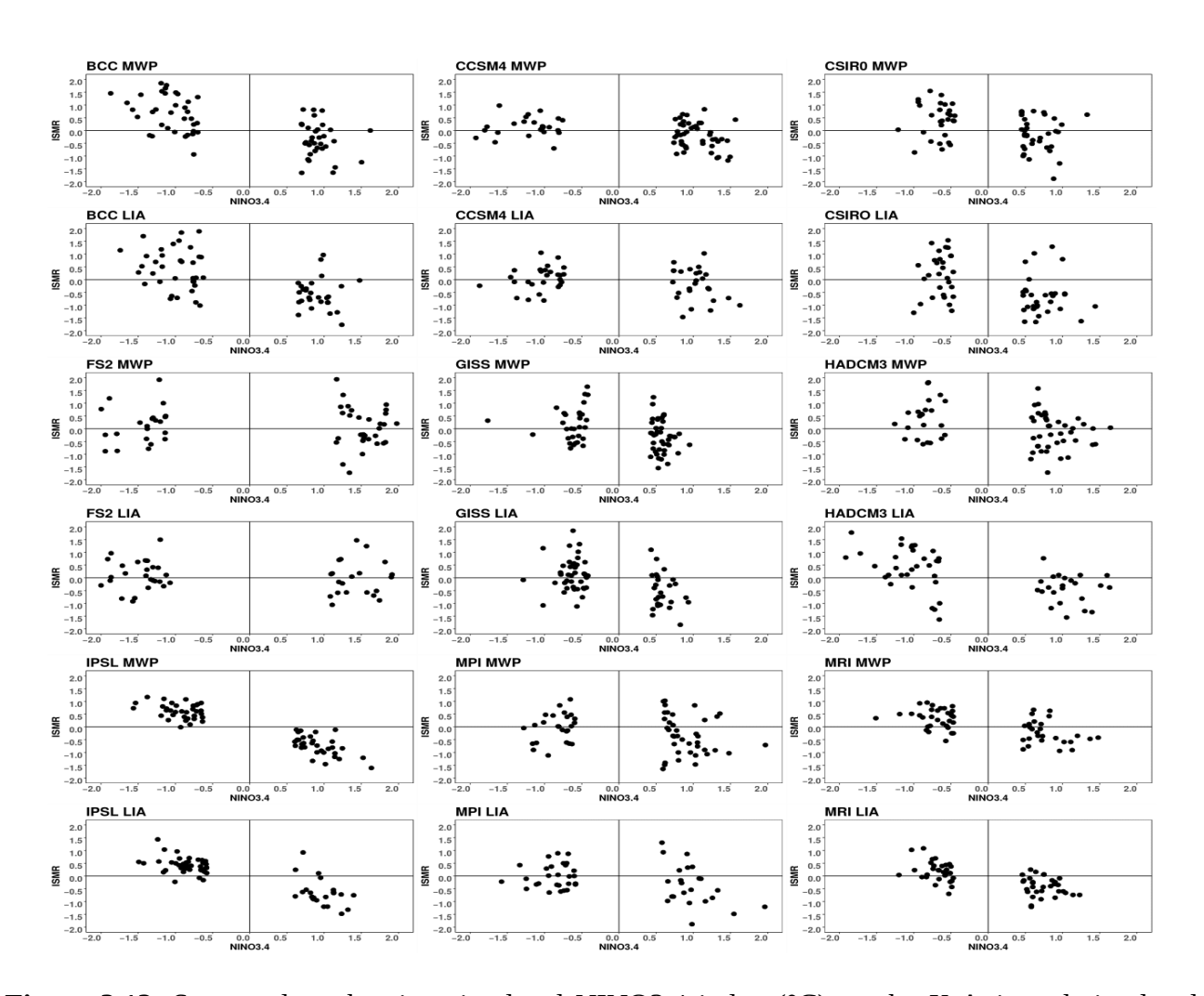


Figure 3.12: Scatter plots showing simulated NINO3.4 index (°C) on the X-Axis and simulated area-averaged ISMR (mm/day) on Y-Axis during both MWP and LIA. The last descriptor string in each panel indicates the name of the model and the period.

Therefore, we infer that the simulated strong La Niñas are apparently more 'efficient' in causing positive AAISMR anomalies during MWP relative to those in LIA. The above results indicate the propensity of the simulated El Niños during the LIA and La Niñas during the MWP to be relatively more 'efficient' in delivering the canonical impact on the summer monsoon rainfall in India, notwithstanding the statistically significant NINO3.4-AAISMR correlations (**Figure 3.10a**). This suggests a possibility of background changes modulating the interannual Indian summer monsoon rainfall-ENSO association. These slow background changes counter the El Niño impacts in several local regions of India. This is why we have a relatively high simulated rainfall over India despite having more El Niños, and the ENSO correlation with the area-averaged rainfall is moderately negative but still statistically significant.

3.3 Dynamics

Figure 3.13 shows the results from the analysis of MMM and the other two representative PMIP3 models to delineate the possible dynamics involved behind the relatively higher ISMR during the MWP period and lesser ISMR during the LIA period over the Indian region. Before going further, we shall briefly ensure that the PMIP3 models were qualitatively able to reproduce the observed zonal convergence/divergence patterns in the tropical Pacific ocean associated with the Walker circulation. We know that the Walker circulation variability is essential for transferring the ENSO impacts on climate elsewhere beyond the eastern tropical pacific.

From the distribution of boreal summer velocity potential at 850 hPa (χ_{850}) simulated by MMM shown in **Figure 3.13**, we see a zone of strong convergence in the central tropical Pacific, flanked by two zones of strong divergence in the equatorial Pacific during the MWP relative to the LM-mean, suggesting a relative westward shift in the Walker circulation during the MWP. This may

suggest a change in background circulation during the MWP compared to the LM-mean and other subperiods such as the LIA.

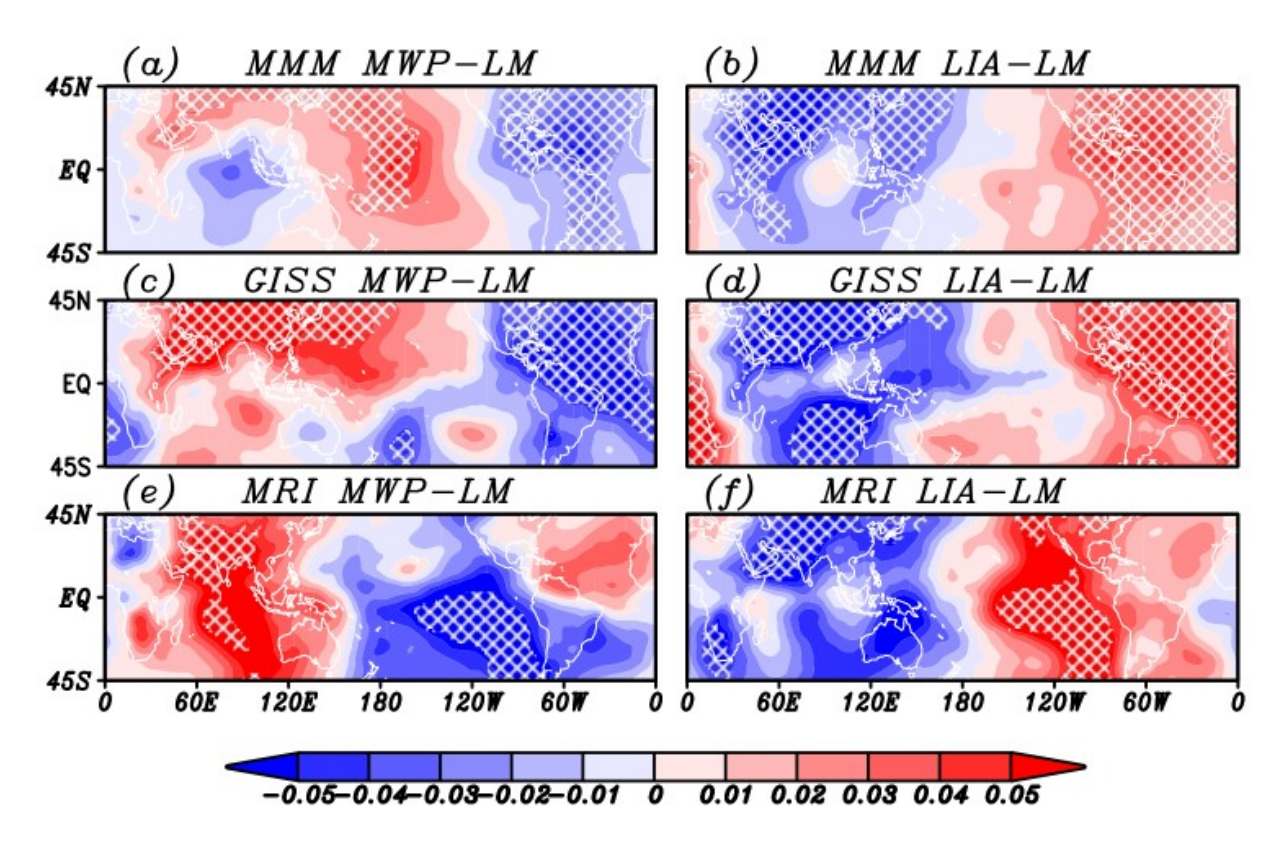


Figure 3.13: Distributions of simulated 850 hPa differences in the time-averaged JJAS velocity potential ' χ 850' (m² s⁻¹) differences. The descriptor string above each panel indicates the name of the model and the periods over which the difference is calculated. The top left panel, for example shows the excess of mean JJAS χ 850 as compared to that for the LM, as simulated by the GISS model. Statistical significance at 80% confidence level from Student's t-test is showed in contours.

Importantly, the simulated strong divergence center in the western pacific extends into the equatorial eastern Indian Ocean, which we believe results in a strong convergence zone over India during the MWP relative to the LM-mean (**Figure 3.13**), and therefore excess rainfall during the MWP as compared to the LM-mean. The differential convergence patterns of the large-scale low-level circulations during the MWP and LIA relative to the historical period (Figures not shown) are qualitatively similar to the anomalous patterns relative to the LM-mean (**Figure 3.13**). Seven models simulate moderately excessive convergence over India during MWP relative to LM-mean, while six models simulate strong divergence over India during the LIA. From **Figure 3.11** and

Figure 3.13, we can say that there is an association in the circulation as mentioned above changes with those in the SST, for example, an increase in low-level convergence of zonal winds over the central equatorial Pacific during the MWP associated with a concurrent increase in the SST relative to the LM-mean condition. The spatial distribution of composite rainfall anomalies over the Indian domain is statistically significant at 0.10 level from a 2-tailed Student's t-test (**Figure 3.14**). Having said this, as a majority of the models indicate a similar sign of anomalies in major portions of the region, the results may qualitatively be considered as conforming across these models. We also see modest warming across the Indian region in all simulations of the MWP (Figures not shown) in agreement with **Figure 3.4b**. The 850 hPa convergence distribution relative to that during the LM (**Figure 3.13**) suggests stronger convergence in the eastern tropical Pacific compared to the LM. An anomalous divergence center over India results in relatively lesser rainfall during the LIA compared to both MWP and LM. From this, it is evident that there is a shift in large-scale Walker circulation patterns.

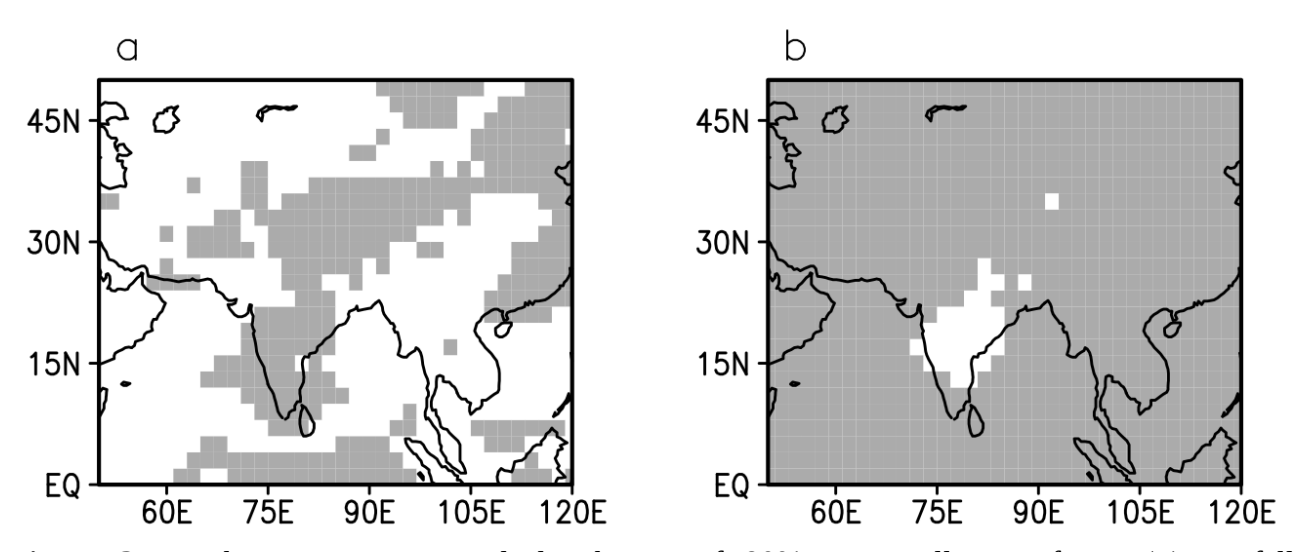


Figure 3.14: The composite spatial distribution of 90% statistically significant (**a**) rainfall anomalies (absolute) (**b**) surface temperature (absolute). Calculated using two sample Student's t-test.

Importantly, we also find a general increase in simulated specific humidity during MWP, particularly in the tropics compared to the LM-mean (**Figure 3.15**). This may indeed be due to an increase in temperature during MWP. We also find an anomalous increase in the simulated moisture transport into the Indian region during the boreal summer monsoon, mostly significant during both the MWP and LIA (**Figure 3.15**). The increased background convergence over India (**Figure 3.13**) during the MWP likely facilitates this inward excess of background moisture transport. This, along with the increase in local moisture retained in the atmosphere owing to the increasing temperature (**Figure 3.15a**), may have resulted in a relative increase in ISMR during the MWP in a majority of the models.

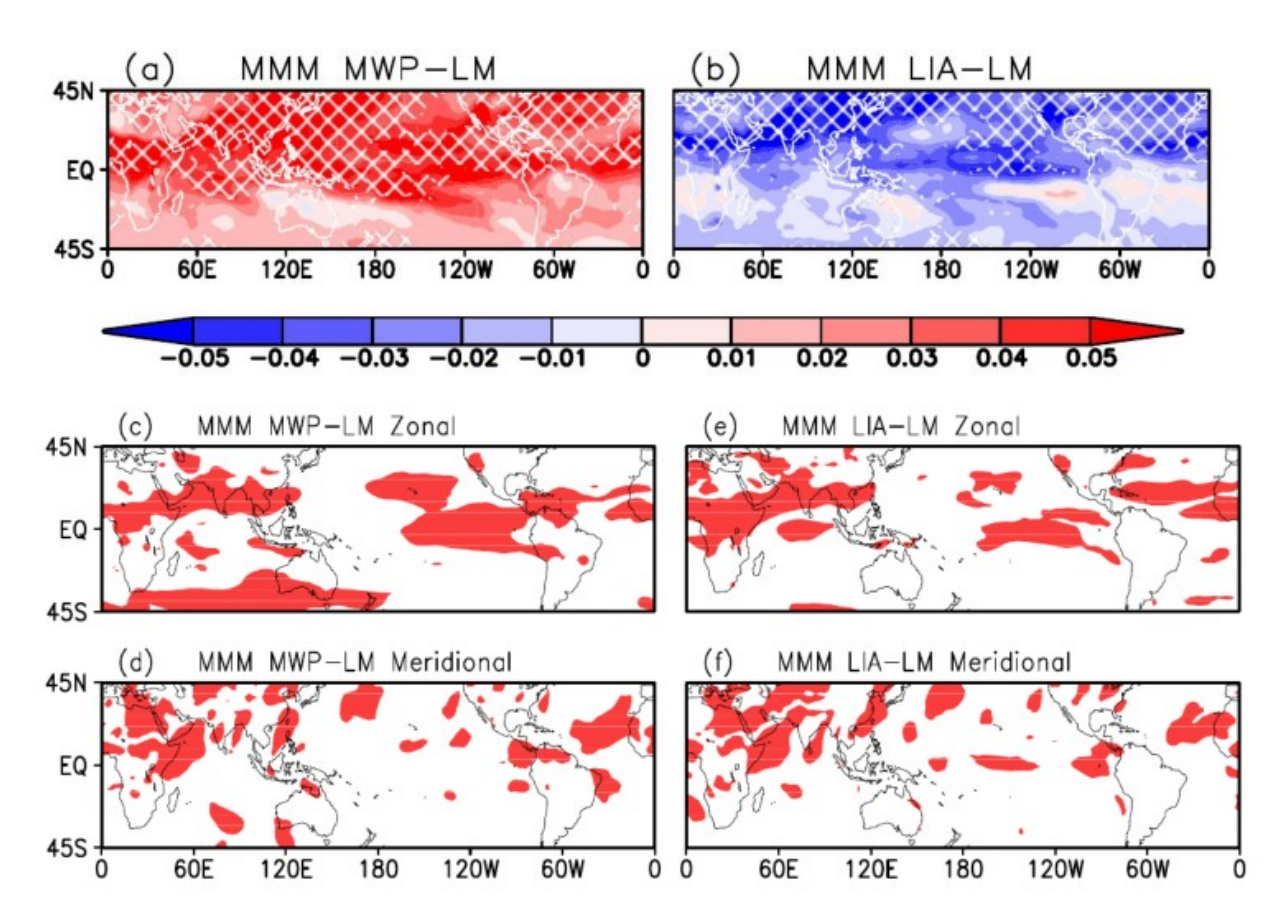


Figure 3.15: The MMM distributions of simulated differences (from the LM mean) in the 850 hPa for JJAS season specific humidity for (a) MWP and (b) for LIA. Statistically significancat specific humidity differences at 95% significance level from two-tailed Student's t-test are marked with hatched region. Panels (c), (d), (e) and (f) show the distributions of JJAS season simulated zonal and meridional for 90% statistically significant moisture transport at 850 hPa from two-tailed Student's t-test in shaded. The descriptor string above each panel indicates the name of the model and the periods over which the difference is calculated.

3.4 Summary

Proxy reconstruction-based studies (Dixit and Tandon, 2016 and references therein) show two significant climate periods in the last millennium (LM): (1) Medieval Warm Period - a relatively warm period (MWP, CE 950–1350) and (2) the Little Ice Age - a relatively cooler period (LIA, CE 1500–1850). Interestingly, the ISM variability regarding the above-mentioned climatic events is relatively less studied from the modeling perspective.

To complement the proxy-studies, We carried out an analysis with the available nine PMIP3 models. I find that all the models simulate the warming MWP and cooler LIA during epochs CE 1000–1199 and CE 1550–1749 roughly commensurate with the proxy-observations. A majority of the models qualitatively reproduces a wetter (drier) Indian summer monsoon season in the MWP (LIA) relative to the mean Indian summer monsoon during the LM. The PMIP3 models simulate a statistically significant ENSO-Monsoon association during the LM similar to the current day climate. Interestingly, we find many strong simulated El Niños (La Niñas) during the LIA (MWP) having a relatively more 'efficient' canonical impact, notwithstanding the statistically significant NINO3.4-ISMR correlation. Importantly, most models simulate more 'strong' El Niños during MWP as compared to 'strong' La Niñas. Furthermore, most models simulate more 'strong' La Niñas during the LIA as compared to 'strong' El Niños. Despite such a relatively high occurrence of strong El Niños relative to the LIA, a relatively westward shift in the simulated anomalous summer Walker circulation compared to the mean LM condition. This change in background circulation is apparently associated with a simulated background change in the tropical Indo-pacific SST in most models. The multi-decadal/centennial shift Walker circulation is reflected in an apparent anomalous divergence in the equatorial eastern Indian Ocean during the MWP, resulting in concurrent anomalous convergence and excess rainfall in the Indian region. Some model studies (e.g., Ashok et al. 2004) indicate that a presence of anomalous low-level divergence in the eastern equatorial Indian Ocean is critical in causing an anomalous divergence over the peninsular Indian region and thereby leading to less than mean rainfall there. All this suggests a modulation of the interannual ISMR-ENSO associated with slow background changes. It is reasonable that the convergence/divergence patterns in the eastern equatorial Indian Ocean, which is more of a peripheral region for ENSO impact, may change depending on the background changes in circulation. Importantly, the relative increase in the simulated ISMR during the MWP is also associated with increased specific humidity and increased moisture transport into the Indian region during the MWP.

Chapter 4

Indian summer monsoon variability during the mid-Holocene

In this chapter, using the paleoclimate modelling intercomparison project phase 3 (PMIP3) and coupled model intercomparison project phase 5 (CMIP5) coupled model simulations, we discuss in detail on the simulated mean Indian summer monsoon during the mid-Holocene (MH; 6 kyr BP) period, its seasonal cycle and interannual variability, mainly the i.e. state, ENSO-ISM relationship, and dynamics involved. The simulations are compared to simulations for the HS (CE 1850-2005) period, which can be deemed as for the 'current period', i.e. 0 kyr BP. The primary difference between the forcings of the MH and HS stems from the solar insolation induced by the changes in orbital parameters (**Table 4.1**). During the MH period, the axial tilt of the Earth is 24.1° which leads stronger solar annual cycle in northern and southern hemisphere. Apart from the axial tilt, the precession during the MH may have facilitated intensification of the Northern hemisphere annual cycle because the perihelion occurs during the boreal summer. This results in the stronger monsoons over the northern hemisphere during the MH comparing to the present day monsoon strength. Keeping this in mind, we will discuss about the mean state, seasonal cycle, and ENSO-ISM relationship during the MH period in comparison with current day climatic conditions, using the multiple coupled model simulations. As discussed in Chapter 2, for this analysis, we use simulations from the twelve models.

Table 4.1: Orbital parameters of the different climatic periods.

Parameters	Time 1	Period
	MH	HS
Eccentricity	0.02	0.02
Obliquity	24.105°	23.446°
PERI-180	0.87°	102.04°

4.1 Annual cycle

In **Figure 4.1,** we show the evolution of the area-averaged seasonal cycle of simulated rainfall and that of the surface temperature for the Indian region the Mid Holocene (MH). The seasonal cycle evolution for the multi-model mean (MMM) is also presented along with those for the individual models. From **Figure 4.1**, it is clear that the seasonal cycle evolution simulated by all the models is similar to those seen in the historical time periods. However, there is inter-model spread in the simulated rainfall (**Figure 4.1a**), which is maximum during the months of June to September, the summer monsoon season.

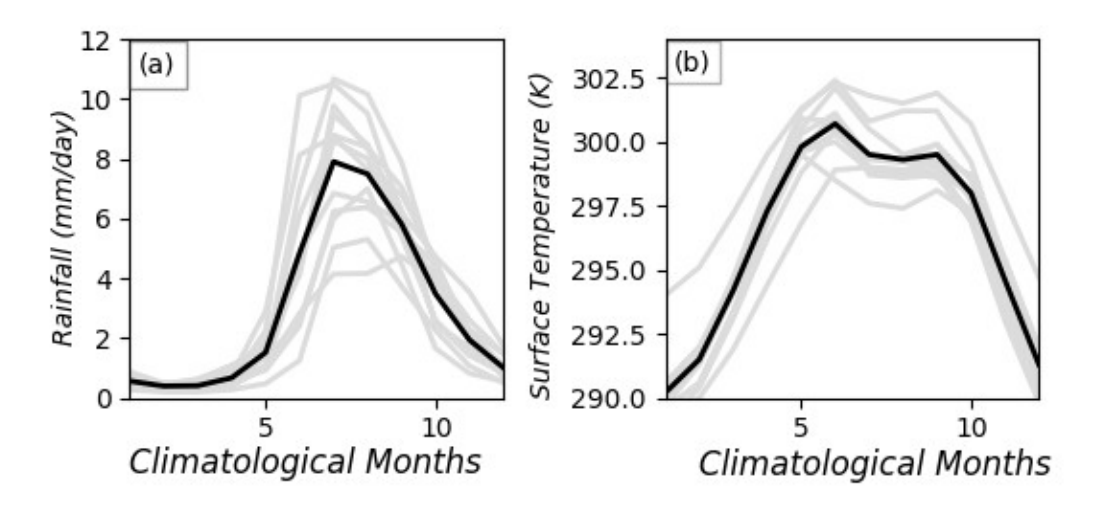


Figure 4.1: Comparisons of simulated area-averaged climatological cycle, for the MH (CE 0850-1849) period (**a**) rainfall and (**b**) surface temperature over the Indian land region (65°E–95°E; 10°N–30°N). MMM is shown as (black line) and PMIP3 models in grey lines.

We also show the spatial distribution of the latitudinally- averaged (over 10°N to 30°N) seasonal cycle of simulated rainfall and surface temperature for the Indian region for MH for the MMM in **Figure 4.2**. From the **Figure 4.2a**, we see that during the summer monsoon months, Eastern Indian region receives more rainfall than the western Indian region. During the pre-summer monsoon months, the central Indian region is warmer compared to the other parts of Indian region in LM (**Figure 4.2b**).

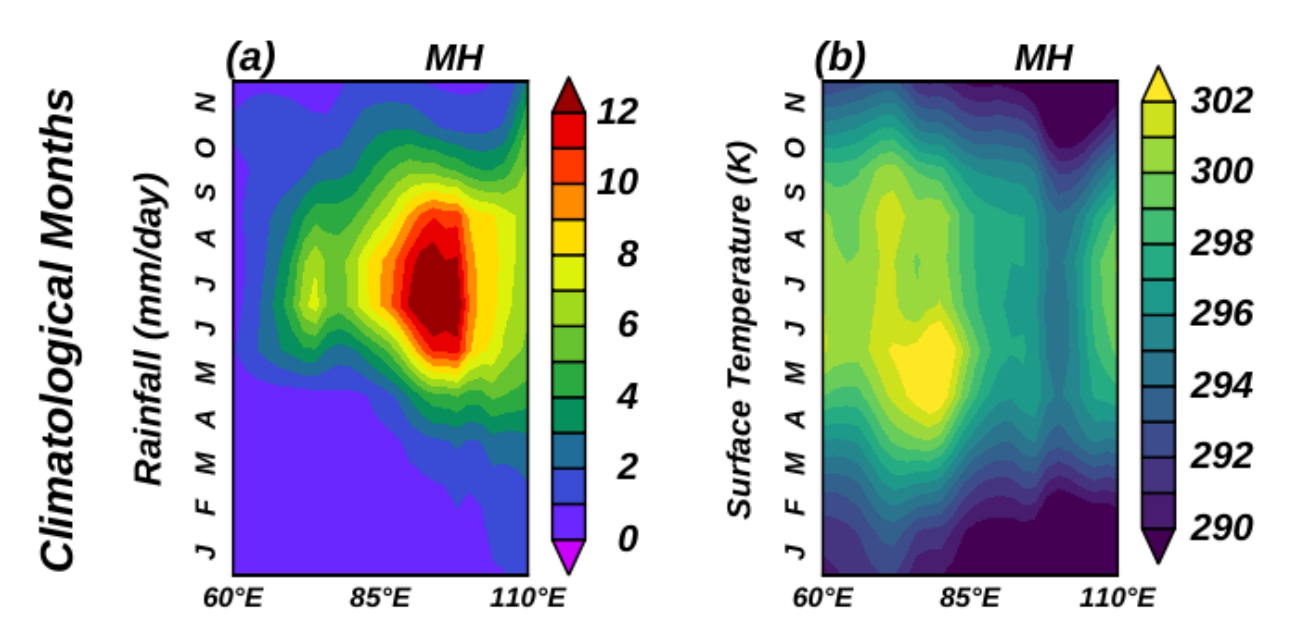


Figure 4.2: Spatial distribution of the latitudinal (10°N to 30°N) averaged seasonal cycle of simulated (**a**) rainfall (mm/day) and (**b**) surface temperature (K) of the Indian region for MH for the MMM.

4.2 Mean state

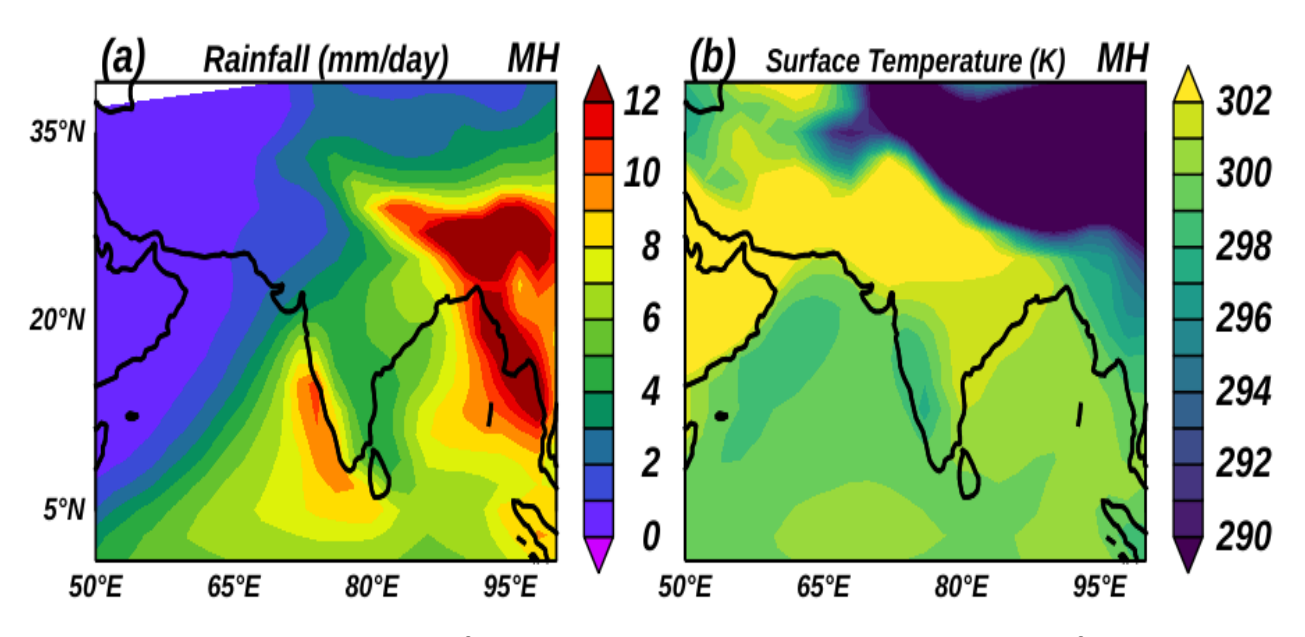


Figure 4.3: Spatial distributions of the simulated mean summer monsoon (**a**) rainfall (mm/day) and (**b**) surface temperature (K) during the MH.

In **Figure 4.3**, we present the mean state of spatial distributions of simulated rainfall and surface temperatures of MH period for the summer monsoon months of June to September (JJAS)

for the MMM. From the **Figure 4.3**, we can see that western ghats and north eastern Indian region received more rainfall during the MH (**Figure 4.3a**) and central to northern Indian regions warmer compared to the rest of the Indian regions (**Figure 4.3b**). The rainfall pattern is dynamically consistent with the surface temperatures over the Indian land region.

4.3 Interannual variability of ISM

In **Figure 4.4**, we show the spatial distributions of the simulated summer monsoon rainfall during the MH climate period relative to HS. We found that all the 12 models simulate a relatively excess summer monsoon rainfall during MH across the Indian region. All the model simulations also show, in general, a cooler MH period relative to the HS (**Figure 4.5**).

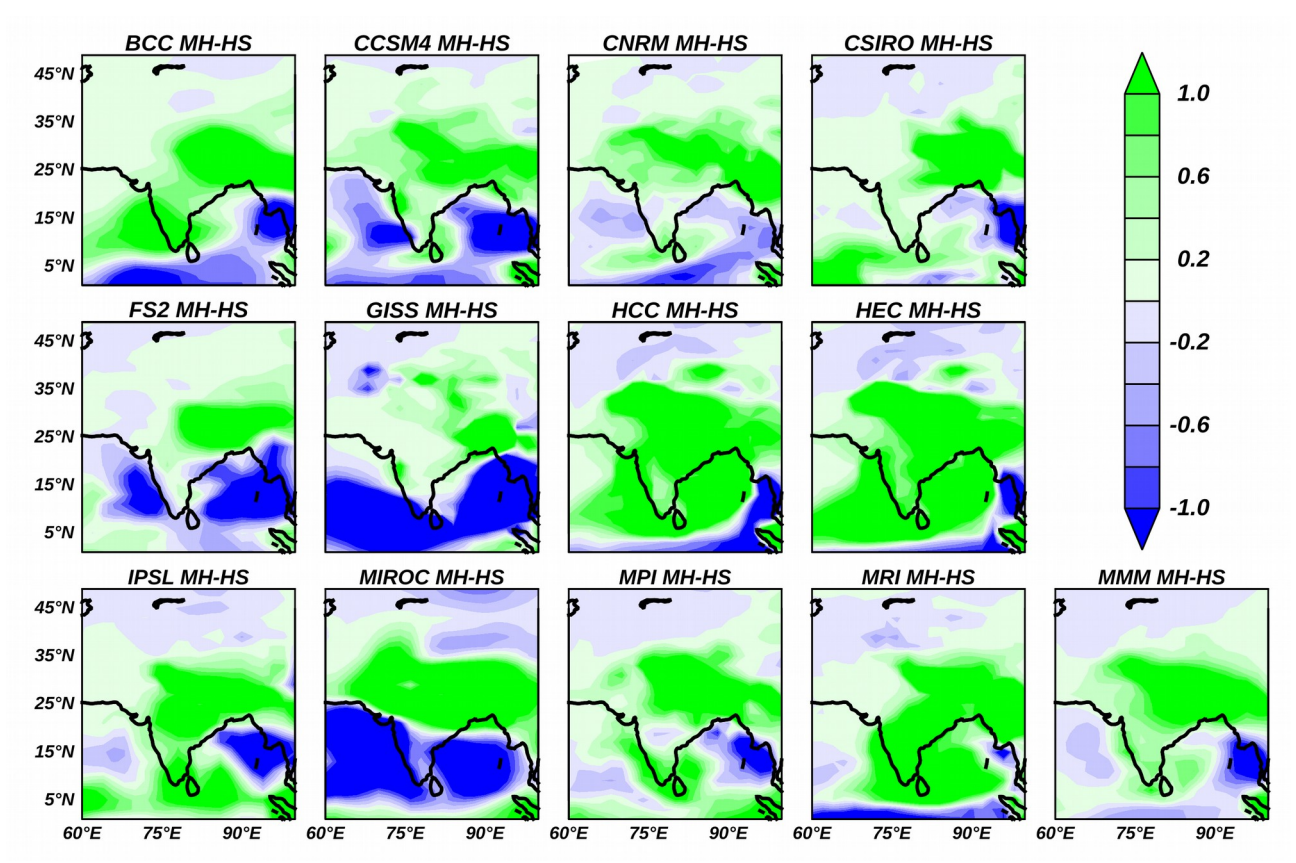


Figure 4.4: Spatial distributions of the simulated summer monsoon rainfall (mm/day) during the MH compared to the HS period. The descriptor string above each panel indicates the name of the model and the periods over which difference is calculated.

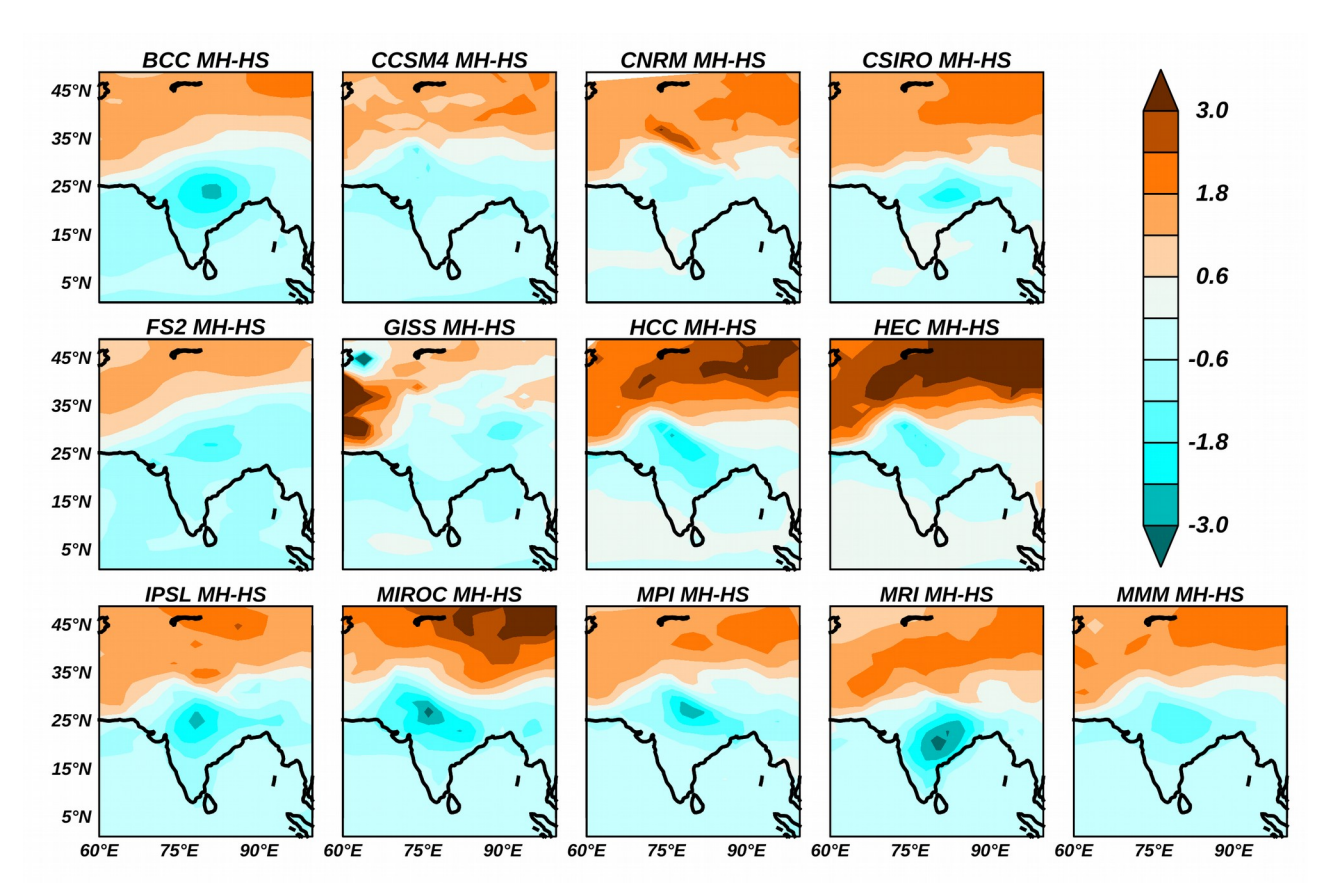


Figure 4.5: Spatial distributions of the simulated summer monsoon surface temperatures (kelvin) during the MH compared to the Hs period. The descriptor string above each panel indicates the name of the model and the periods over which difference is calculated.

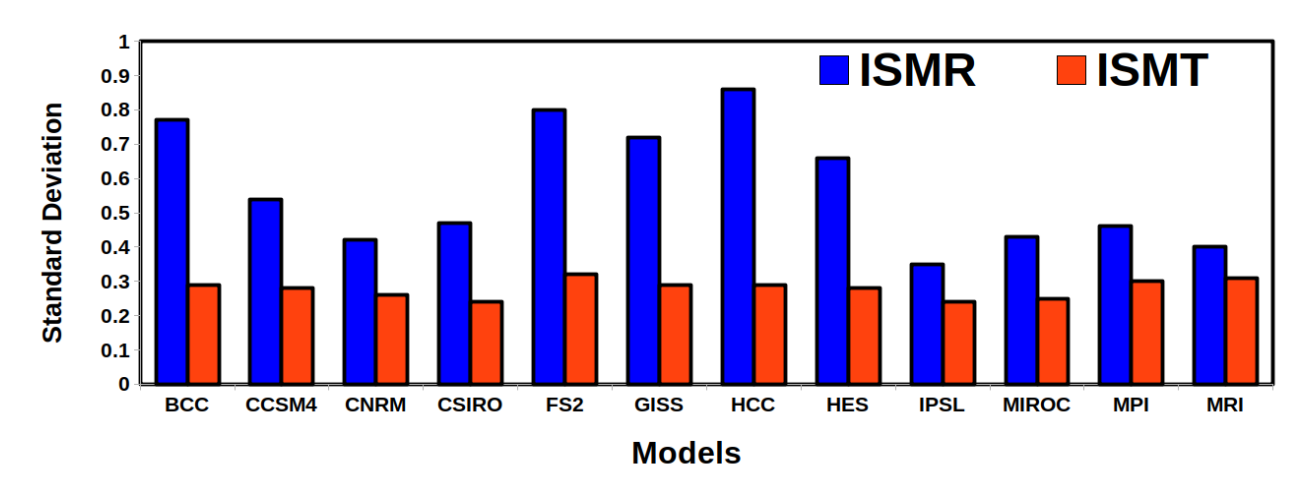


Figure 4.6: Standard deviations of simulated Indian summer monsoon rainfall (ISMR; blue bars) and Indian summer monsoon surface temperatures (ISMT; red bars) for the MH period.

Furthermore, to check the ISM stability, we show the ISM rainfall and ISM surface temperatures variances for all the models in **Figure 4.6**. The simulated ISM rainfall variance is higher in all the models compared to the ISM surface temperatures.

4.4 El-Niño southern oscillation and ISM

ENSO being a major climatic driver for the ISM variability, it will be informative to check the ENSO-ISM association in the simulated MH climate. We have calculated the linear correlations of the NINO3 and NINO3.4 indices with the area-averaged ISM rainfall, and surface temperatures respectively (**Figure 4.7**). It is clearly seen that majority of the PMIP3 models simulate negative ENSO-ISMR correlation during the MH except CNRM, FS2 and MIROC models (**Figure 4.7a**). Also, the PMIP3 models simulate the positive ENSO-ISM surface temperature correlation during the MH except CNRM model (**Figure 4.7b**); most of the correlations, however, are significant at 0.05 level from Student's 2-tailed test.

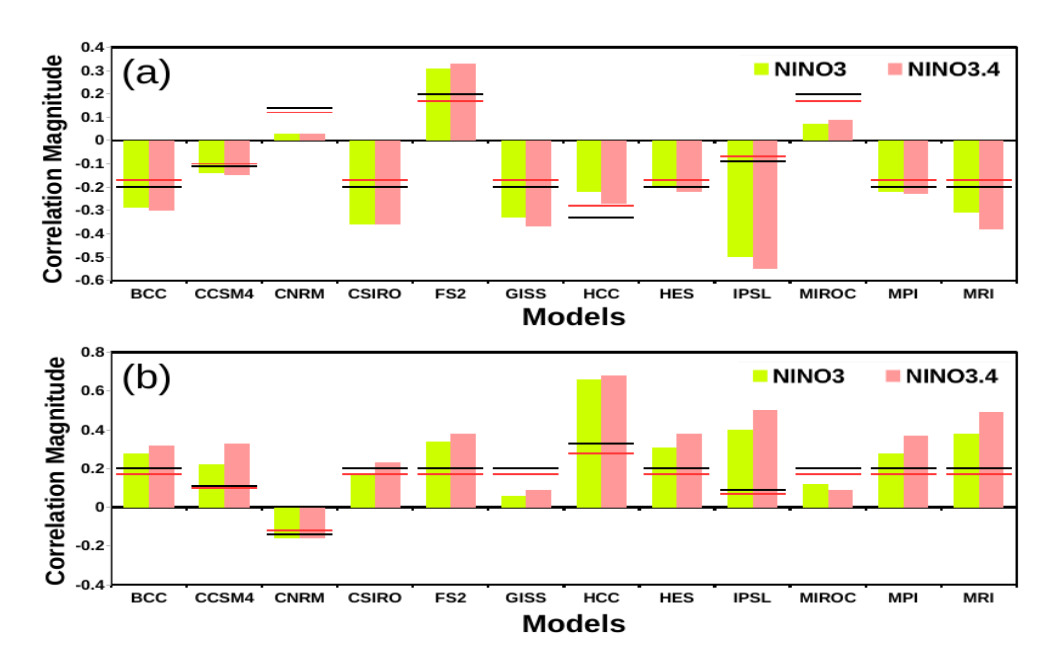


Figure 4.7: Simulated correlations, for each model, during MH of NINO3 index (light green bars) and NINO3.4 index (light red bars) between the (**a**) Area averaged ISMR, and (**b**) Area averaged ISMST. Black line shows the significant value at 0.05 level and Red line show the significant value at 0.10 level from a 2-tailed Student's t-test.

Apart from the area-averaged correlations, we show the spatial plot of the linear correlations between the NINO3.4 index with the area-averaged ISM rainfall (**Figure 4.8**), and surface

temperatures (**Figure 4.9**) respectively. From **Figure 4.8**, we can see that the majority of the models simulated a negative correlations between NINO3.4 Index and ISMR and positive and between NINO3.4 and ISM surface temperatures over the central to north Indian region (**Figure 4.9**). We have also calculated the linear regression coefficients of the NINO3 and NINO3.4 indices with the area-averaged ISM rainfall for both the MH and HS periods (**Figure 4.10**). From **Figure 4.10**, we can see that majority of the models show weak magnitudes during the MH period compared to the HS.

Table 4.2: Boreal summer interannual standard deviations of NINO3 Index(°C) and NINO3.4 Index

(°C), as simulated by CMIP5/PMIP3 MH and HS simulations.

Models	NINO3 Index (°C)		NINO3.4 Index (°C)	
	MH	HS	MH	HS
BCC	-0.29	-0.2	-0.3	-0.19
CCSM4	-0.14	-0.35	-0.15	-0.33
CNRM	0.03	-0.42	0.03	-0.41
CSIRO	-0.36	-0.44	-0.36	-0.43
FS2	0.31	0.01	0.33	0.05
GISS	-0.33	-0.27	-0.37	-0.26
HCC	-0.22	-0.38	-0.27	-0.4
HES	-0.2	-0.4	-0.22	-0.41
IPSL	-0.5	-0.67	-0.55	-0.72
MIROC	0.07	0.02	0.09	0.08
MPI	-0.22	-0.43	-0.23	-0.47
MRI	-0.31	-0.33	-0.38	-0.28

Furthermore, to check the ENSO stability, we compare the simulated JJAS ENSO variance for the MH period compared them with that during the HS period (**Table 4.2**). A majority (eight) of the models show a relatively-weak simulated variance during the MH period compared to the HS. This suggests that despite the significant correlation between the ISMR and the NINO3.4 index, the simulated ENSOs during the MH are relatively weaker.

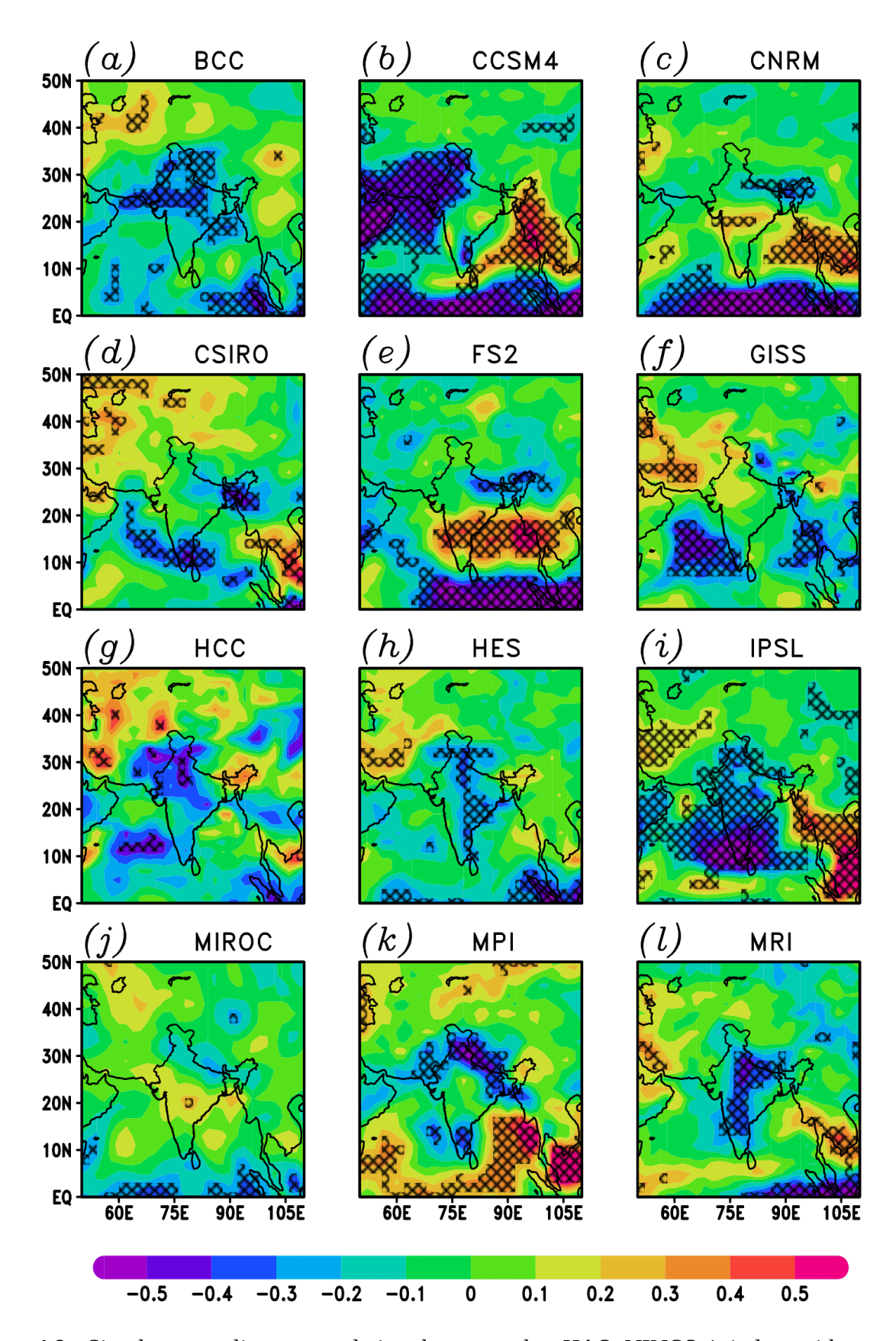


Figure 4.8: Simultaneous linear correlation between the JJAS NINO3.4 index with summer monsoon rainfall for MH period. Hatching indicates significant correlation values at 0.05 significance level from a 2-tailed Student's t-test.

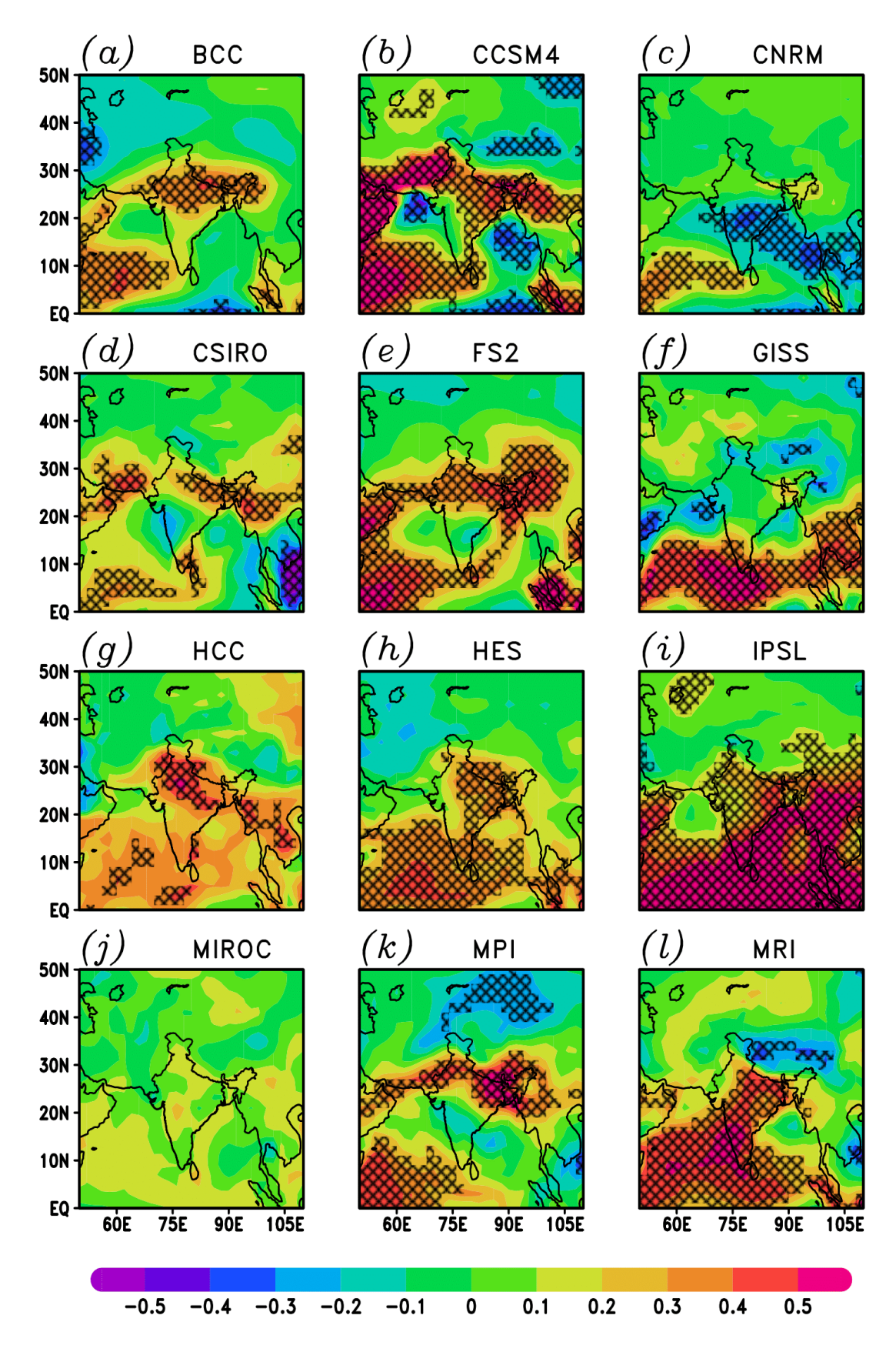


Figure 4.9: Same as Fig. 4.8 but for simultaneous linear correlation between the JJAS NINO3.4 index with monsoon surface temperatures for MH period.

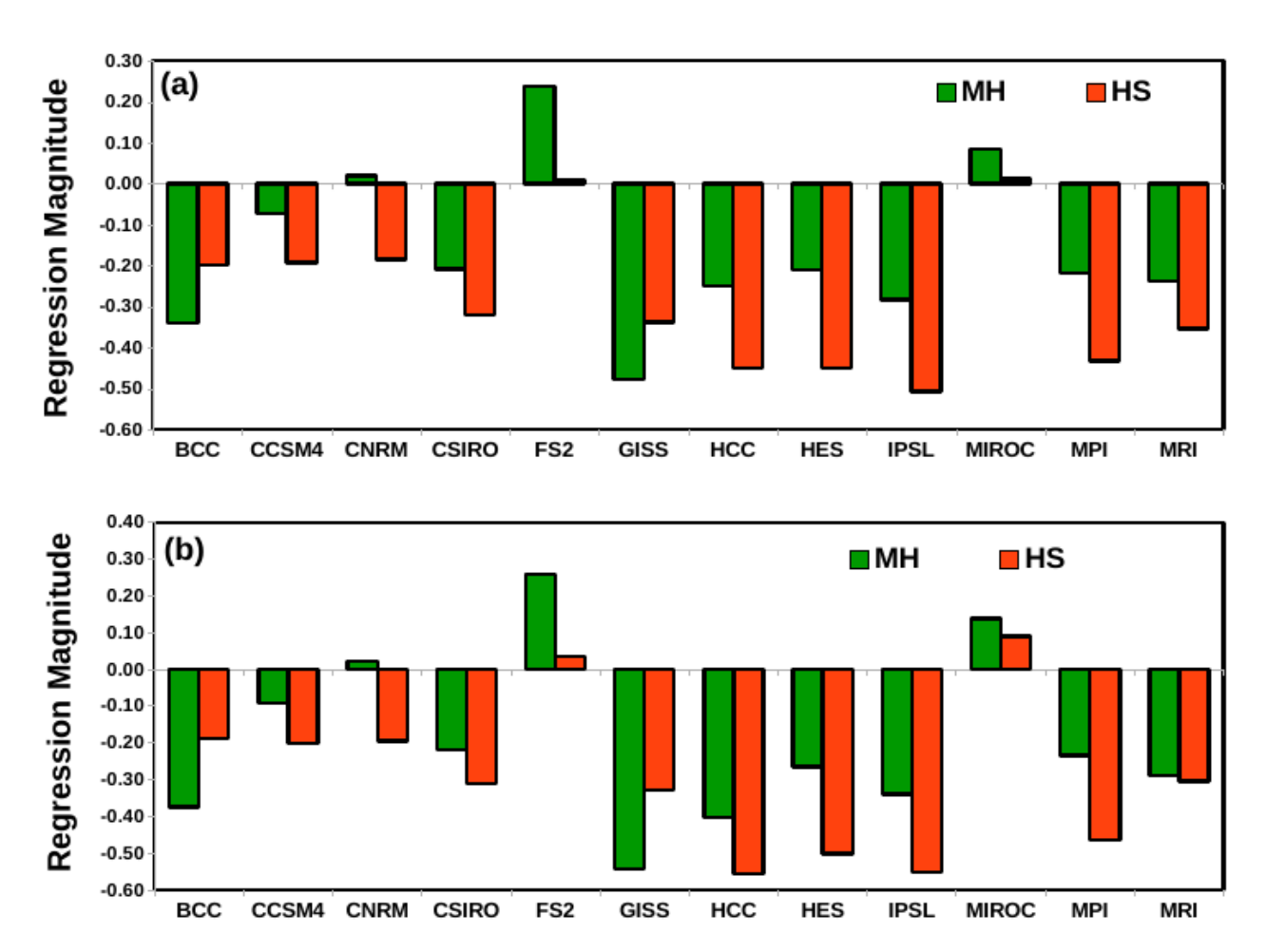


Figure 4.10: Simulated regressions, for each model, during both MH and HS periods between Area averaged ISMR and (a) NINO3 index, (b) NINO3.4 index.

4.5 Possible dynamics

The simulations for the MH suggest that, a major part of the Indian subcontinent received surplus summer monsoon rainfall during the period (**Figure 4.11a**) and relatively cooler region (**Figure 4.11b**) compared to the HS period. A Relatively stronger zonal seasonal mean SST gradient in the tropical Indian Ocean, with a warmer (cooler) eastern (western) tropical Indian Ocean by $0.1^{\circ}\text{C}\sim0.2^{\circ}\text{C}$ (**Figure 4.11c**) relative to the HS, provides a positive IOD-like background. Interestingly, the sea surface temperature difference between the MH and HS from the MMM show

a El Niño type signal in tropical eastern Pacific ocean. During the MH period, we see a stronger lower pressure in the monsoon trough region northward of 20°N relative to the HS (**Figure 4.11d**). This indicates the northward migration of the ITCZ, which is also seen in simulations by a few other AGCMs and coupled models of older vintage (e.g. Zhao and Harrison, 2012); the strengthening of the subtropical high over the western pacific also apparently strengthens the monsoonal circulation over northern India (**Figure 4.11d**). It raises a question of whether the increase in the MH summer rainfall over India during the MH, despite the El Nino is due to a northward shift of the ITCZ.

We show the velocity potential for the MH period relative to that for the HS at 850 hPa and overlaid by the monsoon circulation at the same height in **Figure 4.12a** and same for the at 100 hPa in **Figure 4.12b**. It is evident that the Indian subcontinent was home to large scale low-level convergence during the MH relative to that for the HS period at 850 hPa and high-level divergence 100 hPa. The tropical dynamics suggest that the presence of the entrance of Tropical Easterly Jet (TEJ) over the Bay of Bengal (BoB) facilitates strong convection over BoB and neighbouring coastal regions of India. Briefly, the TEJ originates over the Western Pacific and BoB. The Quasi-geostrophic dynamics Hoskins and Wang (2006, section 9.5.2) suggest that the westward intensification of easterlies in the TEJ over the BoB and adjoining Indian region results in an ageostrophic convergence and upward motion at the mid-troposphere, and consequently, enhanced rainfall. We find an increase in the simulated 500 hPa relative vorticity (**Figures 4.12c**) on the central east coast of India, particularly near to the Head BoB and/or over the neighbouring Indian region, where we see a higher summer monsoon rainfall during MH (**Figures 4.11a**).

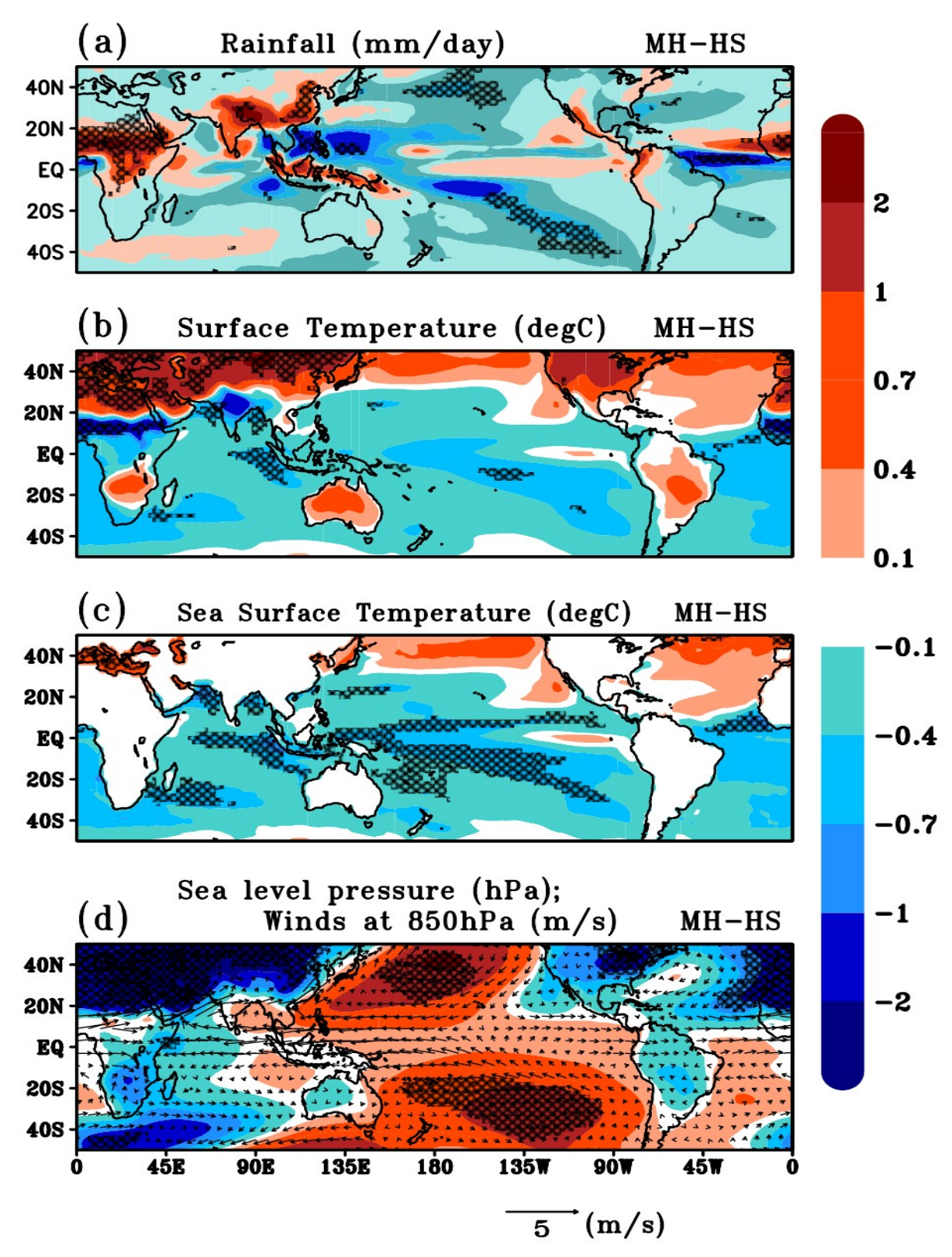


Figure 4.11: Spatial distributions of simulated summer monsoon **(a)** rainfall (mm/day) **(b)** surface temperature (°C) **(c)** sea surface temperatures (°C), and **(d)** sea level pressure (hPa), overlaid by the summer monsoon winds (m/s) at 850 hPa difference in the between MH and HS. Statistical significance at 80% confidence level from Student's t-test is showed in hatched region.

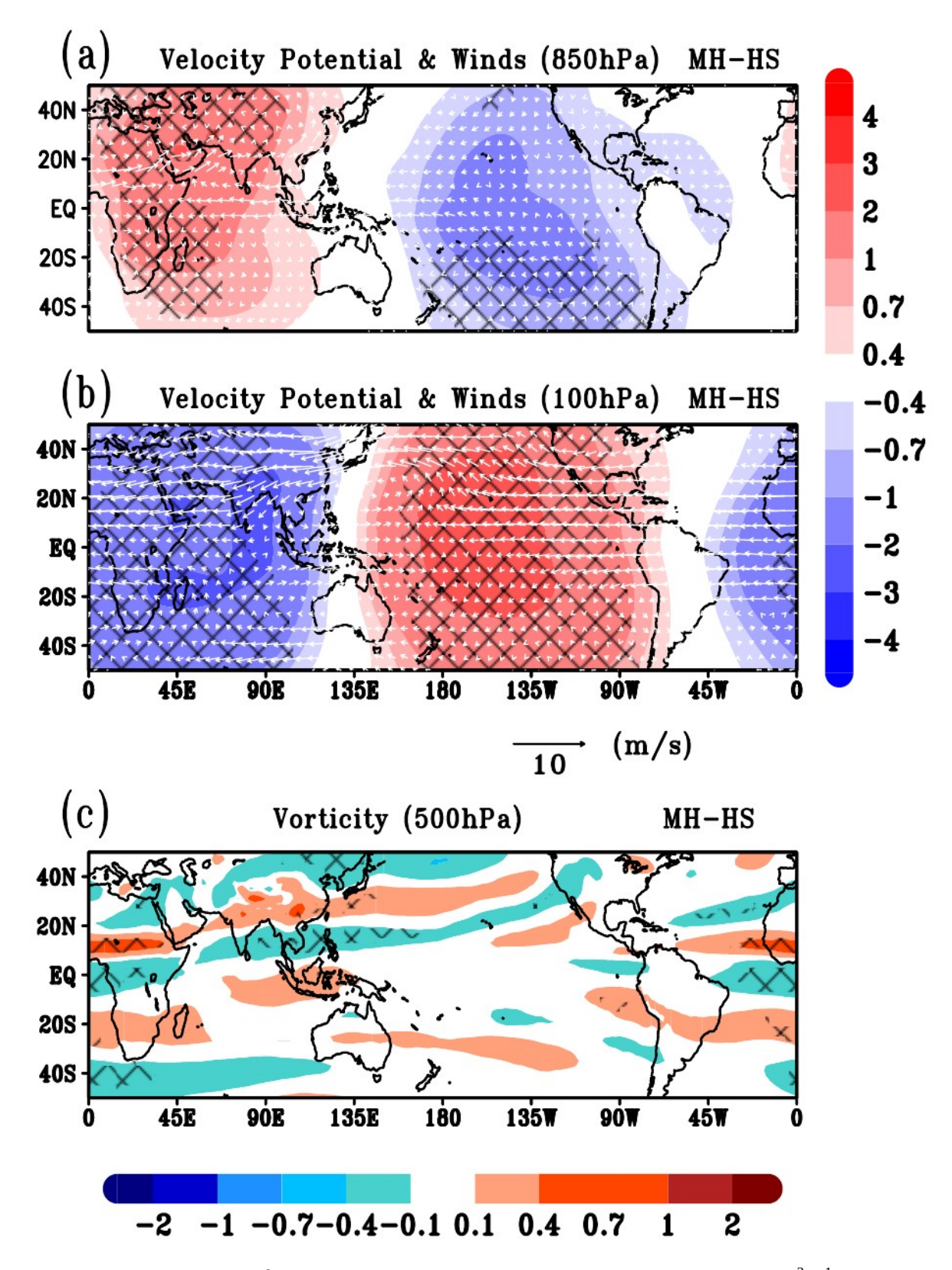


Figure 4.12: Distributions of simulated summer monsoon velocity potential ' χ ' (m² s⁻¹) and overlaid by summer monsoon winds (m/s) differences between MH and HS periods (**a**) at 850 hPa and (**b**) at 100 hPa. Panel (**c**) show Distributions of simulated differences in the summer monsoon vorticity at 500 hPa. Statistical significance at 90% confidence level from Student's t-test is showed in hatched region.

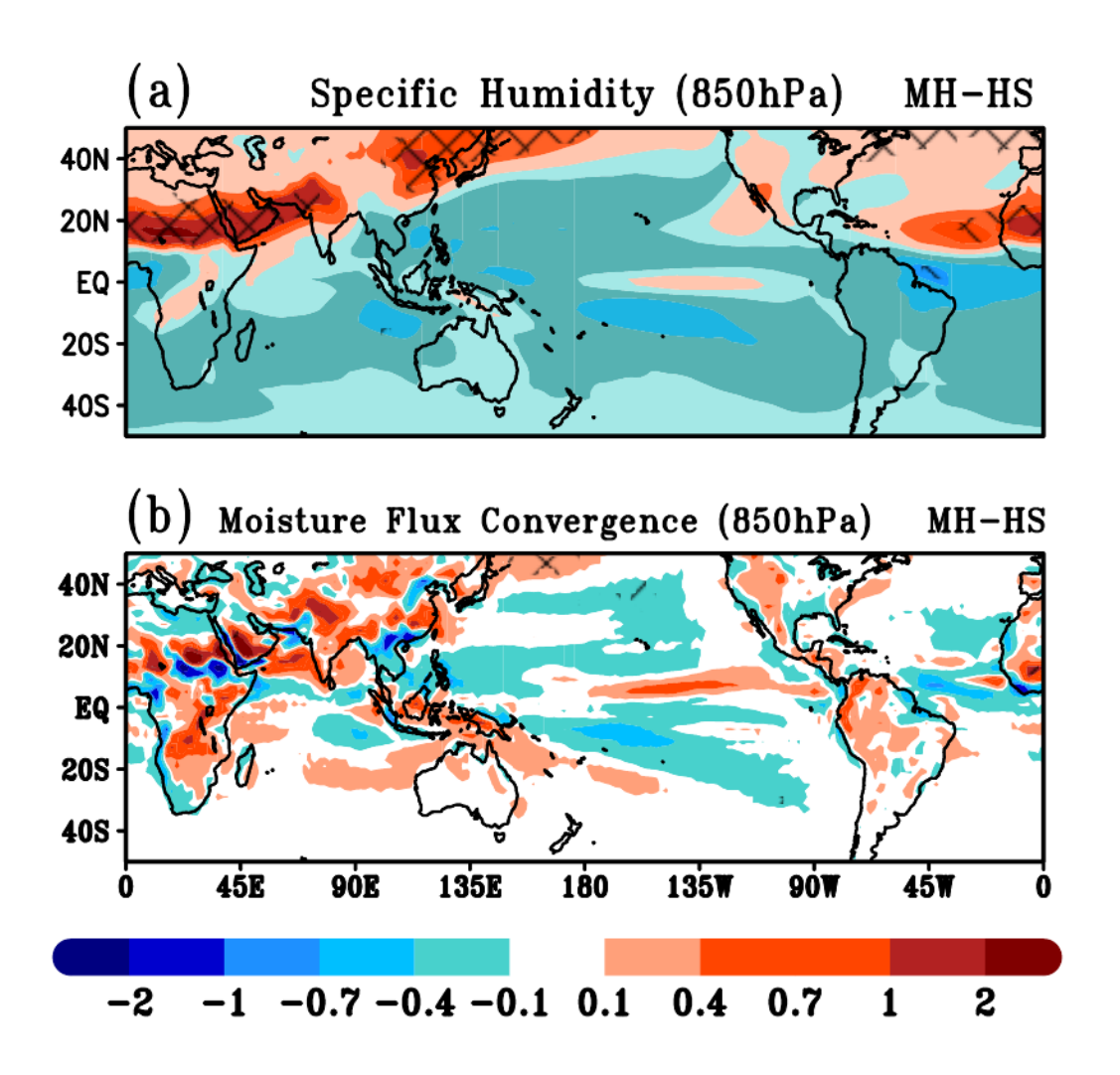


Figure 4.13: Spatial distribution of the simulated 850 hPa differences in the summer monsoon (**a**) Specific humidity (g/kg) and (**b**) Moisture Flux Convergence (X 10⁻⁵ g/(kg-s)). Statistical significance at 80% confidence level from Student's t-test is showed in hatched region.

The differences in the 500 hPa vorticity (**Figure 4.12c**) confirm that the simulated circulation changes are relatively strong over the northern Indian region relative to HS. This suggests that the strengthened TEJ during the MH could be a factor for the enhanced rainfall over the core monsoon region (CMR) during the MH. Such a changing role of the TEJ in enhancing the Indian summer monsoon during the MCA to LIA has also been simulated by the majority of the models, as discussed in the PhD thesis of Bidyabati (2020), and in a related manuscript (Ashok et al., 2021, under revision with the I. J. Climatol.).

We show the simulated low-level simulated specific humidity during the MH relative to the HS in **Figure 4.13a** and the simulated low-level moisture flux convergence change into the Indian region between MH and HS in **Figure 4.13b**. From **Figure 4.13**, we see that during the MH summers, Indian region is associated with high amount of simulated specific humidity and more moisture flux convergence at 850 hPa compared to the HS. These changes in the large-scale low-level circulation, available moisture convergence and strengthened subtropical high etc., during the summer monsoon season are potential reasons for the precipitation changes over India during the MH compared to the HS.

4.6 Summary

Several proxy studies such as Rawat et al., 2015 and Band et al., 2018 suggest that the Indian summer monsoon (ISM) during the mid-Holocene (MH; ~6000 yr BP) was characterized by a wet climate relative to the current day. The few available modeling studies (Kumar et al., 2018 and Tejavath et al., 2020 etc.) also suggest that the ISM was indeed stronger at that time. Interestingly, proxy-based (Mukherjee et al., 2016) and model-based studies suggest that external factors such as changes in the orbital parameters, changes in solar forcing induced by volcanic eruptions, land surface, and vegetation changes, etc., may have played an important role in evolving a distinct climate of the Earth during MH relative to the current day (Crétat et al., 2020).

In this chapter, we report results from an analysis of 12 PMIP3 model outputs have been carried out. Our analysis shows that all the PMIP3 models simulate a wet and cold summer monsoon during the MH period relative to the HS. The rainfall and surface temperature response seems to be homogeneous across all the model simulations analysed for the MH period compared to the HS. We have to bear in mind that the resolution of the models is rather coarse. Consequently,

response at local levels may not adhere to that from the area-averaged analysis. The relatively high Indian summer monsoon simulated for the MH period is in broad conformation with the inferences from proxy studies. The changes in the large-scale low-level circulation patterns and strengthening of the TEJ at the 100 hPa may also have apparently played a major role in the precipitation changes over the Indian during the MH period compared to the HS period.

The simulated variance of the NINO3.4 and NINO3 indices, which represent of the ENSO activity, shows a decrease in variance during the MH period compared to the HS period. The simulated ENSO–ISMR correlations are significantly negative and ENSO-ISM surface temperatures are positive for the majority of the models. However, the variance of these simulated ENSO indices is relatively weak compared to the HS, suggesting a limited role of the ENSOs in Indian summer monsoon variations. It would be important to check whether the changes in large scale summer monsoon circulation during MH could be attributed to the changes in the tropical Indo-pacific characteristics, which themselves may or may not have been modulated by the solar forcing changes.

Chapter 5

Simulating the Indian summer monsoon during Mid-Holocene and Last Millennium

As mentioned in chapter 1 and later, the proxy studies and PMIP simulations suggest the commonalities and distinctions in the simulated the mean Indian summer monsoon and its variability across the during the mid-Holocene (MH; 6 kyr BP), Medieval Warming Period (MWP; 1 kyr BP), Little Ice Age (LIA; 0.35 kyr BP) period compared to the current period (HS; 0 kyr BP). While analysis of coupled model outputs help us in some if the background dynamics, carrying out atmospheric general circulation model (AGCM) sensitivity experiments is often useful in isolating the impact/role of a particular driver (for example, Keshavamurty, 1982; Ashok et al., 2001, 2012, etc.). In this chapter, I report results from various simulation experiments we have carried out with an atmospheric general circulation model (AGCM) with an objective to isolate the role of orbital parameters on the Indian summer monsoon variability during the MH time period.

5.1 The model, experiment setup and methodology

The Community Atmospheric Model Version 5 (CAM5), is the atmospheric component of the well-known Community Earth System Model Version 1.2.0 (CESM1.2.0; Conley et al., 2012). The CESM1.2.0, formerly also known as CCSM4, is a fully-coupled climate model used to generate simulations of the Earth's past, present, and future climate states. For our experiments, we configured horizontal resolution of the CAM5 to 1.9° latitude x 2.5° longitude grids with 30 vertical levels. This configuration of CAM is comparable and compared to the CESM simulations for the Coupled Model Intercomparison Project 5 (CMIP5) and the Paleo-Model Intercomparison Project 3 (PMIP3) simulations. The PMIP3 is a collective initiative endorsed by the World Climate Research

Programme (WCRP) and JSC/CLIVAR working group on coupled models and the International Geosphere and Biosphere Programme (IGBP; PAGES) (Braconnot et al., 2012).

We carried out four suites of multi-ensemble control simulations, for each of the MH, MWP, LIA, and Historical (Present day) periods. Each ensemble of the control experiments in turn contains three individual simulations of 30-year span each. Each of these member simulations starts with January initial conditions of any year, with the condition that none of the initial conditions of member ensembles of a set of ensembles are the same. On the other hand, due care has been taken that the initial conditions of parallel ensembles from each suite are maintained same, that is, only the forcings will be different among them.

The external boundary conditions, e.g., the orbital parameters, trace gases and solar constant imposed in the various control experiments are period-specific (i.e., MH, MWP, LIA, and HS). These have been adopted from the PMIP3 protocols https://pmip3.lsce.ipsl.fr/, and briefly presented in **Table 5.1**. Consequently, the orbital parameters have also been calculated using the PMIP3 protocol https://pmip3.lsce.ipsl.fr/ and are present in **Table 5.2**. The climatological SSTs used in this study for each period are adapted from the simulation outputs from the PMIP3 simulations that were generated with CCSM4 (**Figure 5.1**) corresponding to the concerned period such as the MH. In case of the MH, in addition to the control simulations, we have also carried out sensitivity ensemble experiments simulations for the MH period by forcing the model with different orbital forcings for different periods, e.g., present-day orbital, 8.2 kyr BP orbital, and LGM orbital forcings. The forcings are mentioned in **Table 5.3**. For comparison, the same set of initial conditions have been used in all the complementary experiments.

Table 5.1: Summary of boundary conditions used in different climate periods.

Boundary Condictions	Historical (HS; Present day)	LIA (0.3kyr BP)	MWP (1kyr BP)	Mid-Holocene (6kyrBP)
Orbital parameters	ecc = 0.016724 obl = 23.446 peri-180 = 102.04 orb_iyear = 1850	ecc = 0.016724 obl = 23.446 peri-180 = 102.04 orb_iyear = 1850	ecc = 0.017093 obl = 23.569 peri-180 = 85.79 orb_iyear = 1000	ecc = 0.018682 obl = 24.105 peri-180 = 0.87 orb_iyear = -4050
Date of vernal equinox	March 21 at noon	March 21 at noon	March 21 at noon	March 21 at noon
Trace gases	CO2 = 367 ppm CH4 = 1760 ppb N2O = 316 ppb CFC11 = 653.45 ppt CFC12 = 535 ppt O3 = Modern- 10DU	CO2 = 280 ppm CH4 = 760 ppb N2O = 270 ppb CFC11 = 0 CFC12 = 0 O3 = Modern-10DU	CO2 = 279.265 ppm CH4 = 674.6 ppb N2O = 266.9 ppb CFC11 = 12.48e 12 CFC12 = 0.0 O3 = same as in CMIP5 PI	CO2 = 280 ppm CH4 = 650 ppb N2O = 270 ppb CFC = 0 O3 = same as in CMIP5 PI
Climotological SST	Computed from CCSM4 CMIP5 Historical simulation (CE 1901-1999)	Computed from CCSM4 CMIP5 Last Millennium simulation (CE 1750-1849)	Computed from CCSM4 CMIP5 Last Millennium simulation (CE 1000-1099)	Computed from CCSM4 PMIP3 MidHolocene simulation
Aerosols	Present Day	Same as in CMIP5 PI	Same as in CMIP5 PI	Same as in CMIP5 PI
Solar constant	1,365 W/m2	1,365 W/m2	1361 W/m2	1360.747 W/m2
Vegetation	Interactive	Interactive	Interactive	Interactive
Topography and coastlines	Present Day	Present Day	PMIP3 Past1000	Same as in CMIP5 PI

Table 5.2 Linear approximation of the orbital parameters. < https://wiki.lsce.ipsl.fr/pmip3/doku.php/pmip3:design:lm:final.

Parameter	Linear approximation
Eccentricity	0.017475 - 0.000000382 * Year
Obliquity	23.697 - 0.000128 * Year
PERI-180	68.79 + 0.0170 * Year

Table 5.3: Orbital parameters of the different climatic periods.

Parameters	Time Period				
	MH	HS	8.2 kyr BP	21 kyr BP	
Eccentricity	0.018682	0.016724	0.019199	0.018994	
Obliquity	24.105°	23.446°	24.222°	22.949°	
PERI-180	0.87°	102.04°	319.495°	114.42°	

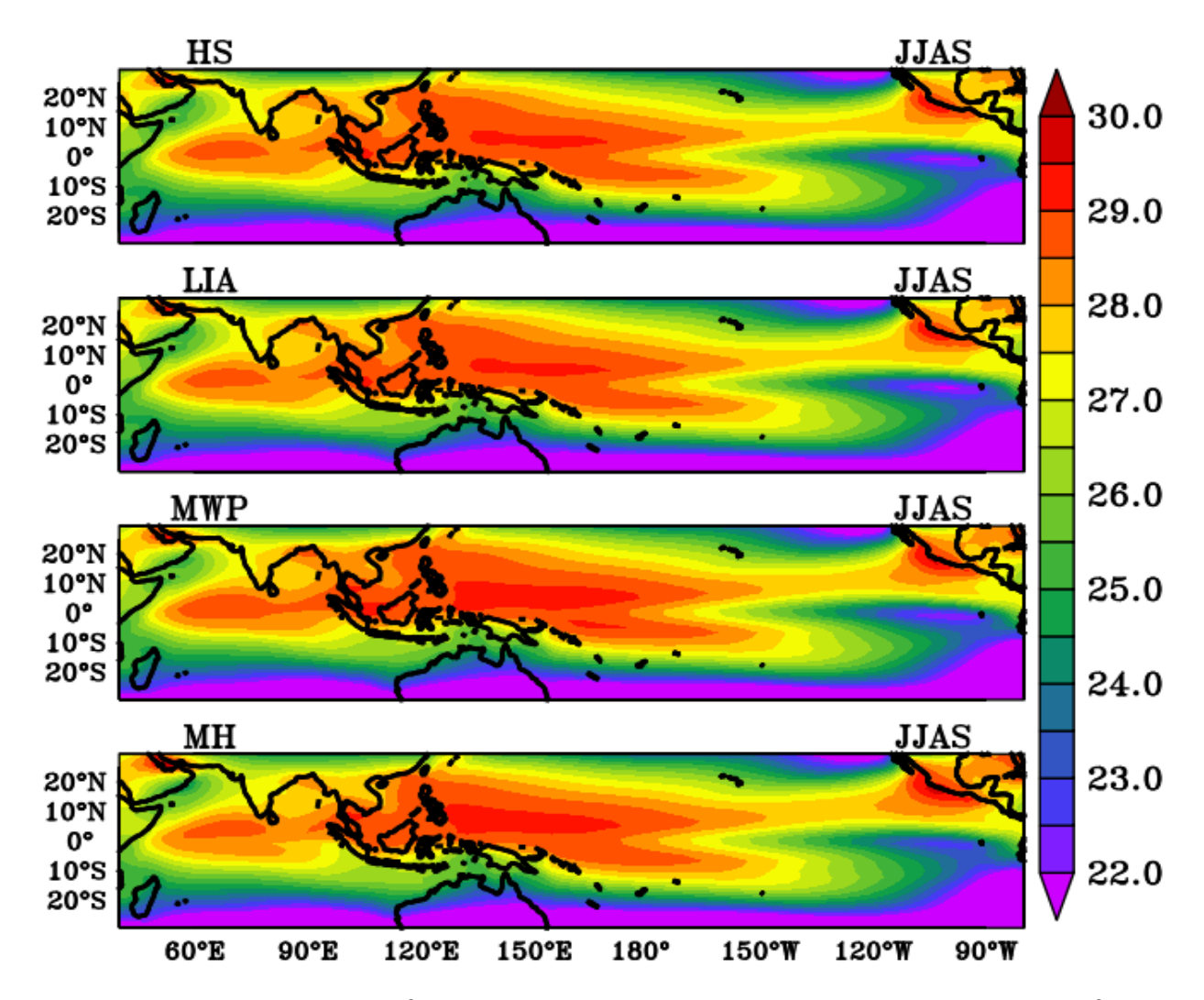


Figure 5.1: Mean JJAS sea surface temperatures (° C) used in the control simulations for MH, MWP, LIA, and HS periods.

Further to these 30-yearlong control and orbital sensitivity simulations, we have also carried out separate suites of simulations of 1-year span (simulation starts in January and ends in December) with 10-individual simulations differing in initial conditions but with the same set of initial conditions across various orbital forcings. The results from the 1-year length simulations are in very good agreement with those from the 30-yearlong simulations, as evidenced by the evolution of the seasonal cycles and mean monsoon rainfall statistics over India (Figures not shown). Therefore, we shall not discuss the results from these runs.

Apart from the control and orbital sensitivity experiments, we have also carried out two sensitivity experiments to gauge the potential relevance of the El Niños during MH, and two more to assess the impact of the La Niñas during the same period. The design of the SST conditions involved, for example in case of the La Niña sensitivity experiments, imposing the La Niña anomalies on the climatological SSTs over the tropical pacific ocean (120°E to 80°W and 30°S to 30°N), which are used in the control experiments, to obtain the lower boundary SSTs representing the La Niña SSTs during the MH, analogous to such sensitivity experiments carried out (e.g. Ashok et al., 2001; 2004; 2009a; 2012; Guan et al., 2003, Ratna et al., 2020). In yet another sensitivity experiment, we impose SST anomalies on the climatological experiments throughout the tropical Indo-pacific ocean (40°E to 80°W and 30°S to 30°N). The SST anomalies imposed in these SST sensitivity experiments for the MH period are shown in **Figure 5.2**. The SST anomalies during the La Niñas (El Niños) were obtained by compositing monthly SST anomalies of all 'typical' La Niñas (El Niños). These typical events, from the CESM outputs for the MH period, are identified as those for which the magnitude of the simulated JJAS NINO3 index is above (below) one standard deviation. In **Table 5.4**, I have briefly listed the simulations carried out in this chapter.

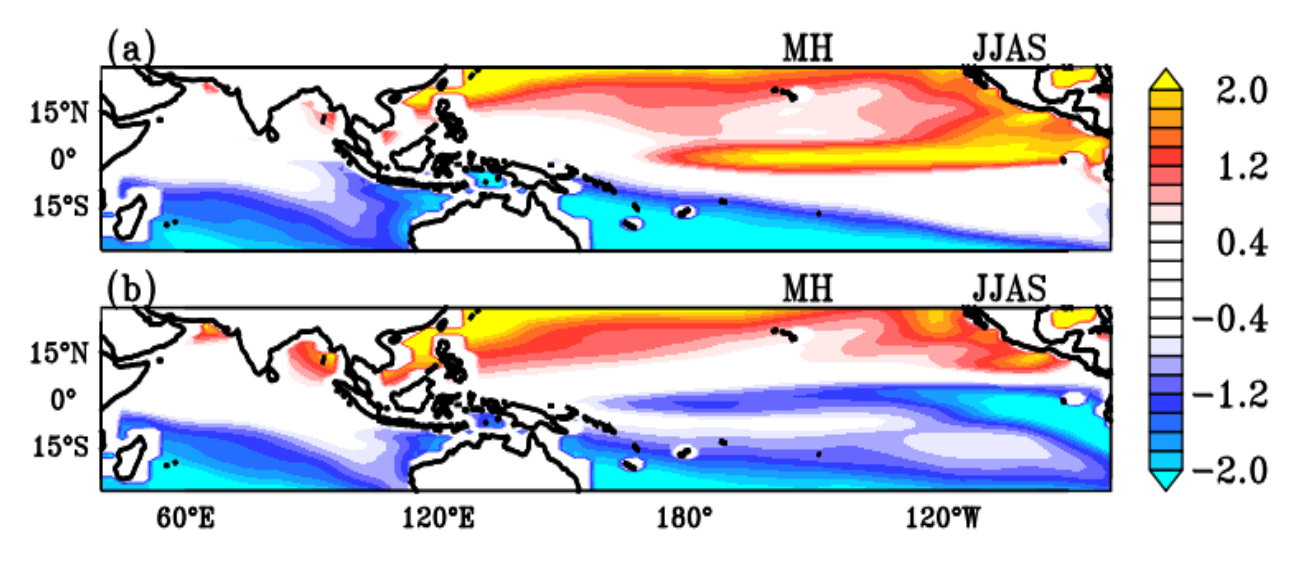


Figure 5.2: The sea surface temperature (°C) anomalies imposed in these SST sensitivity experiments for the MH period over tropical Indo-Pacific oceans (a) El Niño (b) La Niña.

Table 5.4: Brief list of Simulation carried out in this chapter.

S.No.	Time Period	Simulation type
1	HS	Control
2	LIA	Control
3	MWP	Control
4	MH	Control
5	MH	With HS orbital parameters
6	MH	With 8.2 kyr BP orbital parameters
7	MH	With LGM orbital parameters
8	MH	with El Niño type SSTs in the tropical Pacific Ocean
9	MH	with La Niña type SSTs in the tropical Pacific Ocean
10	MH	with El Niño type SSTs in the tropical Indo-Pacific Ocean
11	MH	with La Niña type SSTs in the tropical Indo-Pacific Ocean.

In our analysis, the climatology is taken from entire 30-year runsare taken from PMIP3 CCSM4 simulation, and they are therefore spun up sufficiently. As we are starting our simulation from January, the simulated atmosphere will adjust to the lower boundary SSTs within a couple of months. As it is, such experiments for the current day monsoonal season typically start in the month of May (e.g. Ashok et al., 2001, 2004, 2009, 2012; Guan et al., 2003).

We have calculated the monthly climatological cycles of rainfall and surface temperatures over the Indian land region bounded by 66.5°E–101.5°E; 6.5°N–39.5°N. We analyse the simulated fields of velocity potential-which represent divergence, vorticity, and moisture flux convergence. The moisture flux convergence has been computed as the sum of moisture convergence and advection. The fields of velocity potential, vorticity, and moisture convergence have been computed from the simulated outputs of horizontal winds and moisture through the application of spherical **NCL** details found harmonics using the routines. The can be at https://www.ncl.ucar.edu/Applications/wind.shtml.

5.2 Validation of simulated mean summer monsoon rainfall and surface temperatures over India

Before going any further, we compare our HS simulations with those from the PMIP3 CCSM4 historical simulations, and ascertain their validity through a comparison with various observational and reanalysis data. In **Figure 5.3**, we briefly compare the seasonal cycle evolution of rainfall and surface temperatures of these simulations (PMIP3 CCSM4 and AGCM CAM5) with the ERA-20CM skin temperature (SKT; Hersbach et al., 2015), Climate Prediction Center (CPC) Global Land Surface Air Temperature data (Fan et al., 2004) and the India Meteorological Department (IMD) gridded rainfall (Rajeevan et al., 2006). We present the seasonal cycle validation in **Figure 5.3**. From **Figure 5.3**, we can clearly see that the seasonal cycle evolution of rainfall and surface temperatures are well captured in the AGCM HS.

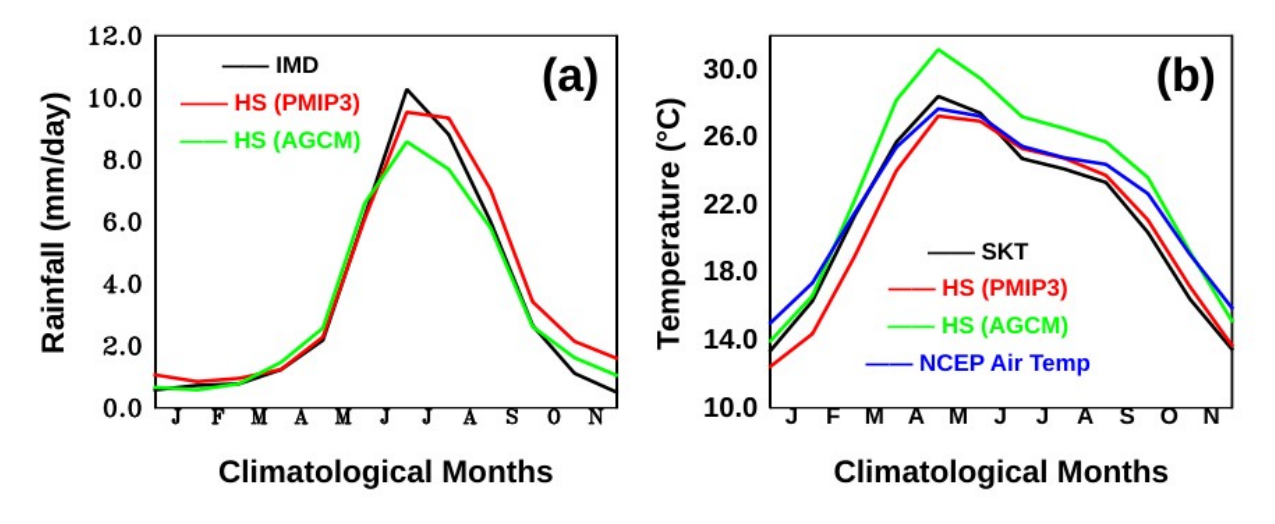


Figure 5.3: Comparisons of PMIP3/CMIP5 CCSM4 simulated area-averaged climatological cycle of rainfall and surface temperature with AGCM simulation rainfall and surface temperatures, with the observational rainfall and surface temperatures respectively. (**a**) for rainfall; (**b**) for surface temperature for HS; The are calculated over the Indian land region (66.5°E–101.5°E; 6.5°N–39.5°N). IMD rainfall climatology calculated from CE 1901-2009, SKT climatology calculated from CE 1901-2009, Climate Prediction Center (CPC) Global Land Surface Air Temperature data from CE 1948-2020.

5.2.1 Mid-Holocene

Figures 5.4a and 5.4c show that simulated summer monsoon rainfall during MH is higher than the HS. Note that we compute the area-averages over the Indian land region only (e.g., see the domain in **Figure 5.4c**). The relatively higher simulated Indian summer monsoon rainfall during MH, particularly around ~ 6 kyr BP, agrees well with results from several coupled model simulations (e.g. Kumar et al., 2018, Tejavath et al., 2020), as well as with the proxy-based studies (Band et al. 2018; Rawat et al. 2015). The simulated area-averaged surface temperature is found to be colder during MH compared to the Present-day period (**Figure 5.4b, 5.4d**), as also indicated by several coupled models of the PMIP3 vintage (Tejavath et al., 2020).

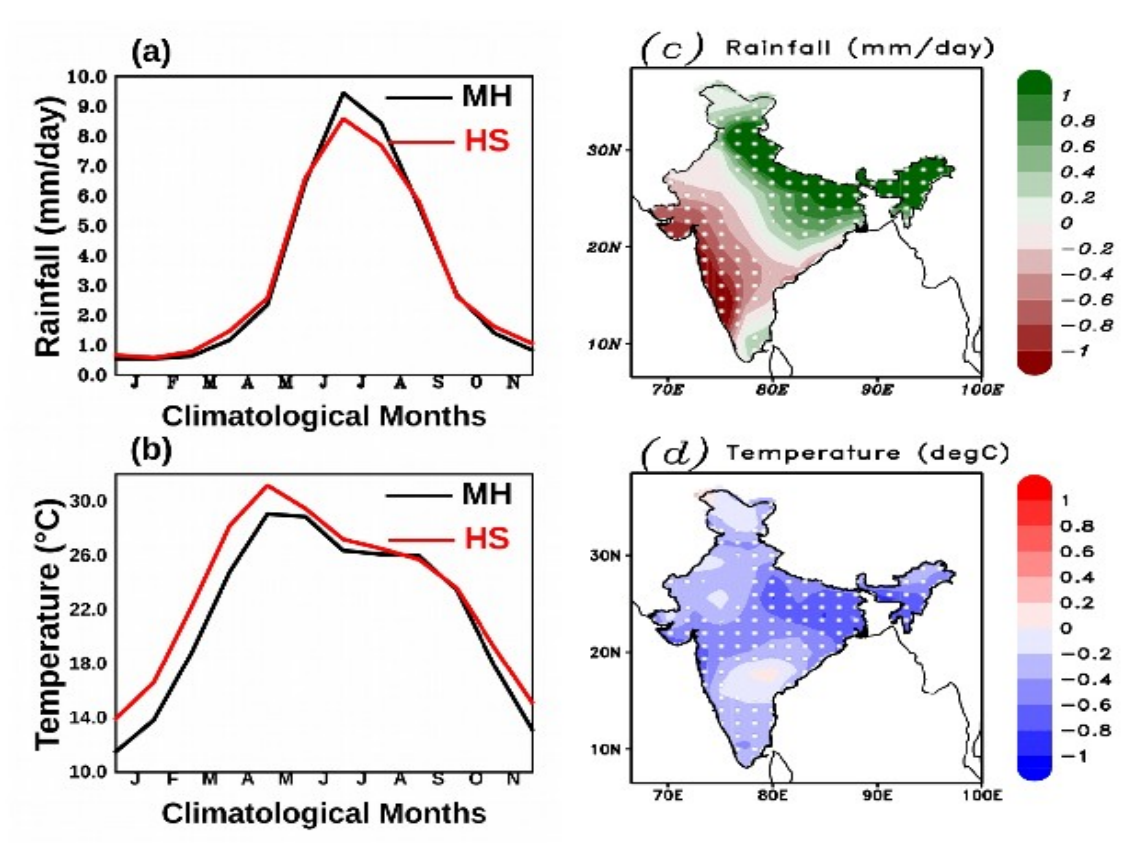


Figure 5.4: Comparison between the area-averaged seasonal cycle of Mid-Holocene (MH) and Historical period, (**a**) is for the simulated rainfall and (**b**) is for the simulated surface temperature over Indian land region. Spatial distributions of the simulated summer monsoon rainfall (mm/day); (**c**) and surface temperature (°C); (**d**) for MH with the difference to HS. The dotted region represents a statistically significant region at a 95% confidence level from a two-tailed Student's t-test.

The simulations suggest, a relatively higher rainfall during the MH relative to the HS in the core monsoon region, northeast India, and foothills of the Himalayas and lower rainfall in the western part of India (Figure 5.4c). Interestingly, despite being a major ISM rainfall region, the simulated rainfall over the western ghats is relatively less rainfall during the MH compared to the HS (**Figure 5.4c**). We have observed a similar kind of pattern in the southern part of western ghats (i.e. Kerala) in PMIP3 CCSM4 coupled model simulations also. This could be potentially because the MH, monsoon winds simulated by the model, as well as those simulated by the PMIP3 CCSM4 (Figure not shown), are weaker over the western ghats region and less moisture availability compared to the HS. Interestingly, the Indus civilization, encompassing the modern-day Rajasthan and neighbouring Pakistan, etc., is said to have thrived during the MH, for which the in which case the local monsoon circulation may have been stronger relative to the HS. However, as can be conjectured from the simulated 850 hPa circulation, the low-level circulation is weaker relative to the historical period, and accompanied by a weak summer monsoon rainfall in the north-western Indian sub-continent. This of course may just be model-specific. We shall explore this aspect further making a detailed PMIP model analysis and sensitivity experiments with multiple AGCMs., A comparatively low-resolution simulation and atmospheric-only configuration could be potential reasons behind it.

5.2.2 MWP and LIA

While the seasonal cycle of the area-averaged Indian summer monsoon for both the MWP and LIA look similar **(Figures 5.5a)**, **Figure5.5c** clearly shows that the area-averaged summer monsoon rainfall during MWP is also higher than LIA, in agreement with a majority of the PMIP3 simulations (e.g., Chapter 3, published as Tejavath et al., 2019). **Figure 5.5b** confirms that the AGCM simulations reproduce the expected surface temperature response to increased greenhouse

gases, from the perspective of increased GHGs in the present day when industrialization has begun (also see **Table 5.1**), and hence considered reliable.

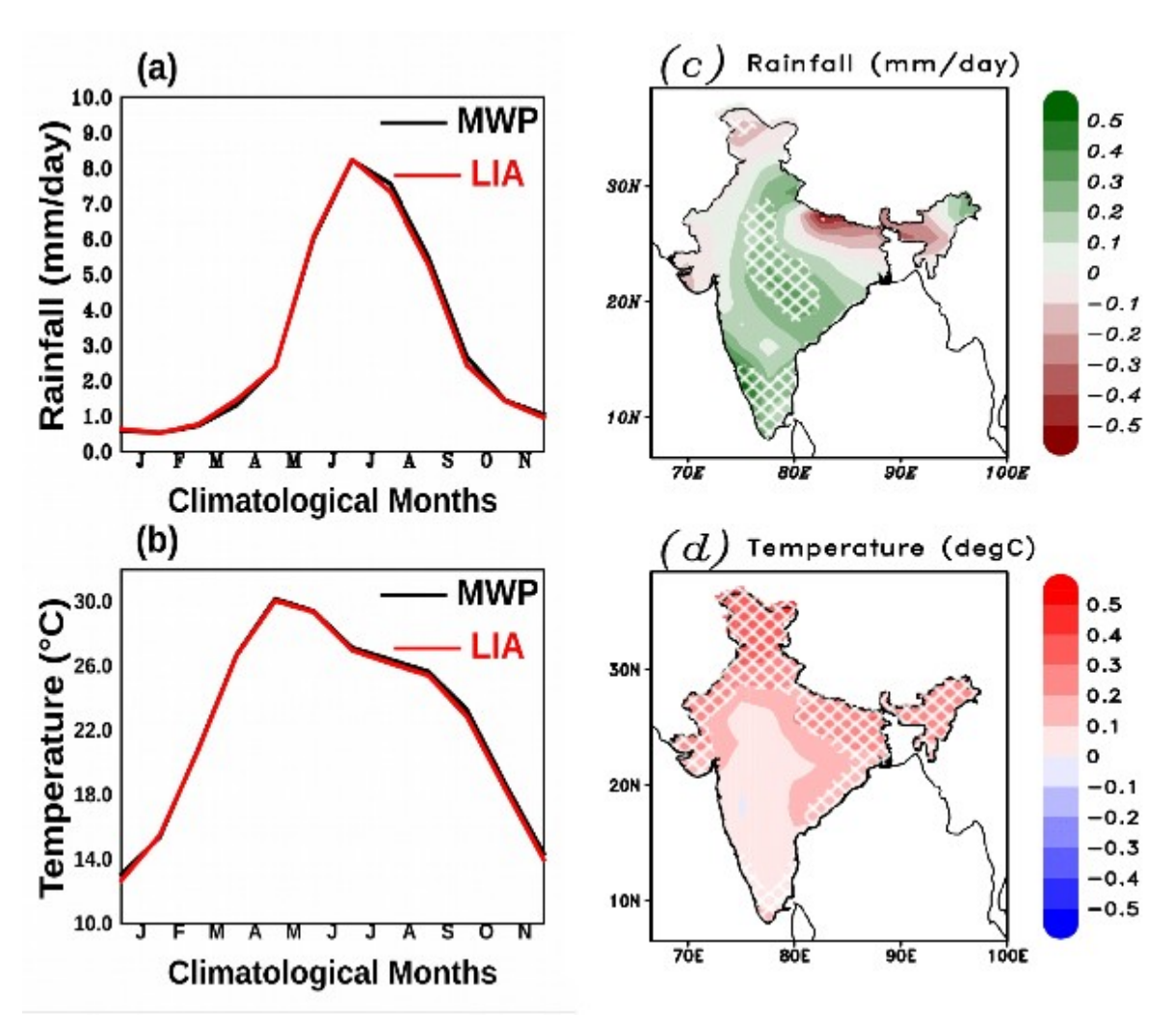


Figure 5.5: Comparison between the area-averaged seasonal cycle of Medieval Warm Period (MWP) and Little Ice Age (LIA) period, (**a**) is for the simulated rainfall, and (**b**) is for the simulated surface temperature over Indian land region. Spatial distributions of the simulated summer monsoon rainfall (mm/day) (**c**) and surface temperature (°C); (**d**) for MWP with the difference to LIA. Hatched region represents a statistically significant region at an 80% confidence level from the two-tailed Student's t-test.

The simulated area-averaged surface temperature during the LIA is cooler compared to the MWP, again as simulated by the coupled models of the PMIP3 vintage (Chapter 3, published as Tejavath et al., 2019) and in agreement with various proxy studies (Dixit and Tandon, 2016 etc.,). Interestingly, the rainfall difference over northeast India indicates a dipolar pattern during the MWP

and LIA (**Figures 5.5c**). When area-averaged, these values are almost negligible, suggesting that the area-averaged summer monsoon rainfall over north-eastern India has not changed across the MWP, LIA, and historical periods, as suggested by a companion study that analyses summer monsoon variability over the northeast India in the simulations from three relatively-high resolution PMIP3 simulations (Bidyabati, PhD thesis, 2021; Ashok et al., 2021, Under review).

Interestingly, several vegetation-based proxy studies suggest differences in the summer monsoon from the MWP to LIA over the northeast India (See the review by Mehrotra et al., 2014). This is unlike for the rest of the Indian summer monsoon for which there is some agreement between the proxy studies and PMIP3 simulations as well as the aforementioned AGCM simulations. Results from a speleothem study (Gupta et al., 2019), and a few other vegetation-based proxy studies however also suggest that the summer monsoon over the northeast India may not have changed much from the MWP to LIA (See the review by Mehrotra et al., 2014). Further discussion on this topic is beyond the scope of this thesis.

5.2.3 Role of tropical Ocean-Atmospheric coupled processes or the lack thereof

We now compare the results from our AGCM simulations with those from the corresponding past climate simulations by CCSM4 (**Figure 5.6**. Recall that, these CCSM4, which have CAM as the atmospheric component, are fully coupled ocean-atmospheric simulations (Schmidt et al. 2012; Taylor et al., 2012).

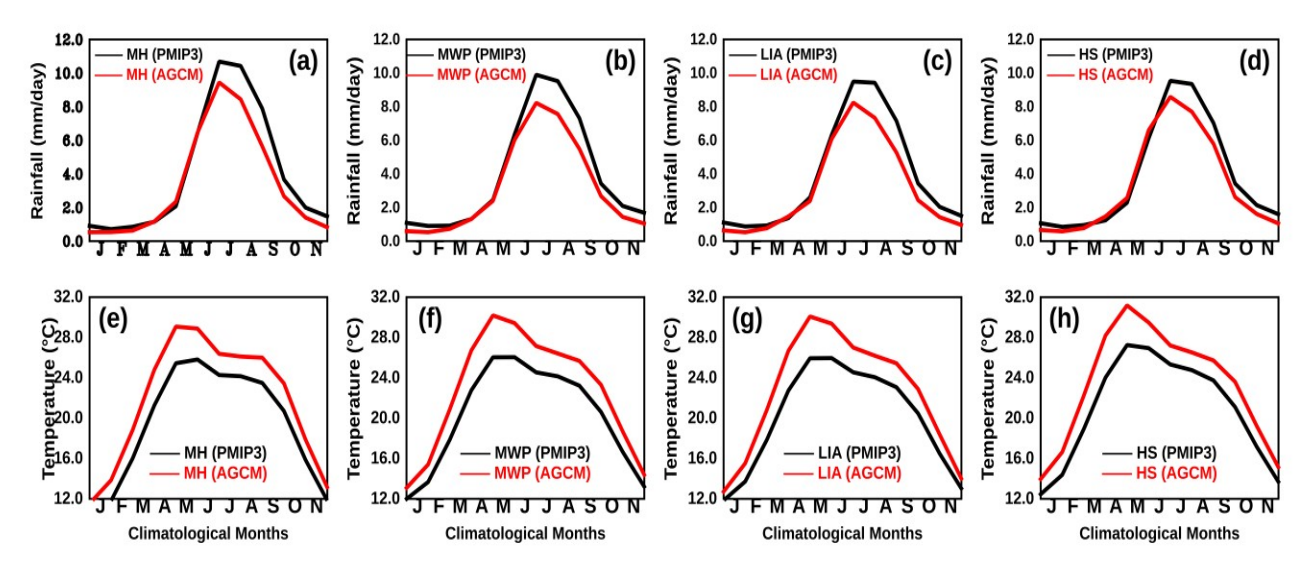


Figure 5.6: Comparisons of PMIP3/CMIP5 CCSM4 simulated area-averaged climatological cycle of rainfall and surface temperature with AGCM simulation rainfall and surface temperatures, respectively. (a), (b), (c), and (d) for rainfall; (e), (f), (g), (h) for surface temperature for past climate periods; The are calculated over the Indian land region (66.5°E–101.5°E; 6.5°N–39.5°N). The legend string of each panel indicates the name of the type of the simulation and the period over which the difference is calculated.

From the panels in **Figure 5.6**, we see that simulated rainfall and surface temperature climatological cycles from our experiments with the CAM AGCM are comparable to those from the CCSM4 in terms of the evolution of the annual cycle. The AGCM simulations are relatively drier and warmer over India during the summer (**Figures 5.6 a-d**) across all the climate periods compared to the coupled CCSM4 simulations. Similarly, we see a warmer bias in AGCM surface temperatures compared to the coupled model simulations. The absence of air-sea coupled processes could be a probable reason behind the dry bias.

5.3 Simulated circulation changes over India

5.3.1 Mid-Holocene

During the MH period, we see a deeper low pressure in the monsoon trough region the Indian sub-continent northward of $\sim 20^{\circ}$ N relative to the HS (**Figure 5.7b**). This indicates a relatively northward migration of the ITCZ. This is also seen in simulations by a few other

AGCMs and coupled models of older vintage (e.g. Zhao and Harrison, 2012). Strengthening of the subtropical high over the western pacific also apparently strengthens the monsoonal circulation over northern India (**Figure 5.7b**).

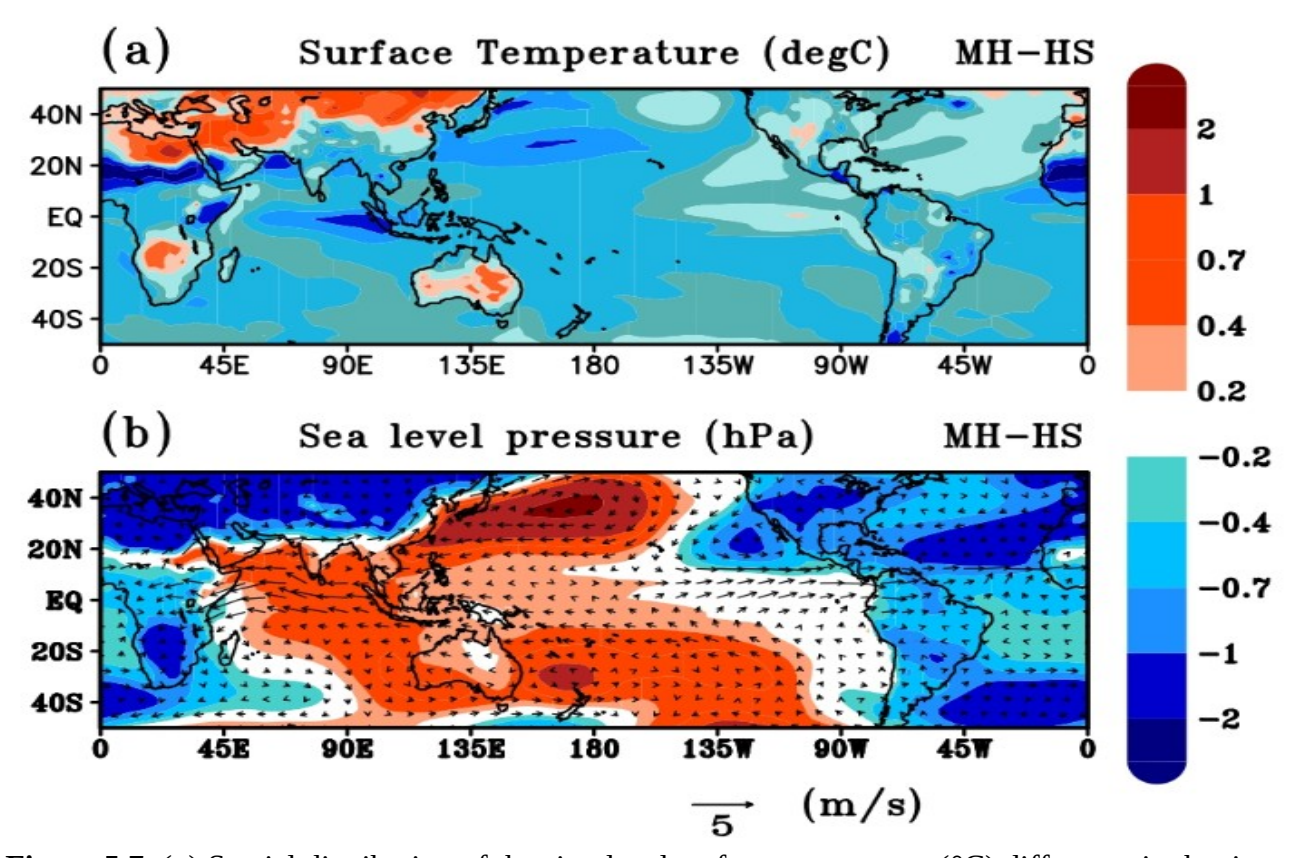


Figure 5.7: (a) Spatial distribution of the simulated surface temperature (°C) difference in the time-averaged JJAS between MH and HS. (b) Spatial distribution of the simulated sea level pressure (hPa) and overlaid by the monsoon winds (m/s) at 850 hPa difference in the time-averaged JJAS between MH and HS.

Apart from these, the Indian subcontinent experienced relatively stronger low-level convergence associated with stronger monsoonal circulation and during MH (**Figure 5.8a**). Other factors such as a stronger zonal seasonal mean SST gradient in the tropical Indian Ocean, with a warmer (cooler) eastern (western) tropical Indian Ocean by 0.1°C~0.2°C (**Figure 5.7a**) relative to the HS, which provides a weak positive IOD-like background, may have marginally contributed to the stronger mean Indian summer monsoon circulation and summer monsoon rainfall. Large scale moisture convergence is seen during the MH (**Figure 5.8b**), consequently giving a relatively

enhanced summer monsoon rainfall in the core monsoon region. Western India is associated with a relatively lower moisture convergence, manifesting as lower rainfall (also see **Figures 5.4a & 5.4c**). Chapter 3 of the thesis (published as Tejavath et al. 2019 during the course of the thesis) and other modeling studies (e.g., Polanski et al. 2014, Ashok et al., under revision, 2021) also show that changes in the large-scale circulation may have facilitated the precipitation changes during the MH period and LM.

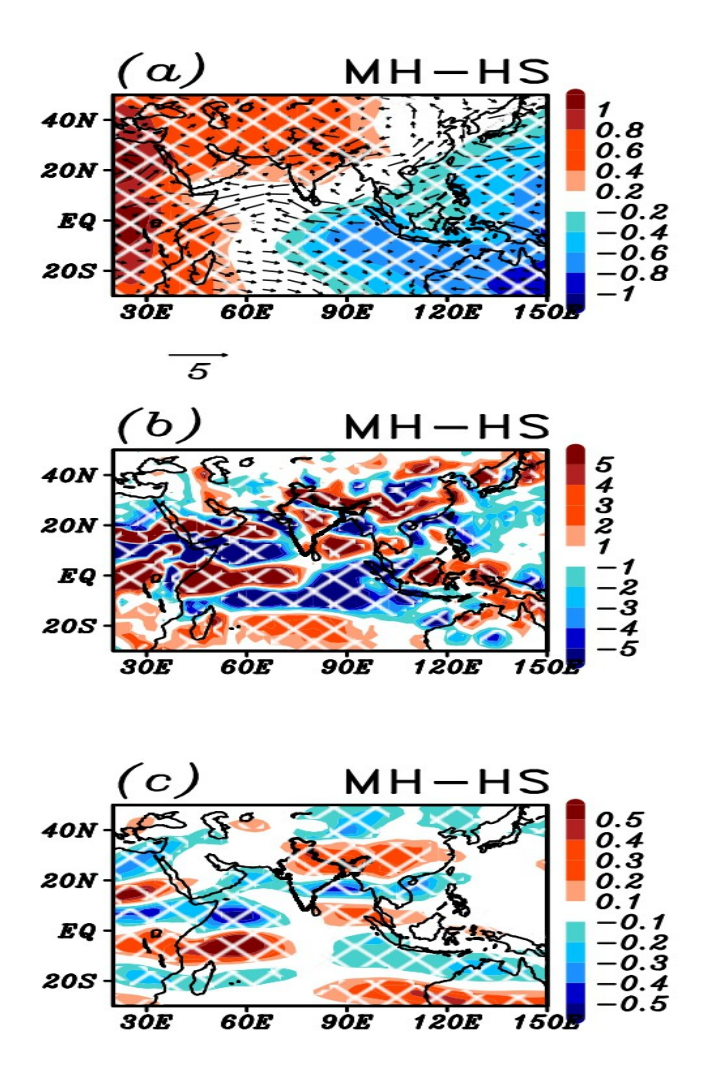


Figure 5.8: (a) spatial distribution of the simulated 850 hPa differences in the time-averaged JJAS velocity potential ' χ 850' (m² s⁻¹; Shaded), and overlaid by the mean monsoon winds (m/s; Vectors) for MH period relative to that for the HS. Panels (b) show spatial distributions of simulated 600 hPa differences in the time-averaged JJAS Moisture Flux Convergence (10^-5 g/(kg-s)). Panel (c) shows spatial distributions of simulated 500 hPa relative vorticity (X 10⁻⁵ S⁻¹) for the MH period relative to that for the HS. Hatched region represents a statistically significant region *at a 95%* confidence level from the two-tailed Student's t-test.

Interestingly, the simulated pre-monsoon (March-May) land-sea temperatures during the MH are cooler compared to the HS (**Figure 5.9**). From this, it seems the pre-monsoon land warming may not be relatively as important as the northward shift in the ITCZ in association with the changes in the subtropical High. The land-sea gradient during the MH from our control run is also relatively weak (Figures not shown), suggesting that this may not be a major factor during the MH.

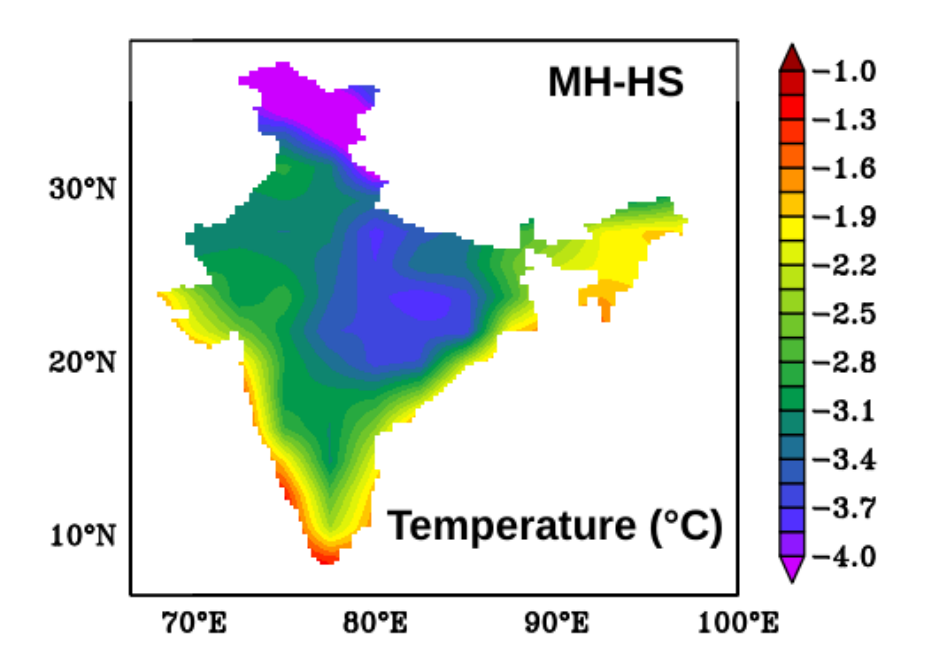


Figure 5.9: Spatial distribution of simulated pre-monsoon (March, April, and May) surface temperatures (°C) difference between the MH and HS.

5.3.2 MWP and LIA

From **Figure 5.10a**, we clearly see that the Indian subcontinent experienced stronger low-level convergence, which is associated with stronger monsoonal circulation during the MWP compared to the LIA. The MWP climate period is associated with strong magnitudes of moisture

convergence compared to the LIA (**Figure 5.10b**). These all resulted in a stronger ISM giving surplus rainfall over the Indian region during the MWP compared to the LIA.

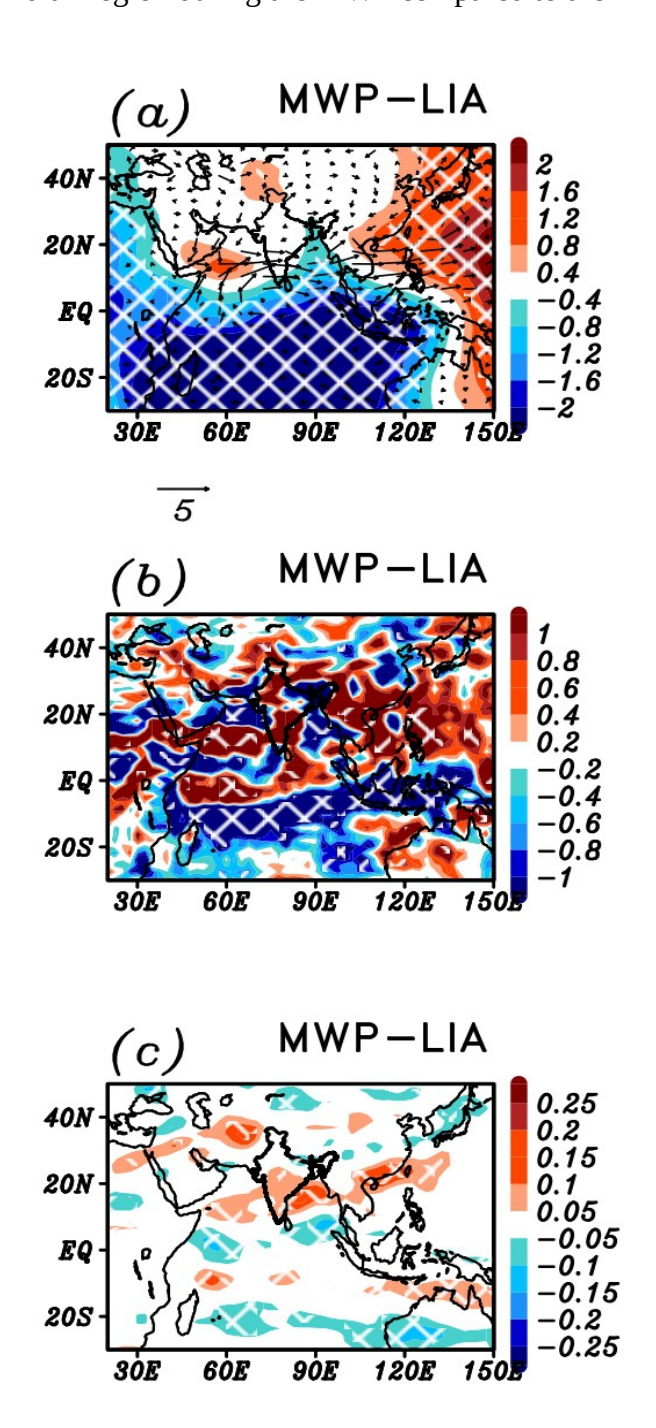


Figure 5.10: (a) spatial distribution of the simulated 850 hPa differences in the time-averaged JJAS velocity potential ' χ 850 ' (m² s⁻¹; Shaded), and overlaid by the mean monsoon winds (m/s; Vectors) for MWP period relative to that for the LIA. Panels (b) show spatial distributions of simulated 600 hPa differences in the time-averaged JJAS Moisture Flux Convergence (10^-5 g/(kg-s)). Panel (c) shows spatial distributions of simulated 500 hPa relative vorticity (X 10⁻⁵ S⁻¹) for the MWP period relative to that for the LIA. Hatched region represents a statistically significant region *at a 95%* confidence level from the two-tailed Student's t-test.

5.3.3 Possible mechanisms for the stronger mid-Holocene summer monsoon

In **Figure 5.11**, we show the differences in the simulated insolation between the MH and the HS climate periods, which are associated with the changes in the obliquity (Table 5.1). From the perspective of the Milankovitch cycles, the obliquity (axial-tilt) of the Earth during the MH is 24.1°, and during the HS is 23.4°. In other words, during the MH, the solar activity was more in the Northern hemisphere compared to the southern hemisphere (**Figure 5.11**). This shows that during the MH climate period, the Indian subcontinent has received more insolation than during the Historical climate period because of the changes in the orbital parameters (**Figure 5.11**).

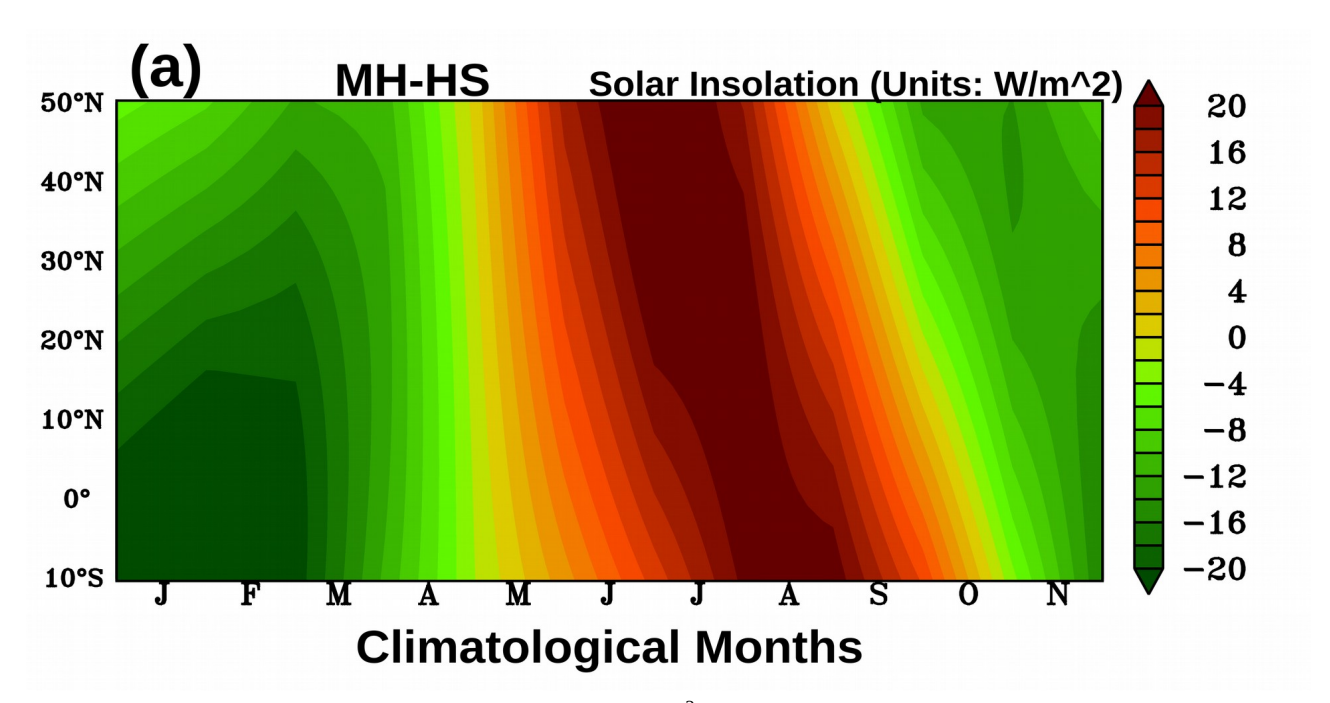


Figure 5.11: Simulated insolation difference (W/m²) between Mid-Holocene and HS (present-day). Averaged over all the longitudes (0°E to 360°E).

A few studies (Bosmans et al. 2012; Zhao and Harrison et al. 2012) suggest that this increased-insolation likely led to deeper thermal lows on the land region and resulted in a higher land-sea thermal gradient because of the difference in thermal inertia between land and ocean. In

general, this can be expected to lead to stronger monsoonal winds into the Indian sub-continent with enhanced moisture flow towards the land region, giving more precipitation (Bosmans et al. 2012; Zhao and Harrison et al. 2012), at least during the onset phase when the land-sea thermal contrast is important. Indeed, the seasonal atmospheric circulation, in general, can also be expected to change as a result of the change in atmospheric energy balance prompted by the strengthening of the summer by stronger insolation (Merlis et al. 2013), and also eventually influence the rainfall. From this perspective, it is interesting to see how the Indian monsoon responded to the changes in orbital parameters, particularly for the mid-Holocene time period using the AGCM.

5.4 The mid-Holocene ISM response to changes in orbital forcings

In this section, we examine the simulated ISM response to changes in orbital forcings through an analysis of our sensitivity experiments, which were discussed in section 5.1.

We have carried out simulations for the MH climate period with different orbital forcings (e.g., present-day orbital, 8.2 kyr BP orbital, and LGM orbital forcings; mentioned **Table 5.2**). The motivation behind choosing the LGM and 8.2 kyr BP orbital parameters apart from HS follows: proxy-based studies suggest that during the LGM, the ISM was weaker and drier compared to the present-day (Chabangborn et al., 2013 and Patnaik et al., 2012). During the 8.2 kyr event, ISM had weakened abruptly (Dixit et al., 2018). Changes in orbital parameters are believed to have played a major role in weakening the ISM during the LGM (Bowen et al., 2009). It must be mentioned that Atlantic teleconnections also had a significant role in the weakening of ISM during the 8.2 kyr BP (Dixit et al., 2018). By applying the orbital parameters of LGM and 8.2 BP kyr for the MH gives an idea for the role of orbital parameters during MH compared to the other climatic periods, although they may possess characteristic differences in capturing the low/high rainfall patterns to these

changes. The simulated MH solar irradiance over the Indian region during the summer monsoon season decreases when the orbital parameters are replaced by those observed during HS and LGM (**Figure 5.12a, and 5.12c**). Furthermore, when the 8.2 kyr orbital parameters have been invoked, the simulated solar irradiance over the Indian region is seen to be slightly higher compared to the MH control simulation (**Figure 5.12b**). The other simulated changes relative to these changes in orbital parameters are discussed in the following subsections.

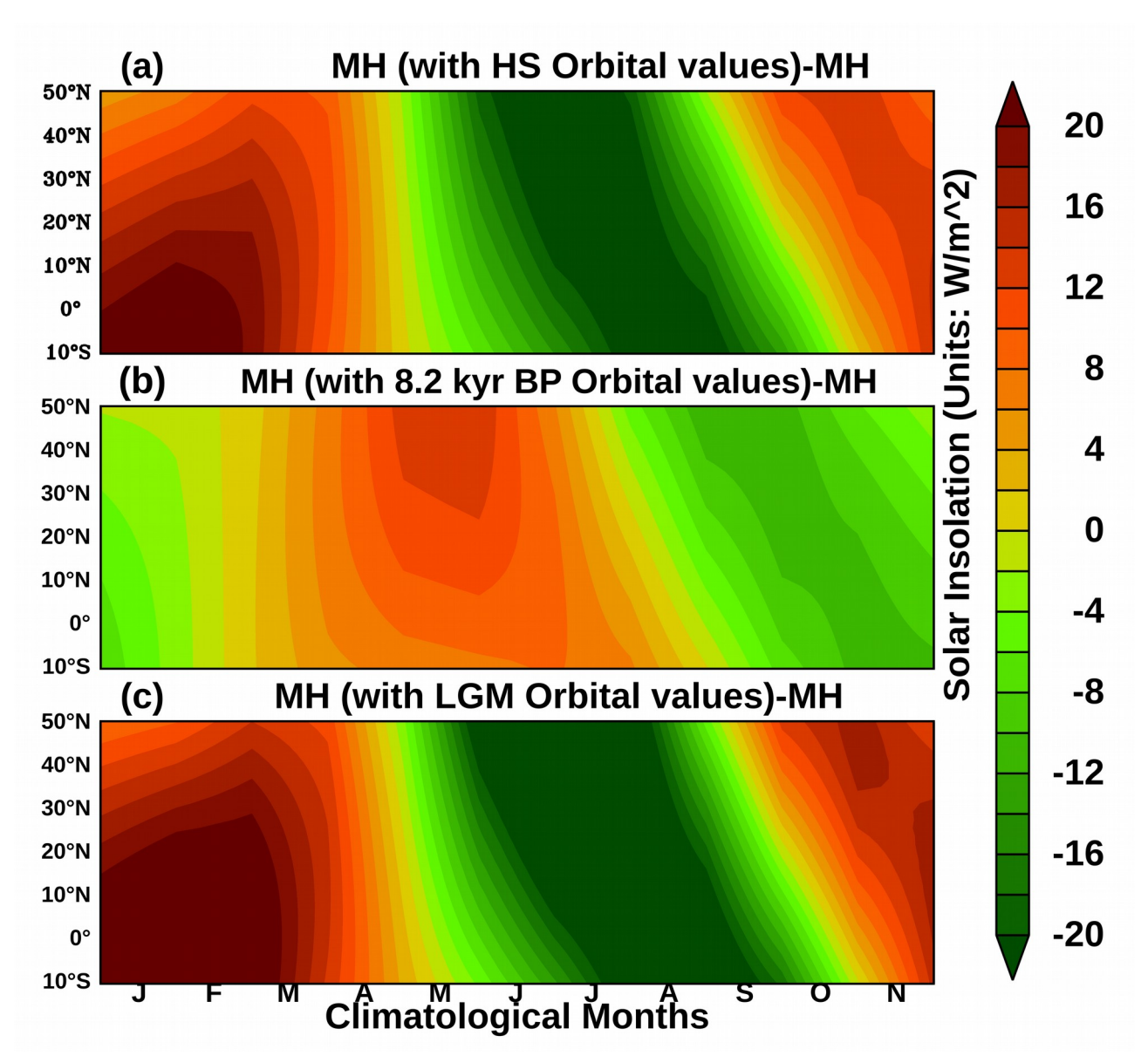


Figure 5.12: Simulated insolation difference (W/m2) between (**a**) MH sensitivity experiment with HS orbital parameters to MH control simulation (**b**) MH sensitivity experiment with 8.2 kyr BP orbital parameters to MH control simulation and (**c**) MH sensitivity experiment with LGM orbital parameters to MH control simulation. Averaged over all the longitudes (0°E to 360°E).

5.4.1 Simulated rainfall and surface temperature

Changing the orbital forcing to that of the HS, and to that of the LGM, reduces the simulated summer monsoon rainfall relative to the MH-control experiment (**Figure 5.13a**). Interestingly, the MH simulations with the orbital forcings pertaining to the 8.2 kyr BP resulted in relatively higher summer monsoon rainfall, contrary to proxy-based observations (Dixit et al., 2018). An earlier coupled model study also suggests that simulating the signatures of the 8.2 kyr BP event seen in proxy-observations is a difficult task (LeGrande et al., 2008). This tells us that apart from the orbital parameters, the North Atlantic teleconnections (Dixit et al., 2018) and, importantly, meltwater forcings (Renssen et al., 2001; Wiersma et al., 2005; LeGrande et al., 2008) may have played a crucial role in the weakening of ISM 8.2 kyr BP event as seen in paleo-data based studies. In this context, the simulated relatively high ISMR with the 8.2 kyr BP may be due to a lack of suitable representation of the fresh-water perturbations, as our experiments are only AGCM-based.

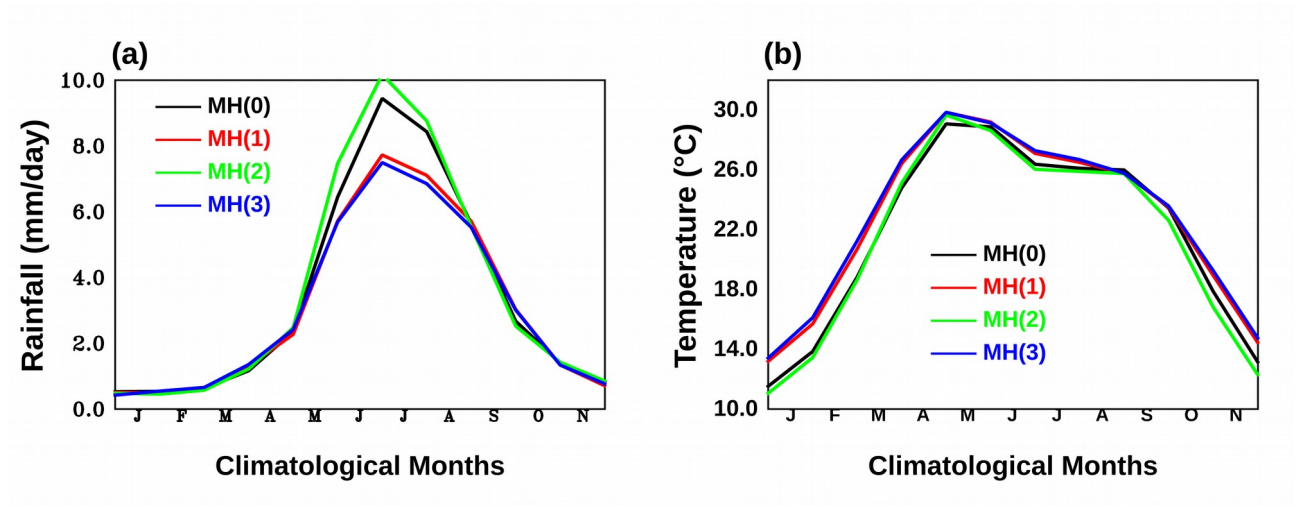


Figure 5.13: Comparison between the area-averaged seasonal cycle of Mid-Holocene (MH) simulations, (**a**) is for the simulated rainfall, and (**b**) is for the simulated surface temperature over the Indian land region. Here, MH(0) is MH Control simulations; MH(1) is MH simulation with HS orbital values; MH(2) is MH simulation with 8.2 kyr BP orbital values; MH(3) is MH simulation with LGM orbital values.

5.4.2 Simulated circulation changes over India

The changing of the orbital parameters to the current day, and in a parallel experiment to that in the LGM time period, caused the weakening of the mean monsoonal winds. This resulted in weakening large-scale low-level convergence over the Indian region (**Figure 5.14a**, and **5.14c**), and a deficit summer monsoon rainfall, particularly over the core monsoon region (**Figure 5.13**).

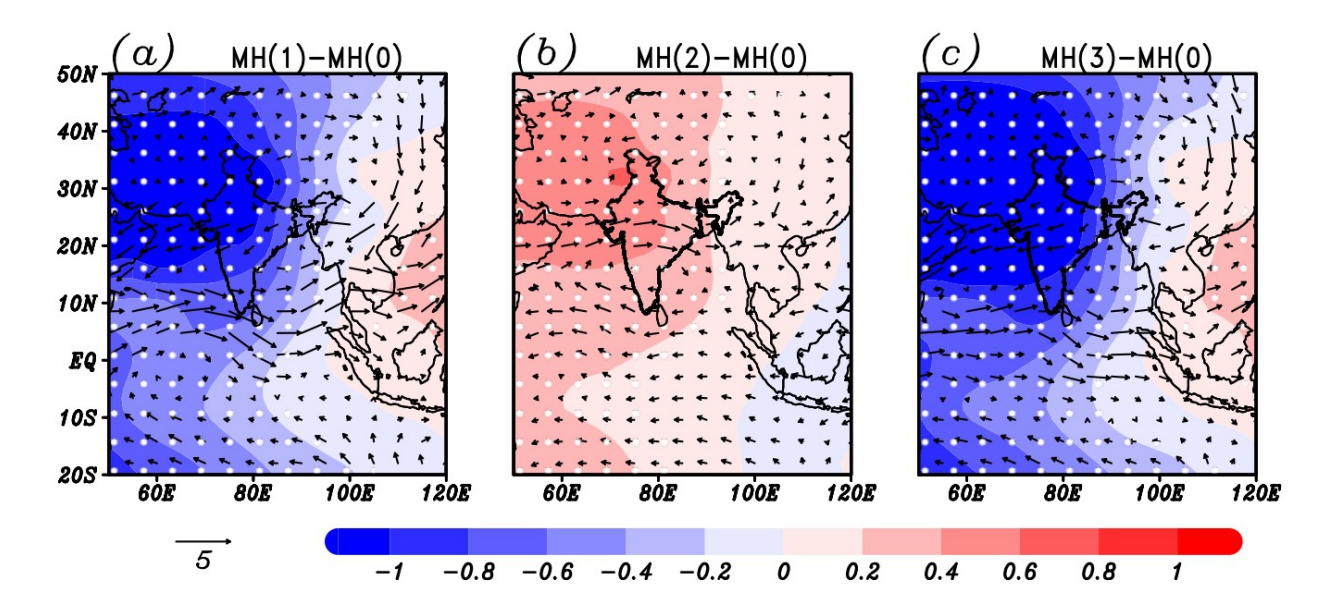


Figure 5.14: Spatial distribution of the simulated 850 hPa differences in the time-averaged JJAS velocity potential ' χ 850' (m² s⁻¹; Shaded), and overlaid by the mean monsoon winds (m/s; Vectors) for MH sensitivity experiments relative to that for the MH control simulation. (**a**) MH sensitivity experiment with HS orbital parameters to MH control simulation (**b**) MH sensitivity experiment with 8.2 kyr BP orbital parameters to MH control simulation and (**c**) MH sensitivity experiment with LGM orbital parameters to MH control simulation.

From **Figures 5.13 and 5.14**, it is evident that the simulated ISMR during the MH has indeed responded to changes in solar irradiance induced by changes in the orbital parameters. This suggests that enhanced solar insolation due to favourable orbital parameters during the MH time period played a crucial role in strengthening the Indian summer monsoon, compared to the HS and LGM. This is also supported by another recent study by Crétat et al., (2020). This also suggests that

changes in orbital parameters had a major role in the strengthening of Indian summer monsoon during the MH than the equatorial ocean-atmosphere dynamical processes at that time.

5.5 Potential role of concurrent ENSO

Recall the details of various sensitivity experiments carried out to gauge the potential role of ENSOs on Indian summer monsoon rainfall from the experimental setup section 5.4. The simulated model response in the experiments carried out with El Niño type of SSTs in the tropical Pacific for the MH period (Experiment ELPMH) resulted in negative summer rainfall anomalies over India (**Figure 5.15**), similar to current day observations (see the review by Ashok et al., 2019; Figure not shown). However, the model response to the La Niña-like lower boundary forcing in the tropical Pacific for the MH (Experiment LNP^{MH}) seems to be contrary to the current day observations(Figure 5.15; also see Table 5.4 for the details of the experiment), as it produces a negative summer monsoon rainfall anomaly over the Indian region. To be sure, studies such as that by Annamalai et al. (2005) suggest that some models may also need the ENSO-associated SST forcing in the tropical Indian Ocean to produce a realistic response over the Indian monsoon rainfall. In addition, recent research by Chowdary et al., (2017) suggests that the ENSO signal in the tropical Indian Ocean, in addition to its signal in the tropical Pacific, may be relevant for the current day monsoon variability. In our experiments as well, for the historical period, the La Niña-related tropical Pacific SST anomalies with, seem to produce above-normal summer monsoon rainfall at least from August for the historical period only when associated with the concurrent Indian Ocean SST anomalies that are associated with La Niña (Figure 5.15). Interestingly, even when we introduce the La Niña-related SSTA in the tropical Indian Ocean to the tropical Pacific SST signals (LNPI^{MH}) for the MH, the model does not simulate above positive summer monsoon rainfall anomalies over India (Figure 5.15). On the other hand, similar experiments carried out with both the El Niño and La Niña type SSTs in both the basins simulate positive summer monsoon rainfall anomalies over India for the HS, MWP, and LIA at least from August through September, while the pacific El Niño signal results in anomalously deficit ISMR **Figure 5.15** as mentioned earlier. This suggests that the impact of the ENSO signal in the Indian Ocean on the Indian summer monsoon may be non-linear. This of course need to be conjectured keeping in mind potential model limitations.

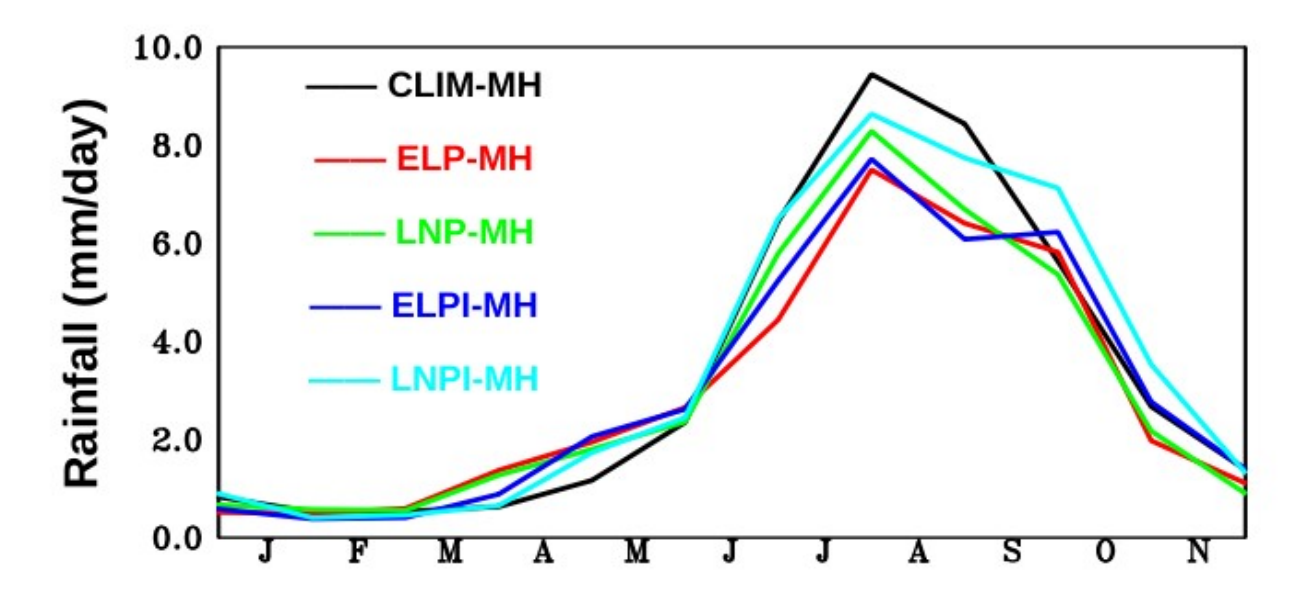


Figure 5.15: Comparision between the area-averaged seasonal cycle of AGCM sea-surface temperature (SST) sensitivity experiments. From Panel (a) CLIM(MH) - MH Control simulations, ELP(MH) - MH simulation with El Niño type SSTs in the tropical Pacific Ocean, LNP(MH) - MH simulation with La Niña type SSTs in the tropical Pacific Ocean, ELPI(MH) - MH simulation with El Niño type SSTs in the tropical Indo-Pacific Ocean, LNPI(MH) - MH simulation with La Niña type SSTs in the tropical Indo-Pacific Ocean.

From the above, based on our model simulations, there may not have be a contribution of the MH La Niñas to the wet MH summer monsoon rainfall. Their contribution to the Indian summer monsoon during MWP and LIA, however, is at least qualitatively palpable, in agreement with the PMIP3 results (Tejavath et al., 2019; 2020).

5.6 Summary

We have carried-out multiple ensemble 30-year simulations for MH, MWP, LIA, and HS climate periods. The results show that the ISMR during the MWP is higher than that of the LIA, but lesser than that of the HS, in agreement with various PMIP3 coupled simulations (Tejavath et al., 2019). Our AGCM experiments simulate relatively higher surplus ISMR during the MH period relative to the HS, supporting proxy observation-based studies (Band et al., 2018) and from other available modeling studies (Chapter 4). Results from our AGCM experiments show that the higher ISMR simulated in the MH is due to a stronger monsoon circulation, northward migration of the ITCZ, strengthening of the subtropical high over the western pacific relative to the HS. To further examine the potential role of orbital parameters on the ISM variability during the MH, we carried out several novel sensitivity simulations for the MH period by changing the orbital parameter with those of the HS, LGM, and 8.2 kyr BP. These sensitivity experiments demonstrate that the higher orbital parameter during the MH, which meant more solar insolation in the northern hemisphere, played a significant role in enhancing the ISM, and consequently, high ISMR.

This suggests that the higher insolation during the MH, around 6 kyr BP, associated with relatively favourable orbital parameters likely played a significant role in enhancing the ISM during the MH compared to the HS. Of course, this is by no means a complete explanation for the high MH rainfall simulated and recorded in several proxies. For example, we have not carried out any experiments to ascertain the potential role of land-surface and vegetation changes in the mid-Holocene, which are said to have facilitated the mid-Holocene climate in West Africa (Messori et al., 2019; Griffiths, 2020; Crétat et al., 2020). Such experiments need a model with an interactive land-surface and vegetation model. The other factors, such as the internal variability such as ENSO, whether generated due to internal coupled dynamics or forced by orbital forcings may have played

their roles. In this context, a few sensitivity simulations carried out by us suggest that our AGCM simulates below normal ISM rainfall during the MH as a response to concurrent El Niño-like SSTs imposed in the tropical Pacific (e.g. Ashok et al., 2004). This is similar to the current day ENSO impact on ISM. But we elicit a relatively low Indian summer rainfall response during the months of June and July when we force the model La Niña type of SSTs in the tropical Pacific ocean or even when the La Niña-associated concurrent SST anomalies are also imposed in the tropical Indian Ocean. Importantly, similar La Niña experiments for the MWP and LIA result in a position ISMR anomaly. This suggests that, at least in our simulations, the La Ninas have not significantly contributed to the relatively wet Indian summer monsoon during the MH, and that the orbital forcings may be relatively more important. To get a comprehensive idea of the relative roles of various internal and external factors and their influences on the Indian summer monsoon during the MH, a more extensive study with a fully coupled land-biosphere-ocean-atmospheric model will be carried out soon. We also plan to revisit the above results by repeating these experiments with multiple AGCMs in order to ascertain our findings reported in this chapter.

Chapter 6

Conclusions and scope for future studies

In this chapter, I provide a summary of the novel and significant findings reported in this thesis so far. I alsi briefly discuss the scope for further research.

The Indian summer monsoon climate variability manifests on interannual to multi-millennial time scales (Ramesh et al., 2010, Chakraborty et al., 2012). Proxy-based studies mention that Indian monsoon precipitation was stronger during mid-Holocene (MH; ~6 kyr BP) period (Rashid et al., 2011, Marzin et al., 2013, Dixit et al., 2014, Rawat et al., 2015). Few modeling studies (Kumar et al., 2018 and Tejavath et al., 2020, etc.,) also suggest that the ISM was indeed stronger during MHat that time. Proxy-based (Mukherjee et al., 2016) and model-based (Crétat et al., 2020) studies suggest that external factors such as changes in the orbital parameters, changes in solar forcing induced by volcanic eruptions, land surface, and vegetation changes, etc., may have played an important role in evolving a distinct climate of the Earth during MH relative to the current day.

However, the two limitations of the proxy-based studies are, (i) they are from a specific location, and so may not necessarily represent the variability of a wider region; (ii) given the sparse observations - which are often based on different proxy types, temporal resolution and localization, it is difficult to understand the potential dynamics that facilitate past-climates. Therefore, models provide a complementary information that can alleviate these issues to a significant extent. This thesis precisely attempts to do so from the Indian context, and focuses on the last millennium (LM) and Mid-Holocene (MH).

The chapter 1 reviews the available proxy and modelling studies for the LM and MH time periods. In chapter 2, I discuss the various datasets used and methodology. Importantly, I also carry out a validation of the simulated Indian summer mosoon climate and its teleconnection to ENSO over the historical period (1901-2005) by the historical simulations of various GCMs. A realistic simulation of the historical Indian monsoon climate gives us a confidence that the corresponding PMIP simulations of various models for the LM and MH periods are also reasonable.

In Chapter 3, we carry out an analysis of the available PMIP3 data sets for the LM period using eleven models. A comparison of the corresponding historical simulations (HS; CE 1901-2000) with the observations, carried out in chapter 2, indicates that nine models successfully replicate the monsoon statistics for the HS. We find that nine models simulate the temperature changes along the LM, particularly the from medieval warming period (MWP) and cooling (LIA). My results shows that all the PMIP3 models simulate a wet and cold summer monsoon over India during the MH period relative to the HS. The simulated rainfall and surface temperature be homogeneous across all the model simulations analysed for the MH period compared to the HS. We have to bear in mind that the resolution of the models is rather coarse, and response at local levels need not adhere to that from the area-averaged analysis. The relatively high Indian summer monsoon simulated for the MH period is in conformation with the inferences from proxy studies.

All the models capture these respective signals during CE 1000–1199 and CE 1550–1749, which periods are roughly commensurate with the proxy-observations. Importantly, most models simulate more 'strong' El Niños during MWP as compared to 'strong' La Niñas. Vice-a-versa during the LIA. Interestingly, as suggested by several proxy-observations, a majority of the models qualitatively reproduces a wetter (drier) Indian summer monsoon season in the MWP (LIA). The models also simulate a statistically significant negative correlation between ENSO-Indian summer

Monsoon rainfall throughout the LM in similar to the current day climate. Despite such a relatively high occurrence of strong El Niños during the MWP relative to the LIA, a relatively westward multi-centennial shift in the simulated anomalous summer Walker circulation as compared to the mean LM condition is simulated by many models. This change in background circulation is apparently associated with a simulated background change in the tropical Indo-pacific SST. The multicentennial shift Walker circulation results in an apparent anomalous divergence in the equatorial eastern Indian Ocean during the MWP (e.g. Ashok et al., 2004), which in turn results in concurrent anomalous convergence and excess rainfall in the Indian region. It is reasonable that the convergence/divergence patterns in the eastern equatorial Indian Ocean, which is more of a peripheral region for ENSO impact, may change depending on the background changes in circulation. Importantly, the relative increase in the simulated ISMR during the MWP is also associated with an increase in specific humidity over Indian region, and increased moisture transport into the Indian region during the MWP. While our results suggest a weakening of the meridional temperature gradient between the area-averaged land temperatures in the Indian region and the Indian ocean to its south.from the MWP to the LIA in majority of the models, the changes are very weak in magnitude.

The simulated variance of the NINO3.4 and NINO3 indices which are the indices of the during the MH period from the PMIP3 models is weaker than that for the HS period. Still, the simulated ENSO–ISMR correlations are negative and ENSO-ISM surface temperatures are positive for the majority of the models. The changes in the large-scale low-level circulation patterns and strengthening of the TEJ at 100 hPa also apparently played a major role in the precipitation changes over the Indian during the MH period compared to the HS period. It would be interesting to check whether the changes in large scale monsoon circulation during summer are attributed to the changes

in the tropical Indo-pacific characteristics, which themselves may or may not have been modulated by the solar forcing changes.

To that end, we have carried-out 30-year long multiple ensemble simulations for MH, MWP, LIA, and Present-day (HS) climate periods. The results show that the rea-averaged Indian summer monsoon rainfall during the MWP is higher than that of the LIA, but lesser than that of the HS, in agreement with various PMIP3 coupled simulations (Tejavath et al., 2019). Our AGCM experiments simulate relatively higher surplus ISMR during the MH period relative to the HS, supporting proxy observation-based studies and from few modeling studies. Results from our novel experiments show that the higher ISMR simulated in the MH is due to a stronger monsoon circulation, northward migration of the ITCZ, strengthening of the subtropical high over the western pacific relative to the HS. To examine the potential role of orbital parameters on the ISM variability during the MH, we carried out several sensitivity simulations for the MH period by changing the orbital parameter with those of the HS, LGM, and 8.2 kyr BP. These sensitivity experiments demonstrate that the higher orbital parameter during the MH, which meant more solar insolation in the northern hemisphere, played a significant role in enhancing the ISM, and consequently, high ISMR.

This suggests that the higher insolation during the MH, around 6 kyr BP, associated with relatively favourable external forcings (e.g. orbital parameters) likely played a significant role in enhancing the ISM during the MH compared to the HS. Of course, this is by no means a complete explanation for the high MH rainfall simulated and recorded in several proxies. For example, we have not carried out any experiments to ascertain the potential role of land-surface and vegetation changes in the mid-Holocene, which are said to have facilitated the mid-Holocene climate in West Africa (Messori et al., 2019; Griffiths, 2020; Crétat et al., 2020). Such experiments need a model

with an interactive land-surface and vegetation model. The other factors, such as the internal variability such as ENSO, whether generated due to internal coupled dynamics or forced by orbital forcings may have played their roles. In this context, a few sensitivity simulations carried out by us suggest that our AGCM simulates below normal ISM rainfall during the MH as a response to concurrent El Niño-like SSTs imposed in the tropical Pacific (e.g. Ashok et al., 2004). This is similar to the current day ENSO impact on ISM. But we elicit a relatively low Indian summer rainfall response during the months of June and July when we force the model La Niña type of SSTs in the tropical Pacific ocean or even when the La Niña-associated concurrent SST anomalies are also imposed in the tropical Indian Ocean. Importantly, similar La Niña experiments for the MWP and LIA result in a positive ISMR anomaly. This suggests that, at least in our simulations, the La Ninas have not significantly contributed to the relatively wet Indian summer monsoon during the MH, and that the orbital forcings may be relatively more important.

Our results are of course are subject to the model uncertainties and inter-model spread. Having said this, an agreement across a majority of the models, and the agreement with the findings from available proxy data, gives us confidence in the results. It will be interesting to examine in more detail the mechanism/reasons for the simulated distinct summer Walker circulation signatures in the tropical Indian ocean during the MWP & LIA. It is also interesting to look at the relative contributions of increase in local moisture over India due to the increased warming in MWP. Another important aspect that we hope to study is to explore whether the models are able to simulate the shrinking of the 'Indo-Pacific' rain belt during the LIA as documented in Denniston et al. (2016) from proxy-data sets, and if they do, whether such a shrinking has a role to play in the changed ENSO-Monsoon links. An important aspect, which has not been ascertained in this study, is whether the relatively higher simulated Indian summer rainfall during the MWP mostly comes from a relatively higher number of extreme rainfall events as compared to the LM-average, a

situation somewhat analogous to warmer and wetter scenario due to the increased saturated water vapour associated with increased temperature in the background of global warming (e.g. Lehmann et al. 2015; Goswami et al. 2006). On another note, It will be worthwhile analyse the future scenarios to identify any analogous or contradicting scenarios to those we see in the PMIP3.

We also plan to revisit the our results from sensitivity experiments carried out with a single AGCM for the MH, reported in Chapter 5, by repeating these experiments with multiple AGCMs in order to ascertain our claims in this thesis. Also, to get a comprehensive idea of the relative roles of a wider internal (e.g. land use land cover changes) and external factors and their influences on the Indian summer monsoon during the MH, a more extensive study with a fully coupled land-biosphere-ocean-atmospheric model will be carried out soon.

Furthermore, the assessment of climate changes on millennial time scales requires a consideration of major components of the earth system typically not represented in the IPCC-type simulations (e.g. interactive ice sheets, marine sediments, etc.) To elaborate, for example, the strong sea-level change suggested to have occurred during the early Holocene, is attributed to the ice sheets that were still melting. Understanding the relevance of changes in sea level to the past climate change of monsoons would not be possible using models without an interactive sea ice component. It is pertinent to recall that "In order to determine the past climate variability of Indian or any other region with better accuracy we have to put our efforts in the synthesis of data model including the comparisons of paleo-simulation outputs and reconstructed paleoclimate proxy data assimilation" (Von Storch et al., 2000, Fang et al., 2016).

References

- Abram N. J, Michael K. Gagan, Zhengyu Liu, Wahyoe S. Hantoro, Malcolm T. McCulloch & Bambang W. Suwargadi. Seasonal characteristics of the Indian Ocean Dipole during the Holocene epoch. Nature. Vol 445| 18 January 2007| doi:10.1038/nature05477.
- Adler, R. F., G. J. Huffman, A. Chang, R. Ferraro, P. Xie, J. Janowiak, B. Rudolf, U. Schneider, S. Curtis, D. Bolvin, A. Gruber, J. Susskind, P. Arkin, and E. Nelkin, 2003: The version 2 Global Precipitation Climatology Project (GPCP) monthly precipitation analysis (1979-present). J. Hydrometeor, 4(6), 1147-1167. Land + Ocean
- Ali Sheikh Nawaz and Coauthors, High frequency abrupt shifts in the Indian summer monsoon since Younger Dryas in the Himalaya. Scientific Reports | (2018) 8:9287 | DOI:10.1038/s41598-018-27597-6.
- Amat, Hemadri & Ashok, Karumuri. (2017). Relevance of Indian Summer Monsoon and its Tropical Indo-Pacific Climate Drivers for the Kharif Crop Production. Pure and Applied Geophysics. 175. 10.1007/s00024-017-1758-9.
- An, S.-I. and Choi, J., Mid-Holocene tropical Pacific climate state, annual cycle, and ENSO in PMIP2 and PMIP3. Clim. Dyn., 2013, 43, 957–970; doi:https://doi.org/10.1007/s00382-013-1880-z.
- Ashok, K., Guan, Z. and Yamagata, T., 2001, "Impact of the Indian Ocean Dipole on the relationship between the Indian Monsoon rainfall and ENSO", Geophys. Res. Lett., 28, 4499-4502.
- Ashok, K., Z. Guan, N. H. Saji, and T. Yamagata, 2004: Individual and combined influences of the ENSO and the Indian Ocean dipole on the Indian summer monsoon. J. Climate, 17, 3141-3155. doi: http://dx.doi.org/10.1175/1520-0442(2004)017<3141:IACIOE>2.0.CO;2
- Ashok K and N. H. Saji (2007), 'Impacts of ENSO and Indian Ocean Dipole Events on the Sub-Regional Indian Summer Monsoon Rainfall', Journal of Natural Hazards, 42: 273–285.
- Ashok, K., S. K. Behera, S. A. Rao, H. Weng, and T. Yamagata (2007), El Niño Modoki and its possible teleconnection, J. Geophys. Res. , 112, C11007, doi:10.1029/2006JC00379
- Ashok, K., Iizuka, S., Rao, S. A., Saji, N. H. and Lee, W. J., 2009, "Processes and boreal summer impacts of the 2004 El Niño Modoki: An AGCM study", Geophys. Res. Lett., 36, L04703.
- Ashok, K., Sabin, T. P., Swapna, P. and Murtugudde, R. G., 2012, "Is a global warming signature emerging in the tropical Pacific?", Geophysical Research Letters, 39, 2, L02701,
- Ashok, K., Feba, F., & Tejavath, C. T. (2019). The Indian summer monsoon rainfall and ENSO. Mausam 70 (3), 443-452

- Ashok. K., Bidyabati. S., Tejavath. C. T., and Cubasch. U. Summer monsoon over northeastern India during the last millennium. (2021), Int. J. Climatol. (Under review).
- Banacos, P. C., & Schultz, D. M. (2005). The use of moisture flux convergence in forecasting convective initiation: historical and operational perspectives. Weather Forecast., 20(3), 351–366.
- Band S, M.G. Yadava, Mahjoor Ahmad Lone, Chuan-Chou Shen, Kaushik Sree and R. Ramesh. High-resolution mid-Holocene Indian Summer Monsoon recorded in a stalagmite from the Kotumsar Cave, Central India. Quaternary International 479 (2018).
- Battisti, D. S., and Hirst, A. C. (1989). Interannual variability in the tropical atmosphere-ocean model: influence of the basic state, ocean geometry and nonlinearity. J. Atmos. Sci., 45, 1687-1712.
- Berkelhammer, M., Sinha, A., Mudelsee, M., Cheng, H., Edwards, R.L., Cannariato, K., 2010. Persistent multidecadal power of the Indian Summer Monsoon. Earth Planet. Sci. Lett. 290, 166-172.
- Berkelhammer, M., Sinha, A., Stott, L., Cheng, H., Pausata, F.S.R., Yoshimura, K., 2012. An abrupt shift in the Indian monsoon 4000 years ago. Geophys. Monogr. Ser. 198, 75-87.
- Blanford HF. 1886. Rainfall of India. Mem. India Meteorol. Dep. 2:217–448.
- Blandford HF (1884) On the connexion of the Himalayan snowfall with dry winds and seasons of drought in India. Proceedings of the Royal Society of London 37: 1–23.
- Bosmans, J. H. C., Drijfhout, S. S., Tuenter, E., Lourens, L. J., Hilgen, F. J., and Weber, S. L.: Monsoonal response to mid-holocene orbital forcing in a high resolution GCM, Clim. Past, 8, 723–740, https://doi.org/10.5194/cp-8-723-2012, 2012.
- Bowen D.Q. (2009) Last Glacial Maximum. In: Gornitz V. (eds) Encyclopedia of Paleoclimatology and Ancient Environments. Encyclopedia of Earth Sciences Series. Springer, Dordrecht. https://doi.org/10.1007/978-1-4020-4411-3_122
- Braconnot, P., et al. (2007a), Results of PMIP2 coupled simulations of the mid-Holocene and last glacial maximum. Part 1: Experiments and large-scale features, Clim. Past, 3(2), 261–277.
- Braconnot, P., et al. (2007b), Results of PMIP2 coupled simulations of the mid-Holocene and last glacial maximum. Part 2: Feedbacks with emphasis on the location of the ITCZ and mid-and high latitudes heat budget, Clim. Past, 3(2), 279–296.
- Braconnot, P., Harrison, S. P., Kageyama, M., Bartlein, P. J., Masson-Delmotte, V., Abe-Ouchi, A., Otto-Bliesner, B., Zhao, Y. (2012). Evaluation of climate models using palaeoclimatic data. Nature Climate Change, 2, 417–424. (doi:10.1038/nclimate1456)
- Cai, W., Borlace, S., Lengaigne, M., and Van Rensch, P.: Increasing frequency of extreme El Niño events due to greenhouse warming, Nature Climate, doi:10.1038/nclimate2100, 2014.

- Chabangborn, A., Brandefelt, J. and Wohlfarth, B., Asian monsoon climate during the Last Glacial Maximum: palaeo-data model comparisons. Boreas, 2013; 10.1111/bor.12032. ISSN 0300-9483.
- Chakraborty S, Goswami BN, Dutta K (2012) Pacific coral oxygen isotope and the tropospheric temperature gradient over Asian monsoon region: a tool to reconstruct past Indian summer monsoon rainfall. J Quat Sci 27(3):269–278. https://doi.org/10.1002/jqs.1541
- Chowdary, J.S., Harsha, H.S., Gnanaseelan, C. et al. Indian summer monsoon rainfall variability in response to differences in the decay phase of El Niño. Clim Dyn 48, 2707–2727 (2017). https://doi.org/10.1007/s00382-016-3233-1
- Cobb KM, CD Charles, H Cheng, and RL Edwards, El Nino/Southern Oscillation and tropical Pacific climate during the last millennium: Nature [Nature]. Vol. 424, no. 6946, pp. 271-276. 17 Jul 2003.
- Collins, M. (2000). The El Nino Southern Oscillation in the Second Hadley Centre Coupled Model and Its Response to Greenhouse Warming, (1997), 1299-1312.
- Conley A.J., et al. (2012) Description of the NCAR Community Atmosphere Model (CAM 5.0).
- Conroy, Jessica L., Restrepo, Alejandra, Overpeck, Jonathan T., Steinitz-Kannan, Miriam, Cole, Julia E., Bush, Mark B., Colinvaux, Paul A., Unprecedented recent warming of surface temperatures in the eastern tropical Pacific Ocean, 2008/12/21/online,vl-2, Nature Publishing Group, http://dx.doi.org/10.1038/ngeo390
- Cook, E. R., Anchukaitis, K. J., Buckley, B. M., D'Arrigo, R. D., Jacoby, G. C., Wright, W. E. (2010). Asian Monsoon Failure and Megadrought During the Last Millenium. Science 328 (5977), 486-9 DOI: 10.1126/science.1185188
- Crétat, J., Braconnot, P., Terray, P. et al. Mid-Holocene to present-day evolution of the Indian monsoon in transient global simulations. Clim Dyn 55, 2761–2784 (2020). https://doi.org/10.1007/s00382-020-05418-9
- Dai, A., and T. M. L. Wigley, 2000: Global patterns of ENSO induced precipitation. Geophys. Res. Lett., 27, 1283–1286.
- Dixit, Y., Hodell, D.A., Petrie, C.A., 2014. Abrupt weakening of the summer monsoon in northwest India ~ 4100 yr ago. Geology 42, 339-342.
- Dixit, Y., Hodell, D. A., Sinha, R. and Petrie, C. A., Abrupt weakening of the Indian summer monsoon at 8.2 kyr BP. Earth Planet. Sci. Lett., 2014, 391, 16–23.
- Dixit Y, Tandon SK (2016) Earth-science reviews hydroclimatic variability on the Indian subcontinent in the past millennium? Review and assessment. Earth-Sci Rev 161:1–15. https://doi.org/10.1016/j.earscirev.2016.08.001

- Dixit, Y., Hodell, D. A., Giesche, A., Tandon, S. K., Gázquez, F., Saini, H. S., et al. (2018) Intensified summer monsoon and the urbanization of Indus Civilization in northwest India. Sci. Rep. 8:4225. doi: 10.1038/s41598-018-22504-5
- Dutt, S., Gupta, A.K., Clemens, S.C., Cheng, H., Singh, R.K., Kathayat, G., Edwards, R.L., 2015. Abrupt changes in Indian summer monsoon strength during 33,800 to 5500 years BP. Geophys. Res. Lett. 42, 5526-5532.
- Emile-Geay, J., M. Cane, R. Seager, A. Kaplan, and P. Almasi (2007), El Nino as a mediator for the solar influence on climate, Paleoceanography, 22, PA3210, doi:10.1029/2006PA001304
- Fallah, B., Cubasch, U., 2014. A comparison of model simulations of Asian megadroughts during the past millennium with proxy reconstructions. Clim. Past Discuss. 10, 2685–2716.
- Fan Y., H. van den Dool (2004), Climate Prediction Center global monthly soil moisture data set at 0.5° resolution for 1948 to present, J. Geophys. Res., 109, D10102, doi:10.1029/2003JD004345.
- Feba, F., Ashok, K. & Ravichandran. M, (2018), Role of changed Indo-Pacific atmospheric circulation in the recent disconnect between the Indian summer monsoon and ENSO. Climate Dynamics, https://doi.org/10.1007/s00382-018-4207-2
- Fedorov, A. V. & Philander, S. G. Is El Nin ~o changing? Science 288, 1997-2002 (2000)
- Gadgil S. 1996. Climate change and agriculture an Indian perspective. In Climate Variability and Agriculture, Abrol YR, Gadgil S, Pant GB (eds). Narosa: New Delhi, India; 1–18.
- Gadgil, S. (2003). THE INDIAN MONSOON AND ITS VARIABILITY. Annual Review of Earth and Planetary Sciences. 31. 429-467. 10.1146/annurev.earth.31.100901.141251.
- Gadgil, S., 2018: The monsoon system: Land—sea breeze or the itcz? Journal of Earth System Science, 127 (1), 1.
- Gao, C., A. Robock, and C. Ammann, 2008: Volcanic forcing of climate over the past 1500 years: An improved ice core-based index for climate models. J. Geophys. Res., 113, D23111.
- Gershunov A, Schneider N, Barnett T (2001) Low-frequency modulation of the ENSO–Indian monsoon rainfall relationship: signal or noise?. J Climate 14:2486–2492.
- Gill, A. E. (1980). Some simple solutions for heat-induced tropical circulation. Quarterly Journal of Royal Meteorological Society, 106, 447-462.
- Gill, E. C., Rajagopalan, B., Molnar, P. and Marchitto, T. M., Reduced-dimension reconstruction of the equatorial Pacific SST and zonal wind fields over the past 10,000 years using Mg/Ca and alkenone records. Paleoceanography, 2016, 31, 928–952 doi:10.1002/2016PA002948.

- Giosan Liviu et al., Fluvial landscapes of the Harappan civilization. Proc. Natl. Acad. Sci., 2012, 109(26), E1688–E1694;doi:10.1073/pnas.1112743109.
- Goswami, B. N. and Shukla, J., Quasi-periodic oscillations in a symmetric general circulation model, J. Atmos. Sci., 41, 20-37, 1984.
- Goswami, B. N., Madhusoodanan, M., Neema, C. & Sengupta, D. A physical mechanism for North Atlantic SST influence on the Indian summer monsoon. Geophys. Res. Lett. 33, L02706 (2006).
- Graham NE, Hughes MK, Ammann CM, Cobb KM, Hoerling MP, Kennett DJ, Kennett JP, Rein B, Stott L, Wigand PE, Xu T (2007) Tropical Pacific mid-latitude teleconnections in medieval times. Clim Change 83:241–285
- Graham, N.E., Ammann, C.M., Fleitmann, D., Cobb, K.M., Luterbacher, J., 2010. Support for global climate reorganization during the Medieval Climate Anomaly. Clim. Dyn. 37, 1217-1245.
- Griffiths, M.L., Johnson, K.R., Pausata, F.S.R. et al. End of Green Sahara amplified mid- to late Holocene megadroughts in mainland Southeast Asia. Nat Commun 11, 4204 (2020). https://doi.org/10.1038/s41467-020-17927-6
- Grove, J. M., The Little Ice Age. Menthuen, London, 1988.
- Guan, Z., Ashok, K. and Yamagata, T., 2003, "Summertime response of the tropical atmosphere to the Indian Ocean sea surface temperature anomalies", J. Meteor. Soc. Japan, 81, 533-561.
- Guhatakurtha P, Rajeevan M (2006) Trends in the rainfall pattern over India. National climate centre (NCC). India Meteorol Dept Res Rep 2:1–23
- Guhathakurta, P. and Rajeevan, M. (2008), Trends in the rainfall pattern over India. Int. J. Climatol., 28: 1453-1469. doi:10.1002/joc.1640
- Gupta, A. K., M. Das, and D. M. Anderson (2005), Solar influence on the Indian summer monsoon during the Holocene, Geophys. Res. Lett., 32, L17703, doi:10.1029/2005GL022685.
- Henke Lilo M. K., F. Hugo Lambert, and Dan J. Charman. Was the Little Ice Age more or less El Niño-like than the Medieval Climate Anomaly? Evidence from hydrological and temperature proxy data. Clim. Past, 13, 267–301, 2017 www.clim-past.net/13/267/2017/ doi:10.5194/cp-13-267-2017
- Hersbach, H., ERA-20CM: a twentieth-century atmospheric model ensemble, 2015, 2350–2375; http://doi.org/10.1002/ qj.2528.
- Hoskins, B., & Wang, B. (2006). Large Scale Atmospheric Dynamics, Asian Monsoon, Ed. Bin Wang, Springer-Praxis publishing, (Chapter 9, Sec. 9.5.2, pp 377-378).
- Iles, C. E., & Hegerl, G. C. (2014). The global precipitation response to volcanic eruptions in the CMIP5 models. Environmental Research Letters, 9(10), 104012.

- IPCC, 2013: Climate Change 2013: The Physical Science Basis. Contribution of Working Group I to the Fifth Assessment Report of the Intergovernmental Panel on Climate Change [Stocker, T.F., D. Qin, G.-K. Plattner, M. Tignor, S.K. Allen, J. Boschung, A. Nauels, Y. Xia, V. Bex and P.M. Midgley (eds.)]. Cambridge University Press, Cambridge, United Kingdom and New York, NY, USA, 1535 pp, 25 doi:10.1017/CBO9781107415324.
- Jain, S., Salunke, P., Mishra, S.K. et al. Performance of CMIP5 models in the simulation of Indian summer monsoon. Theor Appl Climatol 137, 1429–1447 (2019). https://doi.org/10.1007/s00704-018-2674-3
- Jin, F.-F., 1997: An equatorial ocean recharge paradigm for enso. part i: Conceptual model. Journal of the atmospheric sciences, 54 (7), 811–829.
- Jourdain, N.C., Gupta, A.S., Taschetto, A.S. et al. The Indo-Australian monsoon and its relationship to ENSO and IOD in reanalysis data and the CMIP3/CMIP5 simulations. Clim Dyn 41, 3073–3102 (2013). https://doi.org/10.1007/s00382-013-1676-1
- Ju J, Slingo J (1995) The Asian summer monsoon and ENSO. Q J R Meteorol Soc 121(525):1133–1168
- Kalnay et al., The NCEP/NCAR 40-year reanalysis project, Bull. Amer. Meteor. Soc., 77, 437-470, 1996.
- Kanamitsu, M., W. Ebisuzaki, J. Woollen, S.-K. Yang, J. J. Hnilo, M. Fiorino, and G. L. Potter, 2002: Ncepdoe amip-ii reanalysis (r-2). Bulletin of the American Meteorological Society, 83 (11), 1631–1644, doi:10.1175/BAMS-83-11-1631.
- Kao, H. Y., and Yu, J. Y. (2009). Contrasting Eastern-Pacific and Central-Pacific Types of ENSO. J. Climate, 22, 615-632.
- Keshavamurthy RN (1982) Response of the atmosphere to sea surface temperature anomalies over the equatorial Pacific and teleconnections of the Southern Oscillation. J Atmos Sci 39:1241–1259.
- Kitoh, A. (2007). Variability of Indian monsoon-ENSO relationship in a 1000-year MRI-CGCM2.2 simulation. Natural Hazards, 42(2), 261-272. http://doi.org/10.1007/s11069-006-9092-z
- Kothawale, D. R., and H. N. Singh (2017), Recent trends in tropospheric temperature over India during the period 1971-2015, Earth and Space Science, 4, 240 -246,doi:10.1002/2016EA000246
- Kripalani, R. H., and Kulkarni, A.: 1999, Climatological impact of El Niño/La Niña on the Indian monsoon: A new perspective. Weather, 52, 39-46
- Krishnamurthy, L. and Krishnamurthy, V., 2014, "Influence of PDO on South Asian summer monsoon and monsoon-ENSO relation", Climate Dynamics, 42, 2397-2410.
- Krishnamurthy V, Goswami BN. 2000. Indian monsoon–ENSO relationship on interdecadal timescale. J. Clim. 13: 579–595.

- Krishnan, R., Venkatesan, C. and Keshavamurty, R. N., 1998, "Dynamics of upper tropospheric stationary wave anomalies induced by ENSO during the northern summer: A GCM study", Proc. Indian Acad. Sci. Earth Planet Sci, 107, 65-90.
- Krishnan R, Sabin T, Ayantika DC, Kitoh A, Sugi M, Murakami M, Turner AG, Slingo GM, Rajendran R (2012) Will the South Asian monsoon overturning circulation stabilize any further? Clim Dyn 40:187–211
- Krishnan R, Sugi M. 2003. Pacific Decadal Oscillation and variability of the Indian summer monsoon rainfall. Clim. Dyn. 21: 233–242.
- Krishnan R, Kumar V, Sugi M, Yoshimura J (2009) Internal feedbacks from monsoon midlatitude interactions during droughts in the Indian summer monsoon. J Atmos Sci 66:553–578. https://doi.org/10.1175/2008JAS2723.1
- Krishnan, R., Sabin, T.P., Vellore, R. (2016) Deciphering the desiccation trend of the South Asian monsoon hydroclimate in a warming world Clim Dyn 47: 1007. https://doi.org/10.1007/s00382-015-2886-5
- Kug, J.-S., Jin, F.-F., and An, S.-I. (2009). Two-types of El Niño events: Cold Tongue El Niño and Warm Pool El Niño. J. Climate, 22, 1499-1515.
- Kumar KK, Rajagopalan B, Cane MA (1999) On the weakening relationship between the Indian Monsoon and ENSO. Science 284(5423):2156–2159.
- Krishna Kumar, K & Rupa Kumar, K & Ashrit, Raghavendra & Deshpande, Nayana & Hansen, James. (2004). Climate impacts on Indian agriculture. International Journal of Climatology. 24. 1375 1393. 10.1002/joc.1081.
- Kumar, P., Sanwal, J., Dimri, A. P. and Ramesh, R., Contribution of diverse monsoon precipitation over Central and Northern India during Mid to Late Holocene. Quat. Int., 2019, 507, 217–223.
- Lamb, H. H., The early medieval warm epoch and its sequel. Palaeogeogr., Palaeoclimatol., 1965, 1, 13–37.
- Lau, N.-C., and M. J. Nath, 2000: Impact of ENSO on the variability of the Asian–Australian monsoons as simulated in GCM experiments. J. Climate, 13, 4287–4309.
- LeGrande, A. N., & Schmidt, G. A. (2008). Ensemble, water isotope—enabled, coupled general circulation modeling insights into the 8.2 ka event. Paleoceanography, 23(3).
- Lehmann J, Coumou D, Frieler K (2015) Increased record-breaking precipitation events under global warming. Clim Change. https://doi.org/10.1007/s10584-015-1434-y
- Lindzen, R. S., and Nigam, S. (1987). On the role of sea surface temperature gradients in forcing low-level winds and convergence in the Tropics. J. Atmos. Sci., 44, 2418-2436.

- Liu, Z., B. Otto-Bliesner, J. Kutzbach, L. Li, and C. Shields (2003), Coupled climate simulation of the evolution of global monsoons in the Holocene, J. Clim., 16(15), 2472–2490.
- Liu, Fei and Coauthors (2016). Global monsoon precipitation responses to large volcanic eruptions. Scientific Reports. 2016/04/11/online DOI http://dx.doi.org/10.1038/srep24331
- Lu Zhengyao , Zhengyu Liu, Jiang Zhu and Kim M. Cobb A Review of Paleo El Niño-Southern Oscillation. Atmosphere 2018, 9, 130; doi:10.3390/atmos9040130
- Mann, M. E., M. A. Cane, S. E. Zebiak, and A. Clement, 2005: Volcanic and solar forcing of the tropical Pacific over the past 1000 years. J. Climate, 18, 447–456.
- Mann, M. E., Zhihua Zhang, Scott Rutherford, Raymond S. Bradley, Malcolm K. Hughes, Drew Shindell, Caspar A. Global Signatures and Dynamical Origins of the Little Ice Age and Medieval Climate Anomaly Science 27 Nov 2009: Vol. 326, Issue 5957, pp. 1256-1260 DOI: 10.1126/science.1177303
- Marathe, Shamal & Ashok, Karumuri & Panickal, Swapna & T P, Sabin. (2015). Revisiting El Niño Modokis. Climate Dynamics. In press. 10.1007/s00382-015-2555-8.
- Marathe, S., Terray, P. & Karumuri, A. Tropical Indian Ocean and ENSO relationships in a changed climate. Clim Dyn 56, 3255–3276 (2021). https://doi.org/10.1007/s00382-021-05641-y
- Marzin, C., Braconnot, P. and Kageyama, M., Relative impacts of insolation changes, meltwater fluxes and ice sheets on African and Asian monsoons during the Holocene. Clim. Dyn., 2013, 41; 10.1007/s00382-013-1948-9.
- Masumoto and Yamagata (1991) Y Masumoto, T Yamagata. Response of the western tropical Pacific to the Asian winter monsoon: the generation of the Mindanao Dome. Journal of Physical Oceanography, 21 (1991), pp. 1386-1398
- Matsuno, T., 1966: Quasi-geostrophic motions in the equatorial area. J. Meteor. Soc. Japan, 44, 25–43.
- Mayewski Paul A. And Coauthors, Holocene climate variability. Quaternary Research, Volume 62, Issue 3, 2004, Pages 243-255, ISSN 0033-5894, https://doi.org/10.1016/j.vgres.2004.07.001
- Mehrotra, N., Santosh, K. S., & Bhattacharyya, A. (2014). Review of palaeoclimate records from Northeast India based on pollen proxy data of Late Pleistocenee Holocene. Quaternary International, 325, 41–54.
- Messori. G., M. Gaetani, Q. Zhang, P.S.R. Pausata The water cycle of the mid-Holocene West African monsoon: the role of vegetation and dust emission changes Int. J. Climatol. (2018), p. Joc.5924
- Moy, C. M., Seltzer, G. O., Rodbell, D. T. & Anderson, D. M. Variability of El Nino/Southern Oscillation activity at millennial timescales during the Holocene epoch. Nature 420, 162–165 (2002).

- Mujumdar M, Preethi B, Sabin TP, Ashok K, Sajjad S, Pai DS, Krishnan R (2012) The Asian summer monsoon response to the La Niña event of 2010. Meteorol Appl 19:216–225. https://doi.org/10.1002/met.1301
- Mukherjee, P., Sinha, N., Chakraborty, S. (2016) Investigating the dynamical behavior of the Inter-tropical Convergence Zone since the last glacial maximum based on terrestrial and marine sedimentary records. Quat. Int. http://dx.doi.org/10.1016/j.quaint.2016.08.030.
- Murakami T, Ding YH. 1982. Wind and temperature changes over Eurasia during the early summer of 1979. Journal of the Meteorological Society of Japan 60: 183–196.
- Murtugudde, R., McCreary, J. P., & Busalacchi, A. J. (2000). Oceanic processes associated with anomalous events in the Indian Ocean with relevance to 1997–1998. Journal of Geophysical Research: Oceans, 105(C2), 3295–3306.
- Navarra A, Ward MN, Miyakoda K (1999) Tropical-wide teleconnection and oscillation. I: teleconnection indices and type I/type II states. Quart J Roy Meteor Soc 125:2909–2935
- Overpeck, J. T., Anderson, D. M., Trumbore, S. and Prell, W. L., The southwest Indian monsoon over the last 18,000 years. Clim.Dyn., 1996, 12, 213–225; https://doi.org/10.1007/BF00211619.
- PAGES 2k Consortium, 2013: Continental-scale temperature variability during the last two millennia. Nature Geosci., 6, 339–346.
- Pai, D. S., L. Sridhar, M. Rajeevan, O. P. Sreejith, N. S. Satbhai, and B. Mukhopadhyay (2014), Development of a new high spatial resolution (0.25 degrees × 0.25 degrees) long period (1901–2010) daily gridded rainfall data set over India and its comparison with existing data sets over the region, Mausam, 65(1), 1–18.
- Palmer TN, Branković, Viterbo P, Miller MJ (1992) Modeling interannual variations of summer monsoons. J Clim 5:399–417. https://doi. org/10.1175/1520-0442(1992)005<0399:MIVOSM>2.0.CO;2
- Pant, G. B., and K. Rupa Kumar, 1997: Climates of South Asia. J. Wiley and Sons, 317 pp.
- Parthasarathy BA, Munot AA, Kothawale DR. 1988. Regression model for estimation of foodgrain production from summer monsoon rainfall. Agricultural and Forest Meteorology 42: 167–182.
- Parthasarathy B, Rupa Kumar K, Munot AA. 1992. Forecast of rainy-season food grain production based on monsoon rainfall. Indian Journal of Agricultural Science 62: 1–8.
- Pattanaik, D. R., Indian Monsoon Variability, Meteorological Monograph, 2012, vol. 2, Ch. 2, pp. 35–77.
- Philander, S. G. (1990), El Niño, La Niña, and the Southern Oscillation, Academic Press, London, 289 pp.
- Philander, S. G. (1985). El Niño and La Niña. J. Atmos. Sci., 42, 2652-2662.

- Phipps J Steven and Jaclyn N Brown (2010) Understanding ENSO dynamics through the exploration of past climates. IOP Conf. Series: Earth and Environmental Science 9 (2010) 012010 doi:10.1088/1755-1315/9/1/012010.
- Polanski S, Bijan Fallah, Daniel J. Befort, Sushma Prasad and Ulrich Cubasch. Regional moisture change over India during the past Millennium: A comparison of multi-proxy reconstructions and climate model simulations. Global and Planetary Change 122 (2014) 176–185.
- Polanski, S., Fallah, B., Prasad, S. and Cubasch, U., Simulation of the Indian monsoon and its variability during the last millennium, Clim. Past Discuss., 2013, 9, 703–740; doi:10.5194/cpd-9-703-2013.
- Polanski, S., Rinke, A., Dethloff, K., Lorenz, S.J., Wang, Y., Herzschuh, U., 2012. Simulation of the mid-Holocene Indian summer monsoon circulation with a regional climate model. Open Atmos. Sci. J. 6, 42–48
- Prasad, S., Anoop, A., Riedel, N., Sarkar, S., Menzel, P., Basavaiah, N., Krishnan, R., Fuller, D., Plessen, B., Gaye, B., Röhl, U., Wilkes, H., Sachse, D., Sawant, R., Wiesner, B., Stebich, M., 2014. Prolonged monsoon droughts and links to Indo-Pacific warm pool: a Holocene record from Lonar Lake, Central India. Earth Planet. Sci. Lett. 391, 171-182.
- Rajeevan, M., Bhate, J., Kale, J. D. and Lal, B., High resolution daily gridded rainfall data for the Indian region? Anal. Break Active Monsoon Spells, 2006, 91(3).
- Ramage, C. S. (1971) Monsoon Meteorology (Vol. 15 of International Geophysics Series). Academic Press, San Diego, CA, 296 pp.
- Ramesh R, Tiwari M, Chakraborty S, Managave SR, Yadava MG, Sinha DK (2010) Retrieval of south asian monsoon variation during the holocene from natural climate archives. Curr Sci 99(12):1770–1786
- Rao, Y. P. (1976) Southwest Monsoon (meteorological monograph). India Meteorological Department, New Delhi, 366 pp.
- Rashid, H., England, E., Thompson, L., & Polyak, L. (2011). Late glacial to Holocene Indian summer monsoon variability based upon sediment. Terr. Atmos. Ocean. Sci, 22(2), 215–228. https://doi.org/10.3319/TAO.2010.09.17.02(TibXS)1.
- Rasmusson EM, Carpenter TH (1983) The relationship between the eastern Pacific sea surface temperature and rainfall over India and Sri Lanka. Mon Weather Rev 111:517–528
- Ratna, S. B., Osborn, T. J., Joshi, M., Yang, B., & Wang, J. (2019). Identifying teleconnections and multidecadal variability of East Asian surface temperature during the last millennium in CMIP5 simulations. Climate of the Past, 15, 1825–1844. https://doi.org/10.5194/cp-15-1825-2019.

- Rawat, S., Gupta, A. K., Sangode, S. J., Srivastava, P. & Nainwal, H. C. Late Pleistocene–Holocene vegetation and Indian summer monsoon record from the Lahaul, Northwest Himalaya, India. Quat. Sci. Rev. 114, 167–181 (2015).
- Rayner NA, Parker DE, Horton EB, Folland CK, Alexander LV, Rowell DP, Kent EC, Kaplan A (2003) Global analyses of sea surface temperature, sea ice, and night marine air temperature since the late nineteenth century. J Geophys Res 108(D14):4407. doi.org/10.1029/2002JD002670.
- Rehfeld, K., Marwan, N., Breitenbach, S.F.M., Kurths, J., 2013. Late Holocene Asian summer monsoon dynamics from small but complex networks of paleoclimate data. Clim. Dyn. 41, 3–19.
- Renssen, H., Goosse, H., Fichefet, T., & Campin, J. M. (2001). The 8.2 kyr BP event simulated by a global atmosphere—sea ice—ocean model. Geophysical Research Letters, 28(8), 1567-1570.
- Revadekar, J. V, Kothawale, D. R., Patwardhan, S. K., Pant, G. B., & Kumar, K. R. (2012). extremes over India, 1133-1155. http://doi.org/10.1007/s11069-011-9895-4
- Ross Robert S., Krishnamurti T N., Pattnaik Sandeep, Pai D S. Decadal surface temperature trends in India based on a new high-resolution data set. Scientific REPORTS | (2018) 8:7452 DOI 10.1038/s41598-018-25347-2
- Roxy MK, K Ritika, P Terray, R Murtugudde, K Ashok, BN Gowswami Drying of Indian subcontinent by rapid Indian Ocean warming and a weakening land-sea thermal gradient Nature communications, 2015.
- Saji NH, Goswami BN, Vinayachandran PN, Yamagata T (1999) A dipole mode in the tropical Indian Ocean. Nature 401:360–363
- Sandeep, K., Shankar, R., Warrier, A. K., Yadava, M. G., Ramesh, R., Jani, R. A., Weijian, Z. and Xuefeng, L., A multi-proxy lake sediment record of Indian summer monsoon variability during the Holocene in southern India. Palaeogeogr., Palaeoclimatol., Palaeoecol., 2017, 476, 1–14.
- Sano, M., Ramesh, R., Sheshshayee, M., and Sukumar, R.: Increasing aridity over the past 223 years in the Nepal Himalaya inferred from a tree-ring δ 180 chronology, The Holocene, 1-9. 2011
- Sanwal, J., Singh Kotlia, B., Rajendran, C., Masood Ahmad, S., Rajendran, K., & Sandiford, M. (2013). Climatic variability in Central Indian Himalaya during the last ~1800 years:evidence from a high resolution speleothem record. Quaternary International 304, 183–192.
- Schmidt, Michael W. I., Co-authors. Persistence of soil organic matter as an ecosystem property. Nature. 2011/10/06/print, 478, Nature Publishing Group, http://dx.doi.org/10.1038/nature10386
- Schmidt, G. A. et al., Climate forcing reconstructions for use in PMIP simulations of the Last Millennium (v1.1). Geosci. Model Dev., 2012, 5, 185–191; doi:10.5194/gmd- 5-185-2012.

- Sharmila, S., Joseph, S., Sahai, A. K., Abhilash, S., & Chattopadhyay, R. (2015). Future projection of Indian summer monsoon variability under climate change scenario: An assessment from CMIP5 climate models. Global and Planetary Change, 124, 62–78. https://doi.org/10.1016/j.gloplacha.2014.11.004
- Shukla J, Paolina DA (1983) The southern oscillation and long range forecasting of the summer monsoon rainfall over India. Mon Weather Rev 111:1830–1837. doi: 10.1175/1520-0493
- Shukla, J. and J. M. Wallace, 1983, "Numerical simulation of the atmospheric response to equatorial sea surface temperature anomalies", J. Atmos. Sci., 40, 1613-1630.
- Sigl, M., Winstrup, M., Mcconnell, J. R., Welten, K. C., ... Schu, S. (2015). Timing and climate forcing of volcanic eruptions for the past 2,500 years ". https://doi.org/10.1038/nature14565
- Sikka DR (1980) Some aspects of the large-scale fluctuations of summer monsoon rainfall over India in relation to fluctuations in planetary and regional scale circulation parameters. Proc Indian Acad Sci Earth Planet Sci 89:179–195
- Sikka DR, Gadgil S. 1980. On the maximum cloud zone and the ITCZ over India longitude during the Southwest monsoon. Mon. Weather Rev. 108:1840–53
- Sinha, A., Cannariato, K.G., Stott, L.D., Cheng, H., Edwards, R.L., Yadava, M.G., Ramesh, R., Singh, I.B., 2007. A 900-year (600 to 1500 AD) record of the Indian summermonsoon precipitation from the coremonsoon zone of India. Geophys. Res. Lett. 34.
- Sinha, A., Berkelhammer, M., Stott, L., Mudelsee, M., Cheng, H., & Biswas, J. (2011). The leading mode of Indian Summer Monsoon precipitation variability during the last millennium. *Geophysical Research Letters*, *38*(15), 2–6. https://doi.org/10.1029/2011GL047713
- Sinha A, Gayatri Kathayat, Hai Cheng, Sebastian F. M. Breitenbach, Max Berkelhammer, Manfred Mudelsee, Jayant Biswas & R. L. Edwards.Trends and oscillations in the Indian summer monsoon rainfall over the last two millennia. Nature Communications 6, Article number: 6309 (2015) doi:10.1038/ncomms7309
- Sinha, N., Gandhi, N., Chakraborty, S., Krishnan, R., Yadava, M. and Ramesh, R., Abrupt climate change at ~2800 year BP evidenced by a stalagmite record from peninsular India. The Holocene, 2018, 28(11), 1720–1730; https://doi.org/10.1177/0959683618788647.
- Soman MK, Slingo J (1997) Sensitivity of the Asian summer monsoon to aspects of sea-surface-temperature anomalies in the tropical Pacific Ocean. Q J R Meteor Soc 123:309–336 https://doi.org/10.1002/qj.49712353804
- Sreejith OP, Panickal S, Pai S, Rajeevan M (2015) An Indian Ocean precursor for Indian summer monsoon rainfall variability. Geophys Res Lett 42:9345–9354.

- Stepaniak, D. P. and Trenberth, K. E., 2001: Indices of El Ni~no evolution. J. Climate, 14, 1697–1701.
- Stocker, T.F., and Coauthors. (2013): Technical Summary. In: Climate Change 2013: The Physical Science Basis. Contribution of Working Group I to the Fifth Assessment Report of the Intergovernmental Panel on Climate Change. Cambridge University Press, Cambridge, United Kingdom and New York, USA, pp. 33-115, doi:10.1017/ CBO9781107415324.005.
- Staubwasser M, Sirocko F, Grootes PM, Segl M (2003) Climate change at the 4.2 ka BP termination of the Indus valley civilization and Holocene south Asian monsoon variability. Geophys Res Lett 30:1425. https://doi.org/10.1029/2002GL016822
- Steinhilber, F., J. Beer, and C. Fro hlich (2009), Total solar irradiance during the Holocene, Geophys. Res. Lett., 36, L19704, doi:10.1029/2009GL040142.
- Suarez, M. J., and Schopf, P. S. (1988). A delayed action oscillator for ENSO. J. Atmos. Sci., 45, 3283-3287.
- Taylor, K. E., Stouffer, R. J. and Meehl, G. A., An overview of CMIP5 and the experiment design. Am. Meteor. Soc. B, 2012, 93, 485–498; doi:10.1175/BAMS-D-11-00094.1.
- Tejavath, C. T., Ashok, K., Chakraborty, S., & Ramesh, R. (2019). A PMIP3 narrative of modulation of ENSO teleconnections to the Indian summer monsoon by background changes in the Last Millennium. Climate Dynamics, 53, 3445–3461
- Tejavath. C. T., Pankaj. U., Ashok. K., (2020), The past climate of the Indian region as seen from the modelling world. Current Science, Vol. 119, No. 2, 25 July 2020.
- Thamban, M., Kawahata, H., Rao, V.P. (2007). Indian Summer Monsoon Variability during the Holocene as Recorded in Sediments of the Arabian Sea: Timing and Implications. Journal of Oceanography: 2007, vol. 63, no6, pp. 1009-1020.
- Titchner, H. A., and N. A. Rayner (2014), The Met Office Hadley Centre sea ice and sea surface temperature data set, version 2: 1. Sea ice concentrations, J. Geophys. Res. Atmos., 119, 2864-2889, doi:10.1002/2013JD020316.
- Trenberth, K. E., J. M. Caron, D. P. Stepaniak, and S. Worley, Evolution of El Niño–Southern Oscillation and global atmospheric surface temperatures, J. Geophys. Res., 107(D8), doi:10.1029/2000JD000298, 2002.
- Tyagi Ajit, Pai D. S. (2012), Monsoon 2011 A Report. IMD Met. Monograph. Synoptic Meteorology No. 1/2012.
- Ummenhofer C. Caroline, Rosanne D. D'Arrigo, Kevin J. Anchukaitis, Brendan M. Buckley, Edward R. Cook. Links between Indo-Pacific climate variability and drought in the Monsoon Asia Drought Atlas. Clim Dyn (2013) 40:1319–1334 DOI 10.1007/s00382-012-1458-1

- Vidal, C. M., Métrich, N., Komorowski, J., Pratomo, I., Michel, A., Kartadinata, N., ... Lavigne, F. (2016). The 1257 Samalas eruption (Lombok, Indonesia): the single greatest stratospheric gas release of the Common Era. Nature Publishing Group, (June), 1–13. https://doi.org/10.1038/srep34868
- Walker, G. T., Correlation in seasonal variation of weather. Q. J. R. Meteorol. Soc., 1918, 44, 223–234.
- Walker, G. T., 1928, "Quarterly Journal of Royal Meteorological Society", 54, 79.
- Walker, G.T., 1924. Correlation in seasonal variations of weather, IX. A further study of world weather. Memoirs of the India Meteorological Department, 24, (9),275–333.
- Walker, G. T. (1923), Correlation in Seasonal Variations of Weather, VIII: A Preliminary Study of World Weather, Mem. India Meteorol. Dep.
- Wang, C., Weisberg, R. H., and Virmani, J. I. (1999). Western Pacific interannual variability associated with the El Niño-Southern Oscillation. J. Geophys. Res., 104, 5131-5149.
- Webster, P. J., V. O. Magana, T. Palmer, J. Shukla, R. Tomas, M. Yanai, and T. Yasunari, 1998: Monsoons: Processes, predictability, and the prospects for prediction. Journal of Geophysical Research: Oceans, 103 (C7), 14 451–14 510.
- Webster PJ, Moore A, Loschnigg J, Leban M (1999) Coupled dynamics in the Indian Ocean during 1997–1998. Nature 401:356–360
- Wiersma, A. P., & Renssen, H. (2006). Model—data comparison for the 8.2 ka BP event: confirmation of a forcing mechanism by catastrophic drainage of Laurentide Lakes. Quaternary Science Reviews, 25(1-2), 63-88.
- Weisberg, R. H., and Wang, C. (1997). A western Pacific oscillator paradigm for the El Niño-Southern Oscillation. Geophy. Res. Lett., 24, 779-782.
- Wittenberg, A. T. (2009), Are historical records sufficient to constrain ENSO simulations? Geophys. Res. Lett., 36, L12702, doi:10.1029/2009GL038710.
- Xie P, Arkin PA (1997) Global precipitation: a 17-year monthly analysis based on gauge observations, satellite estimates, and numerical model outputs. Bull Amer Meteorol Soc 78:2539–2558
- Yadava, M. G., & Ramesh, R. R. (2005). Monsoon reconstruction from radiocarbon dated tropical speleothems. The Holocene 15:48–59.
- Yanai M, Li C and Song Z 1992 Seasonal heating of the Tibetan Plateau and its effects on the evolution of the Asian summer monsoon J. Meteor. Soc. Japan 70 319-51Yanai, Michio & Wu, Guoxiong & Wang, Bin. (2006). Effects of the Tibetan Plateau. In The Asian Monsoon. 10.1007/3-540-37722-0_13. Yang,

- S. (1996). Enso snow monsoon associations and seasonal interannual predictions. International Journal of Climatology, 16(2), 125–134. https://doi.org/10.1002
- Yanai, Michio, Wu, Guoxiong and Wang, Bin, 2006, "Effects of the Tibetan Plateau", The Asian Monsoon, 513-549,
- Yin M T 1949 A synoptic-aerologic study of the onset of the summer monsoon over India and Burma; J. Meteorol. 6 364–400.
- Zebiak, S. E., and Cane, M. A. (1987). A model El Niño-Southern Oscillation. Monthly Weather Review, 115, 2262-2278.
- Zhao, Y. et al., A multi-model analysis of the role of the ocean on the African and Indian monsoon during the mid-Holocene. Clim. Dyn., 2005, 25(7–8), 777–800.
- Zhao, Y. and Harrison, S.: Mid-Holocene monsoons: a multi-model analysis of the inter-hemispheric differences in the responses to orbital forcing and ocean feedbacks, Clim. Dynam., 39, 1457–1487, 2012.
- Zheng, W., P. Braconnot, E. Guilyardi, U. Merkel, and Y. Yu (2008), ENSO at 6 ka and 21 ka from ocean-atmosphere coupled model simulations, Clim. Dyn., 30(7–8), 745–762.

ng the Indian Summer monsoon and its variability in the Mid-Holocene and Last Millennium - A modelling View by Charan Teja Tejavath

Dr. Karumuri Ashok Professor & Principal Investigator DST-NMKSCC project "simulating...Holocene" Centre for Earth, Ocean & Atmospheric Sciences
University of Hyderabad Hyderabad-500 046, INDIA

Dr. Karumuri Ashok Professor & Principal Investigator DST-NMKSCC project "simulating...Holocene" Centre for Earth Ocean & Atmospheric Sciences University of Hyderabad Hyderabad-500 046, INDIA.

Submission date: 21-Jun-2021 11:10AM (UTC+0530)

Submission ID: 1609899120

File name: Charan_Thesis-V2.pdf (8.62M)

Word count: 25144

Character count: 126790

Modeling the Indian Summer monsoon and its variability in the Mid-Holocene and Last Millennium: A modelling view

ORIGINALITY REPORT

56%
SIMILARITY INDEX

9%
INTERNET SOURCES

54%
PUBLICATIONS

Professor & Principal Investigator
DST-NMKSCC project "simulating...Holocene"
Centre for Earth, Ocean & Atmospheric Sciences
University of Hyderabad
Hyderabad-500 046, INDIA.

STUDENT PAPERS

PRIMARY SOURCES

Charan Teja Tejavath, Karumuri Ashok, Supriyo Chakraborty. "The Importance of the Orbital Parameters for the Indian Summer of Monsoon During the Mid-Holocene, as Deciphered From Atmospheric Model Experiments", Frontiers in Earth Science, 2021

Charan Teja Tejavath, Karumuri Ashok,
Supriyo Chakraborty, Rengaswamy Ramesh.
"A PMIP3 narrative of modulation of ENSO teleconnections to the Indian summer monsoon by background changes in the Last Millennium", Climate Dynamics, 2019

paper 21% hars har hars.)

From the short hars.)

(raper from so.)

Kin hard hars.)

Charan Teja Tejavath, Karumuri Ashok, Supriyo Chakraborty, Rengaswamy Ramesh. "The ENSO teleconnections to the Indian summer monsoon climate through the Last Millennium as simulated by the PMIP3", Climate of the Past Discussions, 2018.

ming sous;), 3 (5),) at - 49); 121

ming sous; (2),), 3 (5), are the sound or and a continued or a conti

Prof. KARUMURI ASHOK

Prof. KARUMURI ASHOR

Prof. KARUMURI Ashnosheric Scientes

Prof

4	Submitted to University of Hyderabad, Hyderabad Student Paper	new 2%
5	link.springer.com Internet Source	1%
6	worldwidescience.org	1 % on
7	Charan Teja Tejavath, Ashok Karumuri, Supriyo Chakraborty, Rengasamy Ramesh. "The Indian summer monsoon climate during the Last Millennium, as simulated by the PMIP3", Climate of the Past Discussions, 2017 Publication	A for how how
8	editor.copernicus.org Internet Source	<1%
9	es.scribd.com Internet Source	<1%
10	journals.ametsoc.org Internet Source	<1%
11	R. Krishnan, C. Venkatesan, R. N. Keshavamurty. "Dynamics of upper tropospheric stationary wave anomalies induced by ENSO during the northern summer: A GCM study", Journal of Earth System Science, 1998 Publication	<1%

Bin Wang. "The Asian Monsoon", Springer Science and Business Media LLC, 2006	<1%
udspace.udel.edu Internet Source	<1%
R. S. Ajayamohan. "Simulation of South-Asian Summer Monsoon in a GCM", Pure and Applied Geophysics, 2007 Publication	<1%
centaur.reading.ac.uk Internet Source	<1%
16 WWW.nature.com Internet Source	<1%
Shinu Sheela Wilson, K. Mohanakumar. "Influence of subtropical circulation systems on the changing El Niño-Indian summer monsoon relationship", Atmospheric Research, 2021 Publication	<1%
Soon-II An, Hayoung Bong. "Feedback process responsible for the suppression of ENSO activity during the mid-Holocene", Theoretical and Applied Climatology, 2017 Publication	<1%
19 Www.m.monsoondata.org Internet Source	<1%

20	Gaurav Srivastava, Arindam Chakraborty, Ravi S. Nanjundiah. "Multidecadal variations in ENSO-Indian summer monsoon relationship at sub-seasonal timescales", Theoretical and Applied Climatology, 2020	<1%
21	Manish P. Kale, Reshma M. Ramachandran, Satish N. Pardeshi, Manoj Chavan et al. "Are Climate Extremities Changing Forest Fire Regimes in India? An Analysis Using MODIS Fire Locations During 2003–2013 and Gridded Climate Data of India Meteorological Department", Proceedings of the National Academy of Sciences, India Section A: Physical Sciences, 2017	<1%
22	"Challenges and Opportunities in Agrometeorology", Springer Nature, 2011 Publication	<1%
23	Submitted to University of Arizona Student Paper	<1%
24	agupubs.onlinelibrary.wiley.com Internet Source	<1%
25	Shraddha Band, M.G. Yadava, Mahjoor Ahmad Lone, Chuan-Chou Shen, Kaushik Sree, R. Ramesh. "High-resolution mid-Holocene Indian Summer Monsoon recorded in a	<1%

stalagmite from the Kotumsar Cave, Central India", Quaternary International, 2018

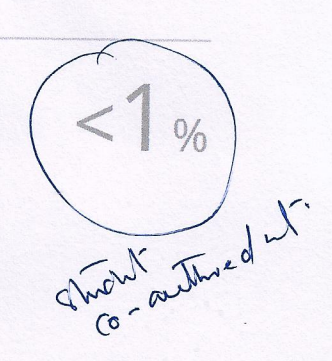
2000-10-months control of the contro		
26	Yama Dixit, Sampat K. Tandon. "Hydroclimatic variability on the Indian subcontinent in the past millennium: Review and assessment", Earth-Science Reviews, 2016 Publication	<1%
27	Roberto Suárez Moreno. "Interdecadal Changes in Ocean Teleconnections with the Sahel", Springer Science and Business Media LLC, 2019	<1%
28	Stella Jes Varghese, Sajani Surendran, Kavirajan Rajendran, Akio Kitoh. "Future projections of Indian Summer Monsoon under multiple RCPs using a high resolution global climate model multiforcing ensemble simulations", Climate Dynamics, 2019 Publication	<1%
29	Submitted to University of Sussex Student Paper	<1%
30	victor Pellet, Filipe Aires, Dai Yamazaki. "Coherent Satellite Monitoring of the Water Cycle Over the Amazon. Part 2: Total Water Storage Change and River Discharge Estimation", Water Resources Research, 2021 Publication	<1%

31	wiki.lsce.ipsl.fr Internet Source	<1%
32	Pandora Hope, Benjamin J. Henley, Joelle Gergis, Josephine Brown, Hua Ye. "Time-varying spectral characteristics of ENSO over the Last Millennium", Climate Dynamics, 2016	<1%
33	R. Seager. "Adjustment of the atmospheric circulation to tropical Pacific SST anomalies: Variability of transient eddy propagation in the Pacific-North America sector", Quarterly Journal of the Royal Meteorological Society, 2010 Publication	<1%
34	Submitted to University of Hong Kong Student Paper	<1%
35	Y. Mao, Q. Li, L. Zhang, Y. Chen, J. T. Randerson, D. Chen, KN. Liou. "Biomass burning contribution to black carbon in the western United States mountain ranges", Copernicus GmbH, 2011 Publication	<1%
36	Akio Kitoh. "Variability of Indian monsoon- ENSO relationship in a 1000-year MRI- CGCM2.2 simulation", Natural Hazards, 2007	<1%

37	Stephanie J. Bush, Andrew G. Turner, Steven J. Woolnough, Gill M. Martin, Nicholas P. Klingaman. "The effect of increased convective entrainment on Asian monsoon biases in the MetUM general circulation model", Quarterly Journal of the Royal Meteorological Society, 2015 Publication	<1
38	Wang, C "ENSO variability and the eastern tropical Pacific: A review", Progress in Oceanography, 200605/06 Publication	<1
39	climatedataguide.ucar.edu	_1

Various de la company de la co		
40	lib.dr.iastate.edu Internet Source	<1%
41	D. Manatsa. "Relative impacts of ENSO and Indian Ocean dipole/zonal mode on east	<1%
	SADC rainfall", International Journal of Climatology, 2010	

Hemadri Bhusan Amat, Maheswar Pradhan, C. T. Tejavath, Avijit Dey, Suryachandra A. Rao, A. K. Sahai, Karumuri Ashok. "Value Addition to Forecasting: Towards Kharif Rice Crop Predictability Through Local Climate

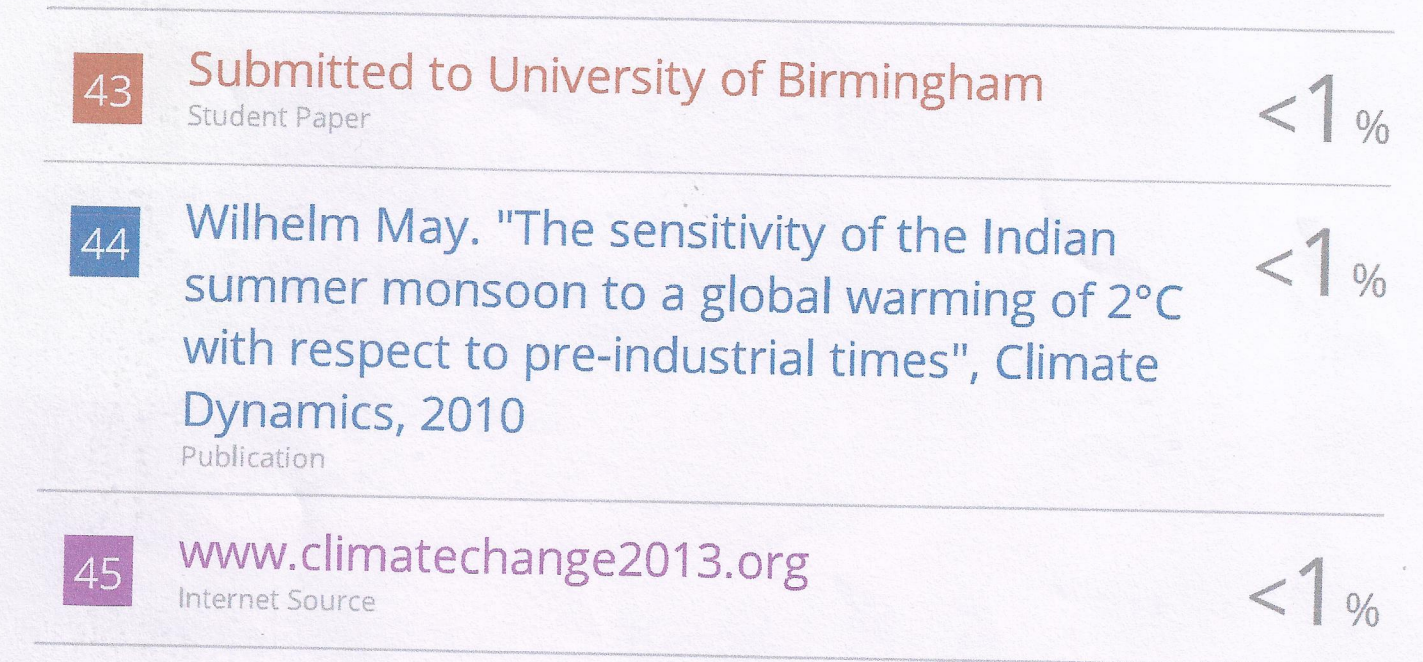


%

9/0

Variations Associated With Indo-Pacific Climate Drivers.", Research Square, 2021

Publication



Exclude quotes Or

Exclude bibliography

Exclude matches

< 14 words